Study on manufacturing and properties evaluation of Mg/Ni/Ti hydrogen storage alloy

Ningning Zhou

Saitama Institute of Technology

October, 2014

Table of content

Chapter 1 Background and applications hydrogen energy

1.1 Development of hydrogen storage materials

The hydrogen is the lightest element in the universe because composed of one proton and one electron. It is also the most abundant element in the universe and making up more than 90%. The using of the abundance of hydrogen energy on earth had been discussed in widely fields [1, 2]. Hydrogen energy can replace fossil fuels as the ideal fuel of the future. Hydrogen, as a clean energy carrier, has great potential to face energy challenges [3-6].

Hydrogen is not an energy source. It is an energy carrier like electricity and is found combined with other elements. For example, hydrogen is combined with oxygen in water [7, 8]. In fossil fuels and many organic compounds, it is combined with carbon as in petroleum, natural gas, coal or biomass. Which is the technological challenge facing researchers: to separate hydrogen from other compounds by using an efficient and economic process. Hydrogen is a new and different energy system. Hydrogen functions as a universal energy carrier converted to energy in fuel cells. Hydrogen is produced from water using renewable energy sources and the energy system holds the potential of zero emission [9- 13].

1.1.1 Necessity of hydrogen storage materials

Currently, hydrogen storage method is compressed gaseous hydrogen by high pressure cylinders or liquid hydrogen in a special bottle. But both methods have the shortcomings which high energy consumption, inconvenient heavy container and unsafe. Thus the wide application is limited [14-17].

Hydrogen storage alloy is an alloy can store hydrogen; its density is greater than the liquid hydrogen, which is called a hydrogen sponge. Not only do not need to consume energy, but could emit heat when the hydrogen was stored

into the hydrogen storage. Releasing the hydrogen needed energy is not high. Therefore, hydrogen storage alloy is the most promising hydrogen storage medium due to low working pressure, operating simple and safe [18].

Hydrogen storage principle is to form reversibly a metal hydride with hydrogen, or hydrogen and alloy formed a compound, hydrogen molecules are decomposed into hydrogen atoms into the inner of the metal [19-22]. The deformations of hydrogen damage, hydrogen corrosion and hydrogen embrittlement were easy to be caused. Moreover, in repeating absorb and release hydrogen process, constantly expanding and shrinking would occur, so that make the alloy be damaged. Therefore, the good hydrogen storage alloy must have the ability to resist the damaging effects [23-27].

Hydrogen storage alloy in research and development is generally constituted of endothermic type metal (e.g., iron, zirconium, copper, chromium, molybdenum, etc.) with an exothermic metal (e.g., titanium, zirconium, lanthanum, cerium, tantalum, etc.) [28,29]. The suitable intermetallic compounds were formed, so that achieved function of the hydrogen storage. Endothermic metal is defined under a certain hydrogen pressure, the solubility of hydrogen is increased with the temperature rises; On the contrary, the exothermic metal was confirmed. Better effect hydrogen storage materials were constituted of magnesium type, calcium type, titanium type and rare earth metals as based hydrogen storage alloys. But there are still some disadvantages to affect performance of hydrogen absorption/desorption [30-36].

The condition of hydrogen absorption was harsh and the rate was slowly. (2) Hydride generated was too stable; the performance of hydrogen absorption kinetics was poor; effective hydrogen absorption was at 573K. (3) The stability absorption and desorption of hydrogen cycle was poor. (4) Corrosion-resistant of alloy electrode in lye was not high, life cycle was low. Above disadvantages of magnesium-based hydrogen storage alloy limits practical application [37, 38]

Table 1.1 Department of Energy Technical Targets: On-board Hydrogen Storage Systems.

Storage Parameter	Deadline:2010
Gravimetric capacity	At least 6wt%
Fill time(5kg H_2)	Within 3 minutes
Volumetric capacity	45kg m^{-3}
Equilibrium pressure	-1 bar；353K
Cycle life	＞1000
Storage system cost	$133

1.1.2 Application of hydrogen storage materials

Hydrogen storage material is a general consensus that the future energy system has to be based on renewable energy sources and not on non-renewable energy sources, which is the main situation today. Renewable energy can be defined as energy obtained from the natural environment. For examples are solar energy, hydro energy and geothermal energy. On the other hand, non-renewable energy can be defined as energy obtained from static stores of energy that remain bound, unless released by human interaction. Examples of these energy sources are nuclear fuels and fossil fuels of coal, oil and natural gas [39, 40].

There is an obvious difference in utilization of these two different types of energy sources where the former one represents conversion of energy from a continuous producing resource, while the latter one represents a release of energy form a natural storage. Hence, conversion of renewable energy has to involve a possibility for energy storage since this energy cannot so easily be converted from the non-renewable sources. Electrochemical storage in different types of batteries, flywheels and thermal storage can serve as intermediate storage possibilities. Furthermore, the direct conversion of hydrogen is believed to be an important technology in future hydrogen energy systems [41].

1.1.3 Research status of hydrogen storage materials

What should be overcome in the utilization of hydrogen energy is effective storage and transportation of hydrogen. The development of zero emission vehicles, electric batteries and fuel cells is the two main power alternatives; in such applications, the demand for efficient energy storage, high volumetric and gravimetric energy densities is a crucial purpose [42-45]. The light and small molecules of hydrogen complicate the storage and transportation of this energy carrier. There are four different storing possibilities for hydrogen in compressed gas form, liquid form, chemical bonding and physical absorption [46].

Storage in the form of compressed hydrogen involves some technical challenges due to the small density of the gas. However, today hydrogen can be compressed in storage tanks with pressures up to 700bar and be used in small industrial projects and in transportation. Liquid hydrogen offers a higher volumetric storage density than compressed gas [47-49]. Hydrogen is liquefied at 20 K, the time and the energy were consumed in the process. However, it has the most gravimetric energy dense fuel in use, which is why it is employed in all space programs and need to be thermal insulated due to the storage tanks are usually large and bulky.

The most safe and volumetric effective way to store hydrogen is by chemical bounding, which can be done in metal hydrides, liquid hydrogen carriers and physical absorption. The hydrogen storage capacity has been subject to a lot of controversy the last 5 years, but the storage potential of such compounds at low temperatures (below 150 K) is well documented. The hydrogen storage potentials of both liquid and metal hydrides are utilized commercially as hydrogen storage alternatives.

The metal hydride and alloys can be considered a gaseous analogy to a water sponge. The interstices in these metal lattices will absorb and desorb hydrogen as a sponge. The absorption/desorption in metal hydrides is a

chemical reaction and not a pure physical action. The chemical reaction during absorption of hydrogen in metal hydrides releases heat, and the heat must be put back in order to release the hydrogen from its bond. It means that the metal hydrides can absorb or desorb hydrogen depending on the temperature.

The metal hydrides are utilized in storage tanks for hydrogen storage and are also used in so-called metal hydride electrical batteries. The latter utilization of the metal hydrides is the topic for the present thesis [50-53].

This hydrogen can be transferred to energy again with very high efficiency (e.g. in fuel cells), thus it can be used to various fields. There are some main hindering factors for the storing hydrogen material. The aim is to store hydrogen in a safe way with the possible highest energy density; it can be stored in tanks under high pressure or at low temperatures, or in absorbed state. Many advanced materials like carbon nano tubes, metals and intermetallic compounds can store hydrogen reversibly. In case of the achievable energy density for same metal-hydrides is higher at 20 K. To understand the application about the hydrogen absorption and desorption processes, the information on the direction of possible future developments must be studied and discussed in detail. Not only the parameters like maximum capacity and rate have to be detected, but also their change when exposed to several absorption-desorption processes would to be analyzed.

1.2 Development of metal hydrides

1.2.1 Species of metal hydrides

In present, metal hydrides had been became a focus, hydrogen storage was achieved in form of metal hydrides and could effectively release out hydrogen under a certain conditions. The process of the cycle had been widely application in various fields. For example, aerospace; communications and electronics as focus had obtained attention from domestic and foreign. Specifically, the development and application of fuel cells cause a great attention. Through the hydrogen storage material had obtained significantly development, there are some malpractices. Expensive material price; not suitable industrial production and the dissociation temperature of metal hydrides was high seriously affected the performance of hydrogen absorption/desorption [54].

Table 1.2 Properties of hydrogen with various metallic hydrides.

Storage medium	H_2 denseness (10^{22}Hatom/cm^3)	Mass%	H_2 desorbed pressure (atm) and temperature
Standard state H_2	5.4×10-3	100.0	-
Liquid H_2(220K)	4.2	100.0	-
MgH_2	6.6	7.6	1(290℃)
TiH_2	9.1	4.0	1(＞600℃)
VH_2	10.5	3.8	4(40℃)
ZrH_2	7.3	2.2	1(＞600℃)
LaH_3	6.9	2.1	1(1100℃)
Mg_2NiH_4	5.6	3.6	1(250℃)
$TiFeH_{1.9}$	5.7	1.8	3(20℃)
$LaNi_5H_6$	6.2	1.4	2(20℃)
$MmNi_{4.5}Mn_{0.5}H_{6.6}$	6.1	1.5	3(20℃)
$MmNi_{4.5}Al_{0.25}Co_{0.25}H_{3.4}$	4.8	1.2	6(20℃)

1.2.2 Research status of metal hydrides

Magnesium-based material, whose light quality, low prices, abundant raw

materials, strong hydrogen storage capacity is considered to be the best promising solid-state hydrogen storage medium. Theoretical hydrogen storage capacity of pure Mg was up to 7.6wt%, and is metal hydrogen storage materials that have the highest storage capacity except Al and Li.

Mg-based hydrogen storage materials not only have the advantages that high hydrogen absorption/desorption platform; abundant resources; low price and so on. But also which have some characteristics from others metal materials, or even superior. For example, Mg-based hydrogen storage materials have varied different form energy to achieve transformed function that heat and hydrogen chemical energy; heat and mechanical energy. For Mg-based, when hydrogen absorption process was achieved, the large number released heat for traditional storage heat material become strong challenge [55]. The prospect of hydrogen storage material was attractive by the characteristics which high-efficiency and no noise from hydrogen pressure work.

Mg alloy and Mg-based hydrogen storage material had been widely applied. In the earth, abundant Mg resources provides widely prospect for the development and produce of Mg alloy materials. In order to challenge the meet of Mg alloy material in current, the researchers put in more power to enhance development effort for Mg alloy and Mg-based hydrogen storage material, so that more perfect various properties of this kind material to develop a new Mg alloy. And based on above, the basis was laid for the formation of metal hydride.

Large scale application of metal hydrides as solid state hydrogen storage medium for the hydrogen economy is by no means the only possibility to commercialize metal hydrides. An overview is given some other types of utilization of metal hydrides. An application of solid state hydrogen storage, which is already used on a large scale, is as anode material in rechargeable nickel metal-Hydride (Ni/MH) batteries. For a detailed description of this battery see paragraph. A metal hydride electrode was used primarily to replace

the Cd-electrode in widely used Ni-Cd batteries, for which the obvious reason was to replace toxic Cd. Other advantages of a MH electrode instead of a Cd electrode include higher (dis)charge rates, a 50% higher capacity and the absence of a memory effect. The hydrogen storage alloy currently used in Ni/MH batteries is a metal-based LaNi5 compound. Much research effort is still aimed at improving properties of this electrode material, such as corrosion resistance, rate-capability and reversible hydrogen storage capacity. Yet, the gravimetric capacity is nowadays in the order of 1.2 wt. % H and it is not expected to rise significantly, simply because the intrinsic capacity is not much higher. In spite of their low gravimetric capacity, large Ni/MH packs are nowadays used in hybrid electric vehicles, like the well-known Toyota Prius and Honda Civic Hybid. Large scale implementation of Ni/MH will of course benefit from improving the gravimetric capacity of the anode. But also small electronic devices, such as mobile phones, personal digital assistants and navigation systems, that are nowadays mainly powered by Li-ion batteries might benefit from improving the capacity of the Ni/MH battery. Replacing Li-ion batteries is preferable as these batteries require expensive special safety equipment that prevents over discharging the battery, whereas Ni/MH batteries do not require any special safety equipment [56, 57].

1.3 Development of Mg-based metal hydride

1.3.1 Species of Mg-based metal hydride

Mg as the lightest element had been attended; many researchers had make contribution for the preparation of alloy phases according to raw material selection and prepared method and obtained significantly achievements. The study shown that the element with H has an affinity can effectively absorb H as hydrogen absorption. Some element produced alloy phase can play obvious catalytic role, so that achieved reversible cycle of hydrogen absorption/desorption. In present, the purpose was to increase the surface of

the specimen. There are still easy to chalking; high hydrogen absorption/desorption temperature and difficult to active [58].

Table 1.3 Characteristics of Mg alloy hydride.

Metal hydride	H mass%	Dissociation pressure (MPa)
MgH_2	7.6	0.1(290℃)
Mg-23.3%Ni-H	6.5	0.5-0.6(343℃)
Mg-10%Ni-H	5.7	0.5-0.6(340℃)
$Mg_2NiH_{4.0}$	3.6	0.1(250℃)
Mg_2Cu-H	2.7	0.1(239℃)
$CeMg_{12}$-H	4.0	0.3(325℃)
$Mg_{51}Zn_{20}H_{95}$	3.6	0.4(200℃)
$Mg_2Ni_{0.75}Cu_{0.25}$-H	3.5	0.1(227℃)
$Mg_2Ni_{0.75}Fe_{0.25}H_{3.1}$	3.6	0.1(253℃)
$Mg_2CaH_{3.72}$	5.5	0.5(350℃)
$CaMg_{1.8}Ni_{0.5}$-H	3.7	0.1(380℃)

1.3.2 Research status of Mg-based metal hydride

Mg is lightweight metal and has many advantages that cheap and readily available. Mg and Mg-based alloys in the form of metallic hydrides such as MgH_2 and Mg_2NiH_4 have been considered as potential materials for solid state hydrogen storage. The theoretical hydrogen storage capacities of MgH_2 and Mg_2NiH4 are 7.6 wt% and 3.6 wt% respectively. Unfortunately, the applications of this kind of materials are marred by their poor sorption/desorption kinetics and high dissociation temperature. Therefore, during the recent years, the main focus of research in this area had been to find the ways to substantially ameliorate the hydration kinetics of Mg-based alloys. In the past, various efforts such as mechanical alloying (MA), GPa hydrogen pressure method, melt spinning, gravity casting, hydriding combustion synthesis, surface modification, alloying with other elements, and adding catalyst have been

undertaken to improve the activation and hydride properties. Zaluska et al. have demonstrated the excellent absorption/desorption kinetics of a milled mixture of Mg_2NiH_4 and MgH_2 at 220-240°C and claimed a maximum hydrogen concentration of more than 5 wt%. Hanada et al. have reported a hydrogen storage capacity of 6.5 wt% after doping of MgH_2 with nanosized- Ni in a temperature range of 150-250°C. Recham et al. have concluded that the hydrogen absorption characteristics of ball-milled MgH_2 can be enhanced by adding NbF_5, and MgH_2 + NbF_5 composite has been found to desorb 3 wt% H_2 at 150°C. Dobrovolsky et al. have synthesized a MgH_2 (50 wt%) + TiB2 (50 wt%) composite by intensive mechanical milling and found that TiB_2 additions lower the dissociation temperature of the MgH_2 hydride about 50°C. The results reported by Cui et al. have testified the capability of amorphous and/or nanocrystalline Mg–Ni-based alloys to electrochemically absorb and also desorb a large amount of hydrogen at ambient temperatures. Kohno et al. had documented a large discharge capacity of 750 mA·h/g at a current density of 20 mA/g for modified Mg_2Ni alloys. Ball-milling indubitably is a very effective method for the fabrication of nanocrystalline and amorphous Mg and Mg-based alloys. This may facilitate the destabilization of MgH_2 or Mg_2NiH_4. However, the milled Mg and Mg-based alloys exhibit very poor hydrogen absorbing and desorbing stability on account of the evanishment of the met stable structures formed by ball milling during the multiple hydrogen absorbing and desorbing cycles. Alternatively, the melt-spun technique has not only overcome the aforementioned shortcoming, but also prohibits the significant degradation of the hydrogen absorbing and desorbing cyclic characteristics of Mg and Mg-based compounds. Furthermore, the melt-spinning technique is a beneficial method to yield a nanocrystalline structure and has been regarded to be the most appropriate for the nanocrystalline Mg-based alloys. It has also been testified that the nanocrystalline alloys produced by melt-spinning method can exhibit excellent hydride characteristics even at ambient temperatures, which is similar to that of the alloys fabricated by the MA

process. Many researchers have prepared Mg_2 (Ni, Y) hydrogen storage alloy with possessing the composition of $Mg_{63}Ni_{30}Y_7$ by rapid solidification process to yield a maximum hydrogen absorption capacity about 3.0 wt%. Huang et al. have concluded that the amorphous and the nanocrystalline Mg based alloy $(Mg_{60}Ni_{25})_{90}Nd_{10}$ prepared by melt-spinning technique displays the highest discharge capacity of 580 mAh/g and the maximum hydrogen capacity of 4.2 wt% H. Our previous work has confirmed that the substitution of Co for Ni significantly improves the absorbing and desorbing kinetics of the Mg_2Ni-type alloys. Therefore, it is very desirable to investigate the influence of substituting the Ni with Cu on the hydrogen storage characteristics of Mg_2Ni-type alloys prepared by melt spinning. The objective of present work is to synthesize the Mg-Ni-based ternary nanocrystalline alloys by melt spinning and to examine their structures and hydrogen storage characteristics [59, 60].

1.3.3 Energy conversion and application of hydrogen energy

The conversion of hydrogen energy had became a new power that improved social development. Common prepared materials divided into powders and alloys, generating alloy phase as main purpose to achieve absorb and release hydrogen under a certain conditions [61]. Metal hydride as carrier achieved the purpose of hydrogen storage.

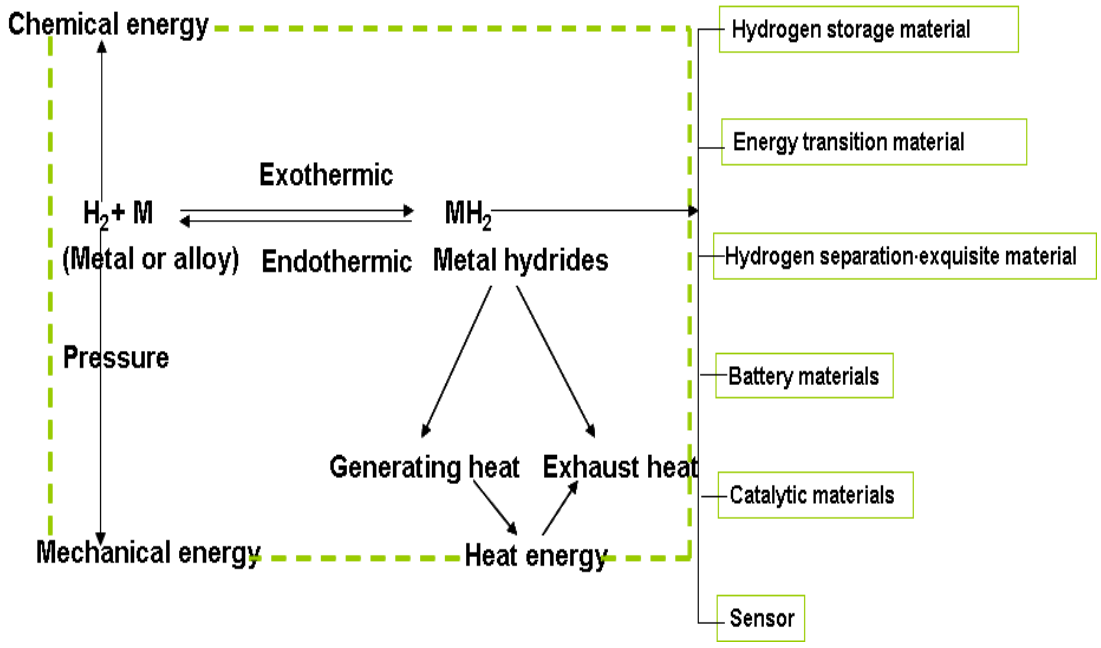

According to above introduction, Mg-based hydrogen storage alloy was still important research object because high hydrogen storage capacity of Mg. Mg was also main composition of multiphase or multivariate hydrogen storage alloy. It is showed that the source of hydrogen storage alloy is widely and could be modulated for the composition and structure of intermetallic compounds by alloying. Based on alloying mechanism, alloy composition and phase structure was optimized, so that the high performance hydrogen storage alloy could be obtained [62].

1.4 Concluding Remarks

Hydrogen is very promising energy source as a new clean energy. However, the safe storage hydrogen is very difficult because of the explosive nature. Solid storage of hydrogen using hydrogen storage materials had been investigated. Magnesium hydride is great interest because of the high storage capacity, low density, and low cost. In the past few years, hydrogen storage had been widely used the several advantages. So it is urgent to develop some new-type materials with higher activation capacity and lower cost in order to enhance the competition ability and to replace expensive materials. Much of the efforts are still intended to improve the properties, such as hydrogen storage capacity. It is known that alloys with high dynamic performance and excellent activation have been considered as new candidates for hydrogen storage applications.

References

[1] F. Stampfer, C.E. Holley and J.F. Suttle, The magnesium-hydrogen system, J. Am. Chem. Soc. 1960, 82, 3504-3508.

[2] K.H.J. Buschow, P.C.P. Bouten and A.R. Miedema, Hydrides formed from intermetallic compounds of two transition metals: a special class of ternary alloys, Rep. Prog. Phys. 1982, 45, 937-1039.

[3] A. Krozer and B. Kasemo, Unusual kinetics due to interface hydride formation in the hydriding of Pd/Mg sandwich layers, J. Vac. Sci. Technol. A 1987, 5, 1003-1005.

[4] J. Rydén, B. Hjörvarsson, T. Ericsson, E. Karlsson, A. Krozer and B. Kasemo, Unusual kinetics of hydride formation in Mg-Pd sandwiches, studied by hydrogen profiling and quartz crystal microbalance measurements, J. Less-common Met. 1989, 152, 295-309.

[5] V.P. Zhdanov, A. Krozer and B. Kasemo, Kinetics of first-order phase transitions initiated by diffusion of particles from the surface into the bulk, Phys. Rev. B 1993, 47, 11044-11048.

[6] K.B. Gerasimov and A. Krozer and B. Kasemo, Unusual kinetics due to interface hydride formation in the hydriding of Pd/Mg sandwich layers, J. Vac. Sci. Technol. A 1987, 5, 1003-1005.

[7] K. B. Gerasimov, The mechanism and kinetics of formation and decomposition of magnesium hydride, Mater, Lett. 1985, 3, 497-499.

[8] C.M. Stander, Kinetics of the formation of magnesium hydride from magnesium and hydrogen, Z. Phys. Chem. Neue Folge 1977, 104, 229-238.

[9] Z. Luz, J. Genossar and P.S. Rudman, Identification of the diffusing atom in MgH2, J. Less-common Met. 1980, 73, 113-118.

[10] J. Töpler, H. Buchner and H. Säufferer, Measurements of the diffusion of hydrogen atoms in magnesium and Mg2Ni by neutron scattering J. Less-common Met. 1982, 88, 397-404.

[11] P. Spatz, H.A. Aebischer, A. Krozer and L. Schlapbach, The diffusion of H in Mg and the nucleation and growth of MgH_2 in thin films, Z. Phys. Chem. 1993, 181, 393-397.

[12] B. Vigeholm, K. Jensen, B. Larsen and A.S. Pedersen, Elements of hydride formation mechanisms in nearly spherical magnesium powder particles, J. Less-common Met. 1987, 131, 133-141.

[13] M. Stioui, A. Grayevski, A. Resnik, D. Shaltiel and N. Kaplan, Macroscopic kinetics of hydrogen in magnesium-rich compounds, J. Less-common Met. 1986, 123, 9-24.

[14] P. van der Sluis, M. Ouwerkerk and P.A. Duine, Optical switches based on magnesium lanthanide alloy hydrides, Appl. Phys. Lett. 1997, 70, 3356-3358.

[15] R.A.H. Niessen and P.H.L. Notten, Electrochemical hydrogen storage characteristics of thin film MgX (X=Sc,Ti,V,Cr) compounds, Electrochem. Solid-State Lett. 2005, 8, A534-A538.

[16] H. Baker (Edt.), ASM Handbook – Alloy Phase Diagrams, vol. 3, ASM International, 1992.

[17] D. Kyoi, T. Sato, E. Rönnebro, N. Kitamura, A. Ueda, M. Ito, S. Katsuyama, S. Hara, D. Noreus and T. Sakai, A new ternary magnesium–titanium hydride Mg7TiHx with hydrogen desorption properties better than both binary magnesium and titanium hydrides, J. Alloys Compd. 2004, 372, 213-217.

[18] P. Villars (Edt), Pearson's Handbook Desk Edition, ASM International, 1997, Vol. 2, 2336,

[19] A.R. West, Solid state Chemistry and its applications, 1st ed., 1984, 367.

[20] T.J. Richardson, B. Farangis, J.L. Slack, P. Nachimuthu, R. Perera, N. Tamura and M. Rubin, X-Ray absorption spectroscopy of transition metal-magnesium hydride thin films, J. Alloys Compd. 2003, 356-357, 204-207.

[21] B. Farangis, P. Nachimuthu, T.J. Richardson, J.L. Slack, B.K. Meyer, R.C.C. Perera and M.D. Rubin, Structural and electronic properties of magnesium-3D transition metal switchable mirrors, Solid State Ionics 2003,

165, 309-314.

[22] L. Vegard, The constitution of mixed crystals and the space occupied by atoms, Z. Physik 1921, 5, 17-26.

[23] E. Zen, Atomic volume and allotropy of the elements, J. Chem. Ed. 1984, 61, 137-142.

[24] O. Friedrichs, L. Kolodziejczyk, J.C. Sánchez-López, A. Fernández, L. Lyubenova, D. Zander, U. Köster, K.F. Aguey-Zinsou, T. Klassen and R. Bormann, Influence of particle size on electrochemical and gas-phase hydrogen storage in nanocrystalline Mg, J. Alloys Compd. 2008, 463, 539-545.

[25] J. Paillier and L. Roue, Hydrogen electrosorption and structural properties of nanostructured Pd-Mg thin films elaborated by pulsed laser deposition, J. Alloys Compd. 2005, 404-406, 473-476.

[26] A. Léon, E.J. Knystautas, J. Huot and R. Schulz, Magnesium films for hydrogen storage, Mater. Sci. Forum 2001, 377, 85-94.

[27] A. Léon, E.J. Knystautas, J. Huot and R. Schulz, Influence of the evaporation rate and evaporation mode on the hydrogen sorption kinetics of air-exposed magnesium films, Thin Solid films 2006, 496, 683-687.

[28] A. Milchev and M.I. Montenegro, A galvanostatic study of electrochemical nucleation, J. Electroanal. Chem. 1992, 333, 93-102.

[29] P.H.L. Notten, M. Ouwerkerk, H. van Hal, D. Beelen, W. Keur, J. Zhou, and H. Feil, High energy density strategies: from hydride-forming materials research to battery integration, J. Power Sources 2004, 29, 45-54.

[30] H Kim, W Myung, K Sumyiama, K Suzuki, Formation and chemical leaching of non-equilibrium $Al_{0.6}(Co_{75}Cu_{25})_{0.4}$ alloy powders by rod milling. J Alloy Compd 2005; 398: 74–9.

[31] K Sumyiama, K Suzuki, Formation and chemical leaching effects of nonequilibrium $Al_{0.6}(Fe_{25}Cu_{75})$ alloy powder produced by rod milling. J Alloy Compd 2003; 360: 168–72.

[32] H Hu, M Qiao, S Wang, K Fan, H Li, B Zong, X Zhang, Structural and catalytic properties of skeletal Ni catalyst prepared from the rapidly quenched

$Ni_{50}Al_{50}$ alloy. J Catal 2004; 221: 612–8.

[33] G Golubkova, O Lomovski, Formation of nanocrystalline structures in a Co–Al system by mechanical alloying and leaching. J Alloy Compd 2003; 351: 101–5.

[34] H Lu, Y Li, F Wang, Synthesis of porous copper from nanocrystalline two-phase Cu–Zr film by dealloying. Scripta Mater 2007; 56: 165–8.

[35] D Ross, Hydrogen storage: the major technological barrier to the development of hydrogen fuel cell cars. Vacuum 2006; 80: 1084–9.

[36] G Duarte, L Bustamante, Hydriding properties of an Mg–Al–Ni–Ng hydrogen storage alloy. Scripta Mater 2007; 56: 789–92.

[37] L Ouyang, H Dong, C Peng, L Sun, M Zhu, A new type of Mg-based metalhydride with promising hydrogen storage properties. Int J Hydrogen Energy 2007; 32: 3929–35.

[38] J Puszkiel, P Larochette, F Gennari, Thermodynamic-kinetic characterization of the synthesized Mg_2FeH_6–MgH_2 hydrides mixture. Int J Hydrogen Energy 2008, doi:10.1016/j.ijhydene.2007.11.030.

[39] E Wirth, D Milcius, C Filiou, D Noreus, Exploring the hydrogen sorption capacity of Mg–Ni powders produced by the vapour deposition technique. Int J Hydrogen Energy 2008; 33: 3122–7.

[40] L Baum, M Meyer, L Mendoza-Zelis, Complex Mg-based hydrides obtained by mechanosynthesis: characterization and formation kinetics. Int J Hydrogen Energy 2007, doi:10.1016/j.ijhydene.2007.10.045.

[41] S Bouaricha, J Dodelet, D Guay, J Huot, S Boily, R Schulz, Hydriding behavior of Mg–Al and leached Mg–Al compounds prepared by high-energy ball-milling. J Alloy Compd 2000; 297: 282–93.

[42] K Yoshimura, Y Yamada, M Okada, Hydrogenation of Pd capped Mg thin films at room temperature. Surf Sci 2004;566: 751.

[43] J Isidorsson, H Arwin, R Griessen, Optical properties of MgH2 measured in situ by ellipsometry and spectrophotometry. Phys Rev B 2003; 68: 115112.

[44] R Westerwaal, C Broedersz, R Gremaud, M Slaman, A Borgschulte, W

Lohstroh, et al, Study of the hydride forming process of in-situ grown MgH2 thin films by activated reactive evaporation. Thin Solid Films 2008; 516: 4351.
[45] J Qu, Y Wang, L Xie, J Zheng, Y Liu, X Li, Hydrogen absorption-desorption, optical transmission properties and annealing effect of Mg thin films prepared by magnetron sputtering. Int J Hydrogen Energy 2009; 34: 1910.
[46] K Higuchi, K Yamamoto, H Kajioka, K Toiyama, M Honda, S Orimo, et al, Remarkable hydrogen storage properties in three-layered Pd/Mg/Pd thin films. J Alloys Compd 2002; 330: 526.
[47] J Ryden, Unusual kinetics of hydride formation in Mg-Pd sandwiches, studied by hydrogen profiling and quartz crystal microbalance measurements. J Less-Common Met 1989;152: 295.
[48] N Bazzanella, R Checchetto, A Miotello, Catalytic effect on hydrogen desorption in Nb-doped microcrystalline MgH_2. Appl Phys Lett 2004;85:5212.
[49] F Tang, T Parker, The Pd catalyst effect on low temperature hydrogen desorption from hydrided ultrathin Mg nanoblades. Nanotechnology 2008; 19: 465706.
[50] J Huiberts, R Griessen, J Rector, R Wijngaarden, J Dekker, et al, Yttrium and lanthanum hydride films with switchable optical properties. Nature 1996; 380: 231.
[51] T Richardson, J Slack, R Armitage, R Kostecki, B Farangis, Switchable mirrors based on nickel-magnesium films. Appl Phys Lett 2001; 78: 3047.
[52] M Pasturel, R Wijngaarden, W Lohstroh, H Schreuders, M Slaman, B Dam, et al. Influence of the chemical potential on the hydrogen sorption kinetics of Mg_2Ni/TM/Pd (TM =transition metal) trilayers. Chem Mater 2007;19: 624.
[53] K Tajima, Y Yamada, S Bao, M Okada, K Yoshimura, Near colorless all-solid-state switchable mirror based on magnesium-itanium thin film. J Appl Phys 2008; 103: 013512.
[54] P van der Sluis, Chemochromic optical switches based on metal hydrides. Electrochim Acta 1999; 44: 3063.

[55] J Paillier, Hydrogen electrosorption and structural properties of nanostructured Pd-Mg thin films elaborated by pulsed laser deposition. J Alloys Compd 2005; 404: 473.

[56] K Tajima, Y Yamada, S Bao, M Okada, K Yoshimura, Flexible all-solid-state switchable mirror on plastic sheet. Appl Phys Lett 2008; 92: 041912.

[57] M Slaman, B Dam, M Pasturel, D Borsa, H Schreuders, et al. Fiber optic hydrogen detectors containing Mg-based metal hydrides. Sens Actuators B-Chem 2007; 123: 538.

[58] M Slaman, B Dam, H Schreuders, R Griessen, Optimization of Mg-based fiber optic hydrogen detectors by alloying the catalyst. Int J Hydrogen Energy 2008; 33: 1084.

[59] M Jurczyk, L Smardz, I Okonska, E Jankowska, M Nowak, K Smardz, Nanoscale Mg-based materials for hydrogen storage. Int J Hydrogen Energy 2008; 33: 374–80.

[60] H Imamura, I Kitazawa, Y Tanabe, Y Sakata, Hydrogen storage in carbon/Mg nanocomposites synthesized by ball milling. Int J Hydrogen Energy 2007; 32: 2408–11.

[61] K Aguey-Zinsou, J Fernandez, T Klassen, R Bormann, Effect of Nb2O5 on MgH2 properties during mechanical milling. Int J Hydrogen Energy 2007; 32: 2400–7.

[62] A Baldi, R Gremaud, D Borsa, C Balde, et al, Nanoscale composition modulations in $MgyTi_{1\_y}Hx$ thin film alloys for hydrogen storage. Int J Hydrogen Energy 2009; 34: 1450–7.

Chapter 2 Design of applications in hydrogen absorption and desorption thermodynamics for Mg-based material microstructure

2.1 Introduction

Many technical field that the rapid rate of hydrogen absorption/desorption for hydrogen storage material, good anti-crushing performance, absorbing and storage in neutron tube, electrode, hydrogen separation and hydrogen chemical synthesis catalyst and so on had been widely applied. The performance of hydrogen was affect by the characteristic from many materials, for example, diffused coefficients of H in metal; hydride nucleation; growth rate; material volume; surface area ratio and surface condition [1-5]. The experiments were conducted for powder and alloy materials by theoretical calculation. But there are some difficulties to achieve isothermal stable conditions and surface contamination for reaction mechanism and the explanation about differences data [6, 8].

For hydrogen absorption and desorption kinetics, many researches are limited under low-pressure hydrogen absorbed range (P_{H2} and P_{eq} are hydrogen absorbed pressure and equilibrium pressure), the chemical absorption only was considered as the rate control procedure. However, in order to promote the rate of hydrogen absorption, the surface penetration, the diffusion and the phase transformed process may be became the rate control procedure of hydride reaction when H pressure is high and after absorbing later period [9].

2.1.1 Hydrogen absorption and desorption kinetics model

Hydrogen absorption and desorption kinetics model as shown in Fig. 2.1, H molecules dissociate on the surface of the specimen at first; H atoms transport

from the surface to substrate. With H gradually dissolve in a specimen, solid solution α forms at first, H atoms from surface h_0 to substrate form concentration gradient; when H reach to supersaturate along the direction from gas-solid interface to the substrate, so that cause γ hydride continuously deposit in supersaturated solid solution [10]. According to γ phase nucleated the difficult degree and the rate in substrate, α phase can be divided three kinds cases: (1) γ phase which easy and rapid to nucleate along the surface to substrate continuous grow by layer and layer, in which the two-phase coexistence region is zero. (2) γ phase nucleating is difficult and slow, but γ phase can grow rapidly; (3) the nucleation and growth of γ phase are difficult and slow and distribute in the whole of the specimen. Therefore, two-phase α+γ forms and single γ phase diffuses from the surface to the substrate.

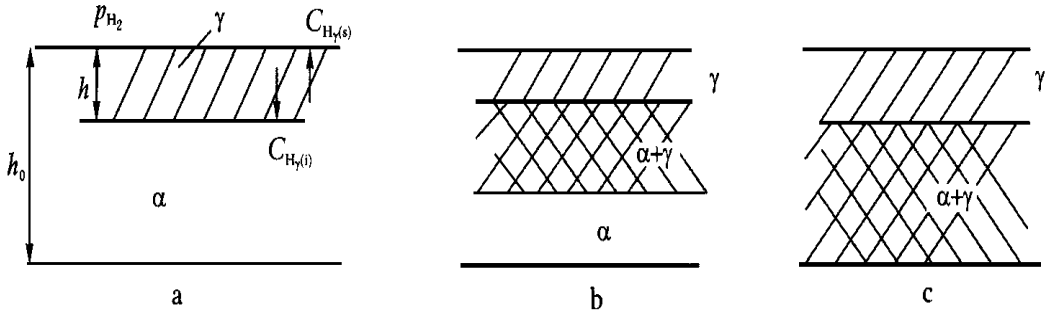

Fig. 2.1 Model of hydriding kinetics.

a- Continuously moving boundary; b- Certain thickness of the two-phase region; c- Two-phase region; CHγ(s)- Hydrogen concentration of hydride phase on inner side of surface; CHγ(i)- Hydrogen concentration of hydride phase on α/γ interface

2.1.2 Dissociation chemically absorption of hydrogen molecules on the surface

Reaction of chemically absorption by hydrogen molecules on the surface as shown in follows:

$$H_2 + 2M(ch) \frac{k_{1f}}{k_{1b}} 2H + M(ph) \quad (1)$$

M(ch) and M(ph) showed an empty chemical and physical adsorption state; k_{1f} and k_{1b} are reaction rate constants of positive and negative directions respectively, T is the absolute temperature. The reaction rate was following:

$$\frac{dn}{dt} = S_0 k_s \left[k_{1f} p_{H_2} (1-\theta) - k_{1b} \theta^2 \right] \quad (2)$$

S_0 is surface area; θ is chemisorbed coverage; k_s is effective chemical adsorption activity score; $k_s=k_0k_e$, k_0 is surface active area ratio; k_e is H atoms occupied activity area. When impurity gas is active absorption, k_e is calculated by follows equation:

$$k_e = \frac{\sqrt{b_H p_H}}{\sqrt{b_H p_H} + \sqrt{b_c} p_c} \quad (3)$$

b_H and b_c are absorbed coefficients of hydrogen and impurity gases; pH and pc are partial pressure of hydrogen and impurity gases. When the reaction reach to equilibrium, $\frac{dn}{dt} = 0$, so that the equation(2) can be converted to:

P_{eq} is equilibrium pressure.

$$\frac{dn}{dt} = k\left(p_0 - p_{eq} - \frac{RT}{V} n \right) \quad (4)$$

$$n = \frac{V}{RT}(p_0 - p_{eq}) \left[\exp\left(-\frac{RT}{V} kt \right) \right] \quad (5)$$

In the equation, $k = \frac{S_0 k_s k_{1f}}{\left(1 + \sqrt{k_d p_{eq}}\right)^2}$, when chemical absorption is non-rate-determining step, chemical absorbing H atoms and gas phase reached equilibrium, so $H_2 + 2M(ch) = 2H(ph)$, equilibrium constant as follow:

$$K_2(T) = \frac{\theta^2}{p(1-\theta)^2} \quad (6)$$

2.1.3 Surface penetration of H atoms

Surface layer of H atoms chemisorbed on surface transferred into hydride can be viewed as one-step diffusion. But the activation energy is different with diffused activation energy.

$$H + M_r(s) \frac{k_{2f}}{k_{2b}} 2H_R(s) + M(ph) \quad (7)$$

$M_r(s)$ is a hole of surface in r phase lattice; $H_r(s)$ is H atom of hydride phase on sub-surface layer. The penetrated rate on surface is showed as bellow:

$$\frac{dn}{dt} = k_s S_0 \left[k_{2f} \theta C_{M_r}(s) - k_{2b}(1-\theta) \right] \quad (8)$$

CM is the concentration on sub-surface and is constant because reached to equilibrium with α/γ interface. When the reaction reach equilibrium, $\frac{dn}{dt} = 0$, combining equation can be obtained as following:

$$\frac{dn}{dt} = k_s S_0 \sqrt{K_2(T)} K_{2F} C_{M_r(s)} \left(\sqrt{p} - \sqrt{p_{eq}} \right) / \left(1 + \sqrt{p K_2(T)} \right) \quad (9)$$

For the experiment under constant pressure, $\frac{dn}{dt} \infty$ is constant.

$$\frac{dn}{dt} = S_0 k_s k_2 \left(\sqrt{p_0 - \frac{RT}{V} n} - \sqrt{p_{eq}} \right) / \left(1 + \sqrt{\left(p_0 - \frac{RT}{V} n \right) K_2(T)} \right)$$

$$= k \left(\sqrt{p_0 - \frac{RT}{V} n} - \sqrt{p_{eq}} \right) / \left(1 + \sqrt{\left(p_0 - \frac{RT}{V} n \right) K_2(T)} \right) \quad (10)$$

$k = S_0 k_s k_2$， $k_2 = \sqrt{K_2(T)} k_{2f} C_{M_r(s)}$. There is numerical solution.

In next reacted process, hydrogen concentration must be equilibrium with gas phase.

$$C_{M_r(s)} = 1 \Big/ \sqrt{K_3(T) p} \quad (11)$$

2.1.4 Diffusion

H atom diffuses from hydride region sub-surface to α/γ interface and the

diffused rate as shown in bellow:

$$\frac{dn}{dt} = -\frac{S_0 D_\delta n_f}{\sqrt{K_3(T)} h_0 n}\left(\frac{1}{\sqrt{p}} - \frac{1}{\sqrt{p_{eq}}}\right) = -k\frac{1}{n}\left(\frac{1}{\sqrt{p}} - \frac{1}{\sqrt{p_{eq}}}\right) \quad (12)$$

$k = \frac{S_0 D_r nf}{\sqrt{K_3(T)} h_0}$, if p is constant，so $\frac{dn}{dt} \infty \frac{1}{n}$.

2.1.5 Hydride generation on interface

Finally, the reaction in two-phase region is the formation of new hydride in α/γ phase interface. Reacted equation is as shown in following:

$$Me(\alpha) + H \frac{k_{4f}}{k_{4b}} MeH + r(i) \quad (13)$$

M_e is metal. The reacted rate can be calculated.

$$\frac{dn}{dt} = S_0\left(k_{4f} - k_{4b} C_{r(i)}\right) \quad (14)$$

When the reaction reach to equilibrium, $k_{4b} = \frac{k_{4f}}{C_{r(i)_{eq}}} = k_{4f}\sqrt{K_3(T) p_{eq}}$， the equation can be became, as shown in below:

$$\frac{dn}{dt} = S_0 k_{4f}\sqrt{p_{eq}}\left(\frac{1}{\sqrt{p_{eq}}} - \frac{1}{\sqrt{p}}\right) = k\left(\frac{1}{\sqrt{p_{eq}}} - \frac{1}{\sqrt{p}}\right)$$

The hydrogen absorption capacity was calculated as time curves by different hydrogenated reaction rate as shown in follow Figure. The pressure variation by absorbing hydrogen could be been neglected due to hydrogen absorption pressure was high. In according to diffusion model, other hydrogen absorption rates with time had linear relations. The initial rate of diffused model was higher than that of other models [11]. The above kinetic model showed the absorbing hydrogen range in two-phase region. Two-phase coexist region start from absorbing hydrogen. Therefore, when the phase conversion completed into γ phase, the equilibrium pressure is dissociation equilibrium pressure for γ phase correspondingly and the hydrogen absorption constituted of three steps. In addition, when deriving kinetic equations, it is assumed that only one step

deterred the rate of hydrogen absorption. Although different hydrogenated reaction rate might be produce in each steps of absorbing hydrogen; but whether in two-phase region or γ phase region, the diffusion became finally determining step of hydrogenated reaction rate because H concentration gradient was very small when absorbing hydrogen process closed to equilibrium [12].

Figure 2.2 is the curve of hydrogen absorption pressure in two-phase region for varieties rate of hydrogen absorption kinetics. When the pressure is small, the absorbing rate on surface is small and is controlled by the reacted rate. With increasing pressure, other reacted steps became slowly, it will become control steps of hydrogen absorption kinetics. For affect of surface pollution on hydrogen absorption kinetics, with pollution degree aggravating, the absorbing and penetrating rate on surface will be significantly slowed down. Therefore, hydrogenation time by controlling process for surface will increase and the pressure of absorbing hydrogen will also increase [13].

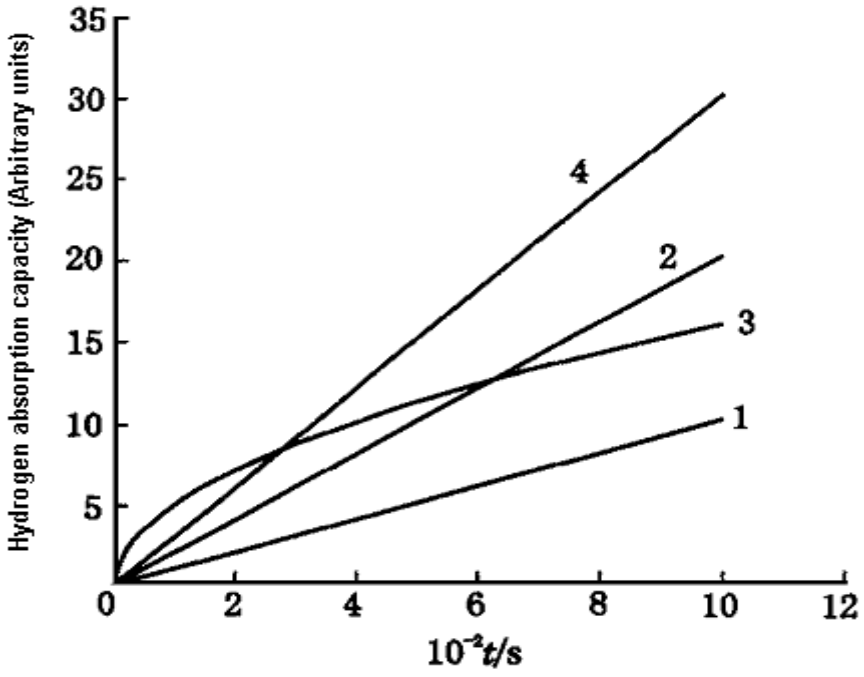

Fig. 2.2 Relation between absorbed hydrogen and time; 1- Surface absorption;

2- Surface penetration; 3- Diffusion; 4- Hydride generation.

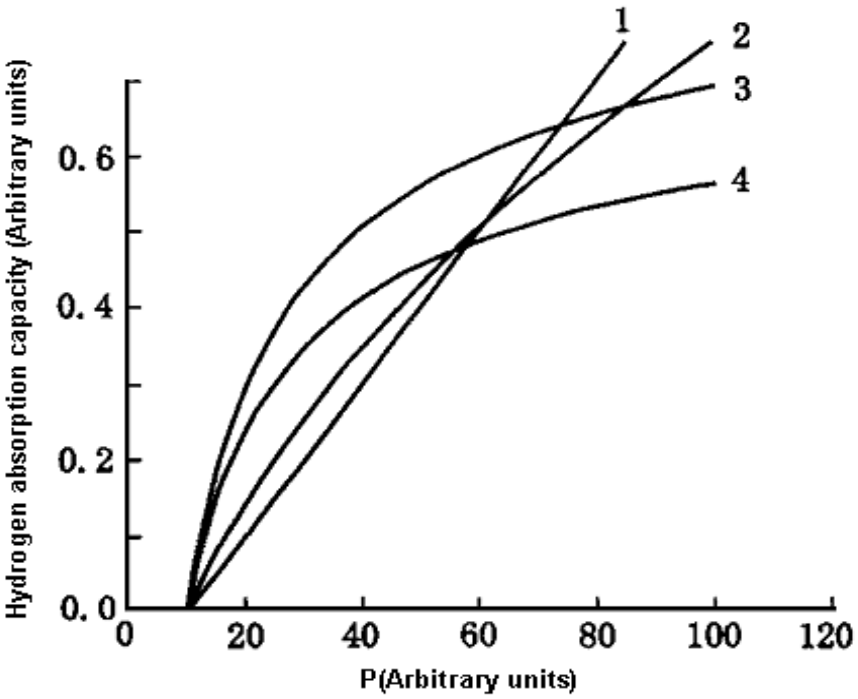

Fig. 2.3 Relation between rate and pressure; 1- Surface absorption; 2 – Surface penetration; 3 – Diffusion; 4 - Hydride generation.

2.2 Thermodynamic calculations of hydrogen absorption and desorption

Through detecting PCT curve of hydrogen absorption and desorption under different conditions, the conclusion about the performance of hydrogen storage of the temperature was obtained, in which H_2 pressure had significantly effects. According to the micro- structure of the material and heating temperature X-ray calculating, two kinds of alloy phases generated in the composite material. The performance of hydrogen storage could be studied by thermodynamic calculations [14].

According to thermodynamic equation of chemical reactions:

$$K_P = \frac{\alpha_{MH}}{\alpha_M P_{H_2}^{\frac{1}{2}}} \quad (5)$$

Kp is a equilibrium constant; α is substance activity; M, MH is the standard state; α_{MH} and α_M are activity; P_{H2} is equilibrium H_2 pressure.

According to the standard Gibbs free energy formulas:

$$\Delta G = -RT \ln K_P \tag{6}$$

$\triangle G^0$ is standard Gibbs free energy amount of change; R is gas constant; T is thermodynamic temperature.

Substituting formula (5) to (6):

$$\Delta G = -RT \ln \frac{\alpha_{MH}}{\alpha_M P_{H_2}^{\frac{1}{2}}} \tag{7}$$

$$\Delta G = -RT \ln P_{H_2} \tag{8}$$

According to the basic equations of thermodynamics

$$\Delta G = \Delta H - T\Delta S \tag{9}$$

$\triangle H$ and $\triangle S$ respectively represent the standard enthalpy and entropy changes.

Substituting formula (8) to (9)

$$\ln P_{H_2} = \frac{\Delta H}{RT} - \frac{\Delta S}{R} \tag{10}$$

The formula (11) shows the equilibrium pressure P_{H2} of the system and temperature T when the reactions reach equilibrium, standard enthalpy and entropy changes amount could be obtained.

For the experiment, the determination of hydrogen absorption and desorption was conducted under the different conditions:

(1) Constant temperature- Constant H_2 pressure

(2) Constant temperature-Changing H_2 pressure

(3) Constant H_2 pressure-Changing temperature

(4) Changing temperature-Changing H_2 pressure

According to four kinds of different conditions, the formulas were respectively used to calculate $\triangle H$ and $\triangle S$.

Under constant temperature-H_2 pressure state, the study could directly

convert formula to obtained △H，△S，△G. The period was an activated process, H molecules physically adsorbed on the surface of the composite. In order to discuss the effects the temperature and H_2 pressure for producing hydrogen absorption and desorption, the study respectively detected for constant temperature-changing H_2 pressure and constant H_2 pressure-changing temperature and according to the same formula to calculate enthalpy (△H) , entropy（△S）and Gibbs free energy（△G）, the formulas as follows:

$$K = \frac{\alpha_{MH_X}}{\alpha_M \left(f_{H_2}\right)^{\frac{X}{2}}} \tag{11}$$

$$\left(\ln P_{H_2}\right)^{\frac{-x}{2}} = \ln \frac{\alpha_{MHx}}{\alpha_M \left(f_{H_2}\right)^{\frac{X}{2}}} \tag{12}$$

$$\left(\ln P_{H_2}\right)_{673K} = \frac{\Delta H}{RT} - \frac{\Delta S}{R}; \quad \left(\ln P_{H_2}\right)_{523K} = \frac{\Delta H}{RT} - \frac{\Delta S}{R} \tag{13}$$

Through formulas (11), (12) and (13), enthalpy (△H) and entropy（△S）were obtained. Enthalpy (△H) and Entropy (△S) were 125KJmol^{-1} and 80JK^{-1}mol^{-1}. Enthalpy (△H) at 250°C is small and easy to lead the plateau pressure become higher, so that conducive to release hydrogen. It is showed that the effect on hydrogen desorption is more obviously. Based on the above measurement results, the rate and the capacity of hydrogen absorption and desorption under different conditions were discussed in detail.

2.3 Grain structure

X-ray diffraction is observed when electromagnetic radiation impinges on periodic structures with geometrical variations on the length scale the wavelength of the radiation. The interatomic distances in crystals typically amount to 0.15-4.0nm. when X-rays with a wavelength (λ) and an angle of incidence (θ) exactly fit once or n times, where n is an integer, constructive interference is observed in the form of a diffraction peak between the crystal

planes separated by a distance d; it is represented by the Bragg equation [15-17].

$$n\lambda = 2\,d\,sin\theta$$

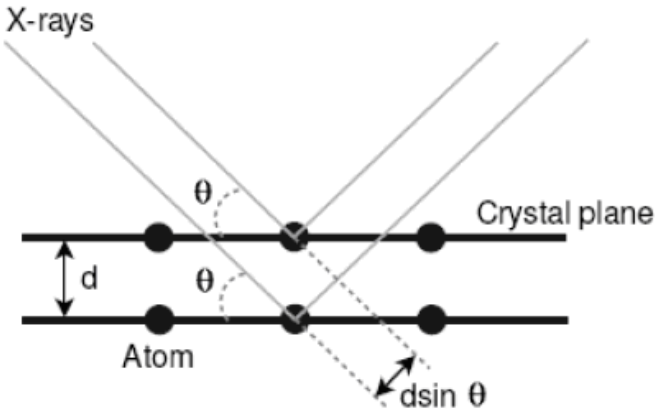

Fig. 2.4 Diffraction of X-ray.

In a crystal the positions of the atoms are periodic in three dimensions and form the crystal lattice. It is possible to determine unit cell to describe structure of entire crystal by translation into three dimensions. The unit cell is characterized by the lattice parameter a, b and c that represents lengths of crystallographic unit cell, while α, β and γ are angles between them. Directions with repeating units in crystals are described by the Miller indices h, k and l, which defined a set of lattice planes (hkl). Miller indices specify points of intersection of lattice planes with unit cell axes.

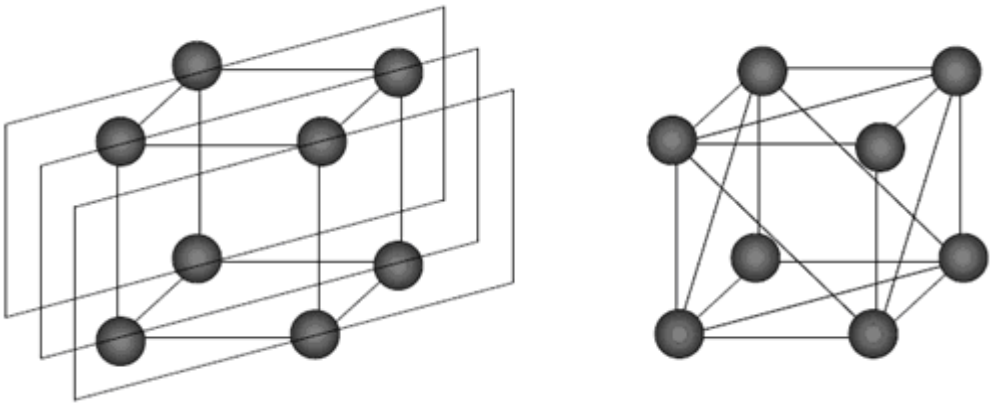

Fig. 2.5 Lattice planes with Miller indices in a simple cubic lattice.

The distance between two adjacent planes is given by the interplanar distance (d_{hkl}) with the indices specifying Miller indices of appropriate lattice

planes. For orthogonal lattices, the d_{hkl} spacing is calculated by bellow equation:

$$d_{hkl} = \frac{a}{\sqrt{h^2 k^2 l^2}} \quad (1)$$

The material prepared in this experiment had uniform crystal structure and transitional layer that promoted hydrogen absorption and desorption. The different diffused layers were composed based on the same size pure Mg ingot as substance; the different transitional layers were connected between each diffused layers and had good continuity, so that improved the performance of hydrogen absorption and desorption. Distribution of elemental and continuous diffusion layers was observed by microstructure characterization; through analyzing metal hydride formation mechanism to discuss principle of hydrogen absorption/desorption. In the paper, confirming temperature range of hydrogen desorption as research focus was calculated by high temperature X-ray diffraction and laid a foundation for the determination of actual value about hydrogen absorption and desorption.

Through above crystal phase standardized, the occupying of the atoms was calculated. As shown in Fig. 2.6(a), Ti replaced atoms Ni in Mg_2Ni alloy phase. In the diffused process, Ni and Ti in form of simple substance reacted with Mg to form Mg_2Ni alloy phase on the surface, with forming coherent transited layers of Ni, Ti and Mg_2Ni constantly diffused, Ti replaced occupying of Ni in Mg_2Ni, at the same time, NiTi formed on transited layers under a certain temperature, so that formed the transited layers in each diffused layers. The bonding of the diffused layers became more density, but crystal structure had obviously pores and effective surface area in each diffused layers. As shown in Fig. 2.6(b), H atoms enter into octahedral and tetrahedral of lattices in the hydrogen absorption process; cell expansion was caused and lattice spacing reduced obviously. As shown in Fig. 2.6(c), under a certain temperature and H_2 pressure, atoms H was released lead to the lattice spacing increase. The experiment applied the theoretical basis to conduct a cycle of

hydrogen absorption/desorption again. It helped to promote the capacity and the rate of the cycle because lattice spacing increased. As shown in Fig. 2.6(d), the result showed the cell volume appeared obvious expansion after hydrogen absorption and desorption.

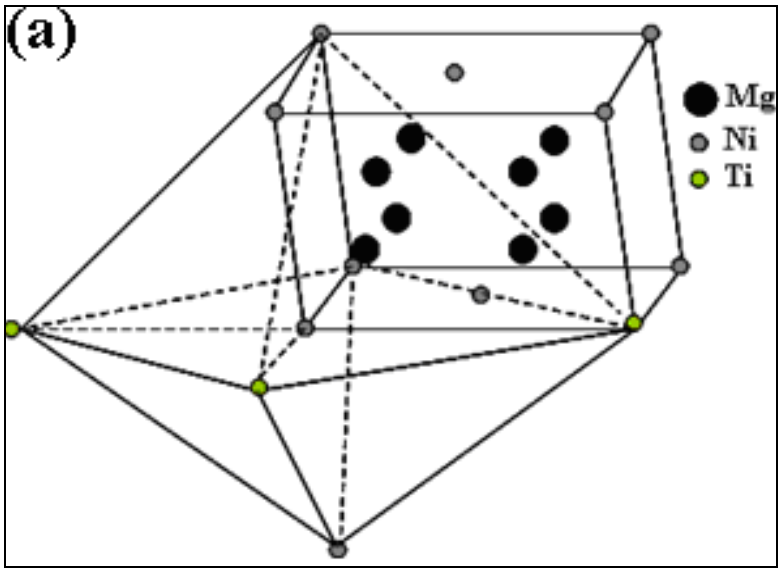

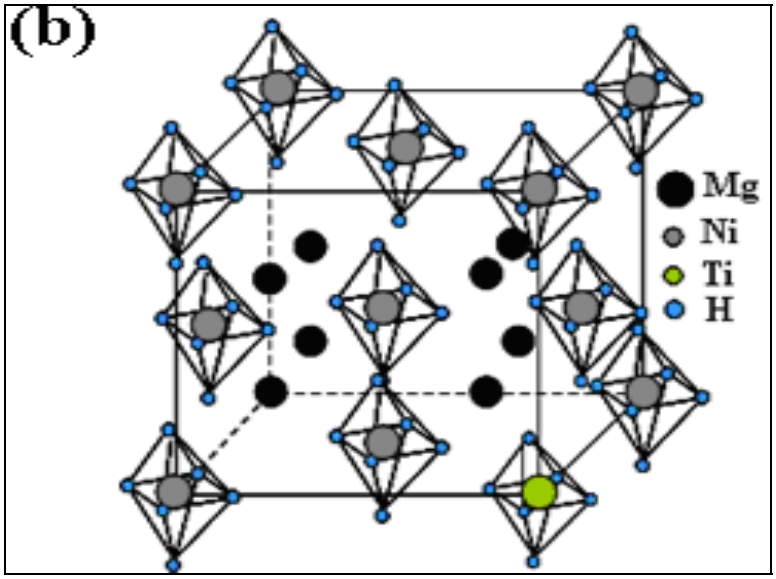

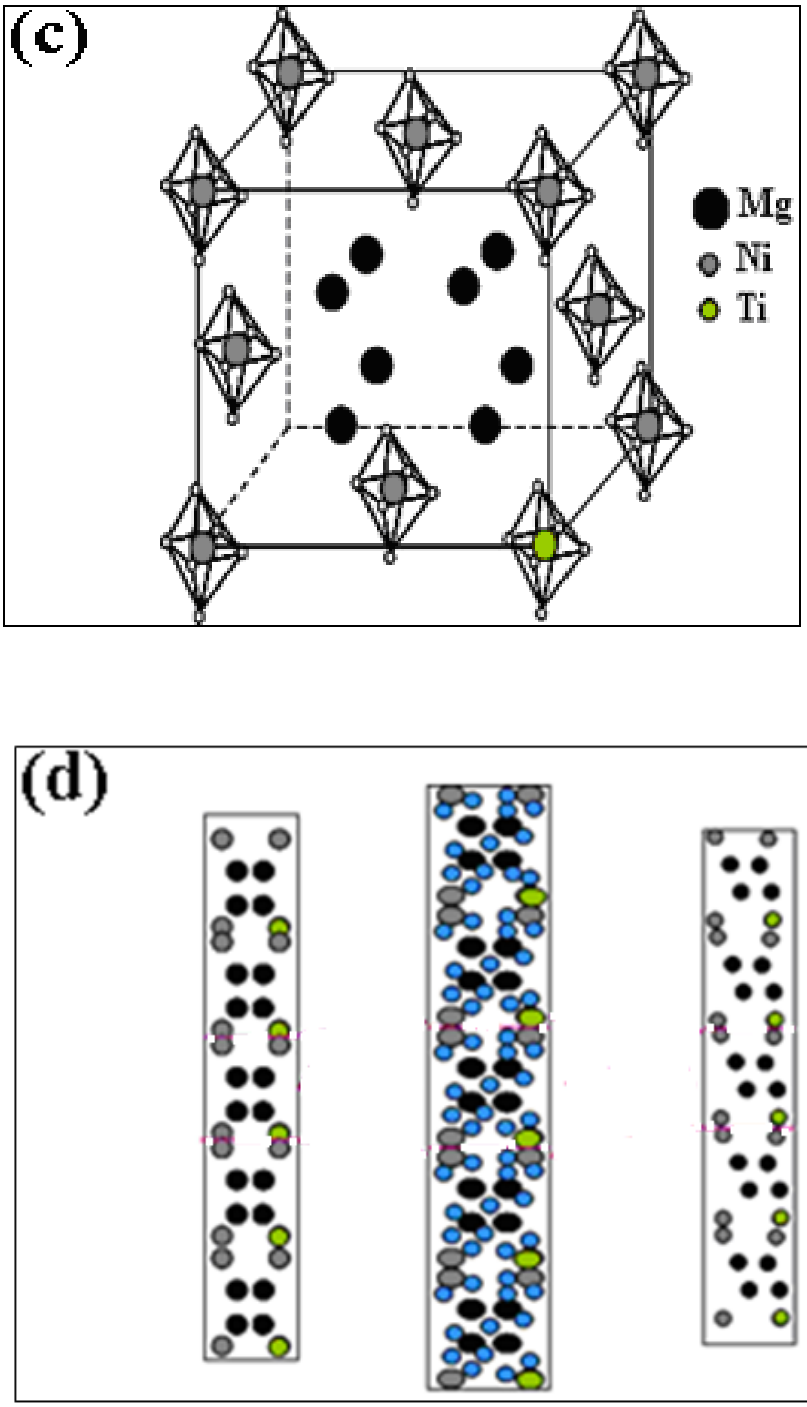

Fig. 2.6 Crystal structure (a) Mg, Ni and Ti occupying model; (b) After absorbing H; (c) After desorbing H; (d) cell volume.

2.4 Crystal grain size

The temperature range of the composite start release hydrogen was investigated by high temperature X-ray, equipped with a Cu source and an X' Celerator detector. Besides the dimensions and symmetry of unit cells in the crystalline solid, another property that can be analyzed by XRD is the grain size. To quantify the grain size, the Scherrer equation can be used.

$$D = \frac{K\lambda}{\beta COS\,\theta} \quad (1)$$

In order to confirm hydrogen absorption/desorption range, the special method that calculated crystal grain size was proposed to distinguish conventional experimental conditions, in which the crystal grain size was calculated after absorbing hydrogen in order to accurately control an experimental temperature. The hydrogen desorption temperature range would be as the test standard. In the hydrogen absorption process, the sample was put into the homemade device under H_2 state and the gas was held circulate for 2 hours. The experiment through calculating the size of the crystal grains analyzed that the temperature range was easy to be enlarged because deviations of hydrogen absorption/desorption.

The growth process of metallic hydrides $NiTiH_{0.5}$ and the $Mg_2NiH_{0.3}$ were calculated by high temperature X-ray diffraction. As shown in Fig. 2.7, Full width half maximum $NiTiH_{0.5}$ and $Mg_2NiH_{0.3}$ reached 0.096 under room temperature; but FWHM increased to 0.197 at 250°C. It indicated that the release of H in the heating temperature process led to the smaller lattice spacing between unit cells. It is showed that the crystalline particle size reduced obviously because the constantly increasing of lattice deformation with the heating temperature when FWHM increased with further heating, the finding was that the process of releasing H was achieved at 250°C. The experimental condition of the hydrogen desorption could be confirmed at the

temperature of 250°C or so. The hydrogen absorption/desorption range laid the foundation for evaluating the actual capacity.

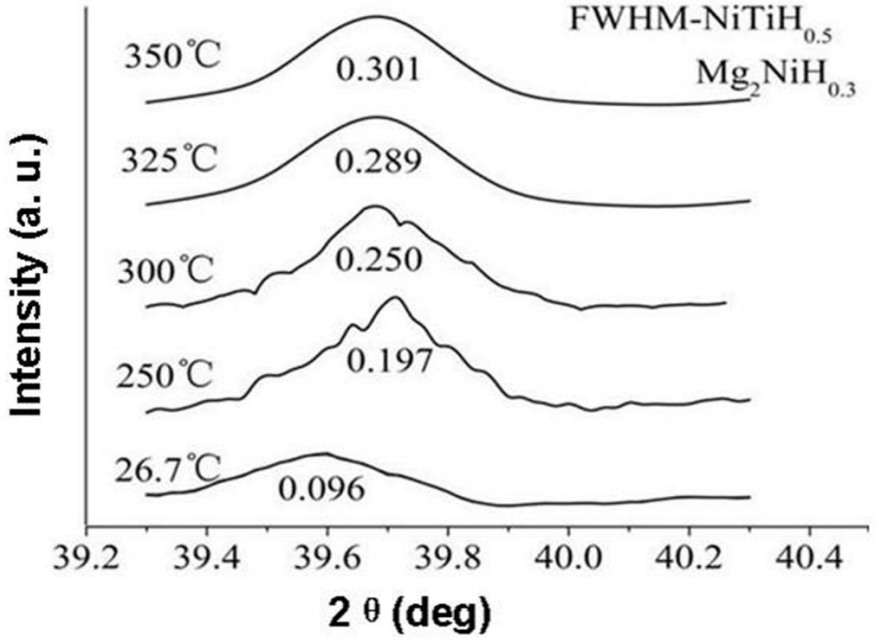

Fig. 2.7 High temperature XRD pattern of $NiTiH_{0.5}$ and $Mg_2NiH_{0.3}$.

Table 2.1- Temperature range of hydrogen desorption after absorbing hydrogen

Temperature (°C)	β	2θ (deg)	D (nm)
26.7	0.096	39.6	87.27
250	0.197	39.75	42.38
300	0.250	39.69	33.41
325	0.289	39.67	28.90
350	0.301	39.67	27.73

2.5 Concluding Remarks

The experiment confirmed basic characteristics and hydrogen absorption capacity by dynamics and thermodynamics analysis. There are some drawbacks for traditional specimen, for example, high absorbing hydrogen temperature and slow cycle rate. The study confirmed the most suitable temperature of hydrogen absorption and desorption for mentioned

shortcomings; according to grain calculation, the change degree of grain size under the absorption and desorption temperature was verified; the detected conditions were proved by the mechanism calculation of expansion and contraction for the crystal grain. It is showed that the most suitable temperature of generating Mg_2Ni and NiTi alloy phases was 600-800°C and the most suitable desorbing hydrogen temperature was about 250°C.

References

[1] W．Kohn，L．J．Sham, Self-consistent Equations Including Exchange and Correlation Effects．Physical Review A，1965，140：1 133·l 138．

[2] J．P．Perdew，K．Burke, Comparison Shopping for a Gradient-corrected Density Functional．International Journal of Quantum Chemistry，1 996，57：309-3 1 9．

[3] D．R．Hamann，M．Schluter，C．Chiang, Norm—conserving Pseudopotential．Physical ReviewLetters,1979，43：1494-1497．

[4] D．Vanderbilt, Soft Seit-consistent Pseudopotential in a Generalized Eigenvalue Formolism．Physical Review B，1 990，43：7892—7895．

[5] D．J．Siegel C．Wolverton,V．Ozolins，Reaction Energetics and Crystal Structure of Li4BN3Hlo from First Principles．Physical Review B，2007，75：014101．

[6] E．Weidner, F．Doici，J．Hu,W．Wiebke，T．Hansen，D．J．Bull，M．Fichtner, Hydrogenation Reaction Pathway in $Li_2Mg(NH)_2$．Journal of Physical Chemistry C，2009，l 1 3：1 5772-1 5777．

[7] R．L．Davis，C．H．L．Kennard, Structure of Sodium Tetradeuterobrate，$NaBD_4$．Journal of Solid State Chemistry，1 985，59：393-396．

[8] M．D．Segall，R．Shah，C．J．Pickard,M．C．Payne, Popuimion Analysis of Plane·wave Electronic Structure Calculations of Bulk Materials．Physical Review B，1 996，54：163 17．16320．

[9] C．G．Van de Walle，J．Neugebauer, First-principles Calculations for Defects and Impurities：Applications to Hl—nitrides．Journal ofApplied Physics，2004，95：3851-3879．

[10] H．Y．Leng，T．1chiwawa,S．Hino，T．Nakagawa,H．Fujii, Mechanism of Hydrogenation Reaction in the Li-Mg-N-H System．Journal of Physical Chemistry B，2005，109：10744．10748．

[11] W．I．F．David,M．O．Jones，D．H．Gregory，C．M．Jewell，S．R．

Johnson, A. Walton，P. P. Edwards, A Mechanism for Non·stoichiometry in the Lithium Amide／Lithium Imide Hydrogen Storage Reaction. Journal of the American Chemistry Society，2007，129：1594-1601.

[12] H. Wu. Structure of Ternary Imide $Li_2Ca(NH)_2$ and Hydrogen Storage Mechanisms in Amide, Hydride System. Journal of the American Chemistry Society，2008，130：6515-6522.

[13] T. Ichikawa, N. Hanada, S. Isobe，H. Y. Leng, H. Fujii, Mechanism of Novel Reaction from $LiNH_2$ and LiH to Li_2NH and H_2 aS a Promising Hydrogen Storage System. Journal of Physical Chemistry B，2004，l 08：7887-7892.

[14] W. Luo，K. Stewart, Characterization of NHa Formation in Desorption of Li—Mg-N-H Storage System. Journal ofAlloys and Compounds，2007，440：357-361.

[15] H. Y. Leng，T. Ichiwawa, H. Fujii, Hydrogen Storage Properties of Li-Mg-N-H System with Different Ratios of LiH／$M_{90}(H_2)_2$. Journal of Physical Chemislry B 2006，l 10：12964. 12968.

[16] T. Nakagawa, T. Ichikawa, R. Iida, H. Y. Leng，N. Takeichi，T. Kiyobayashi，H. Takeshita, H. Fujii, Observation of Hydrogen Absorption／Desorption Reaction Processes in Li-Mg·N·H System by in-situ X-ray Diffractmetry. Journal of Alloys and Compounds，2007，430：21 7. 221.

[17] S. Isobe，T. Ichikawa, H. Y. Leng，H. Fujii，Y. Kojima, Hydrogen Desorption Processes in Li—Mg-N·H Systems. Journal of Physics and Chemistry of Solids，2008，69：2234—2236.

Chapter 3 Preparation and evaluation of Ni/MgO powder

3.1 Introduction

Ni/MgO powder had been applied in many fields, such as the efficient reaction of organic synthesis and reduction reactions. Especially for fields of battery materials and alloy binder metal, Ni/MgO is applied widely as a catalyst that improve thermal conductivity, the heat resistance and dynamic performance of hydrogen storage materials[1-3]. Specially, the structure of the Ni catalysts is also important in the liquid-phase reaction [4]. Much attention had been paid to the elemental substance of Ni [4]. In this paper, it had been achieved under certain conditions that Ni powder homemade process effectively reduced the presence of impurities and oxidation/reduction was used in order to further refine the powder [5-9]. Gas plays a vital role in protecting process, not only prevented re-oxidation at high temperatures, but also conducted reduction reaction with the oxide formed during sintering, so that the oxide is reduced sufficiently. Greater impact on the grain size to the crystal structure and elemental distribution was caused [10-15].

In this experiment, a trace amount of H_3BO_3 was added after the nickel is prepared, the purpose is to make the grain more uniform and refinement by chemical reaction. We used uniform refinement method based on co-precipitation to obtain Ni/MgO [16-20], in which controlled the molar ratio of $NiCl_2 \cdot 6H_2O$ and $MgCl_2 \cdot 4H_2O$ solution. Then H_3BO_3 was added into the Ni/MgO sintering powder and was sintered at 800°C，900°C and 1000°C. Through evaluated results of crystal structure and microstructure, we found that adjunction and grinding of H_3BO_3 promote grain refine at the second sintered process and grain size is about 1μm.

3.2 Experimental methods

3.2.1 Preparation of powder Ni by high temperature X-ray

The mixed powder was prepared by co-precipitation. The ammonium oxalate [$(NH_4)_2C_2O_4 \cdot H_2O$] of 25g, 1.4mol/L $NiCl_2 \cdot 6H_2O$ 32g were used as starting materials to prepare Ni powder. It was confirmed that the solute of the aqueous solution was completely dissolved at 50°C; aqueous solution mixed was stirred at the rate of 300rpm for 2 hours. The next, aqueous solution stirred was filtered with the funnel and filter paper.

The mixed powder was sintered at 10°C /min to 1000°C by using the apparatus of high temperature X-ray. In the prepared process, As shown in Fig. 3.1 and Tab. 3.1, $Mg_3O(CO_3)_2$， $NiCO_3$ and $MgNiO_2$ formed at 200°C. With the temperature increasing, the grain of $Mg_3O(CO_3)_2$ became smaller and disappear at 300°C. In which $Mg_3O(CO_3)_2$ was thermal decomposed , so that the grain of $MgNiO_2$ grew up and a small amount of Ni was restored out. It is indicated that $C_2O_4^{2-}$ was decomposed to CO and CO_2 while generated NiO oxides. With generated CO was releasing, which make NiO be reverted Ni in heating process of the powder at 350°C. Heating up 400°C to 600°C, the grain size of Ni powder continues increase and is to 49.904nm. The grain size was refined obviously with temperature to 800°C and the grain size is 39.886nm. But temperature continues up to 1000°C, crystal particles begin to dilate, so that leading to the formation of agglomeration. The above results show the most suitable temperature is 600-800°C**.**

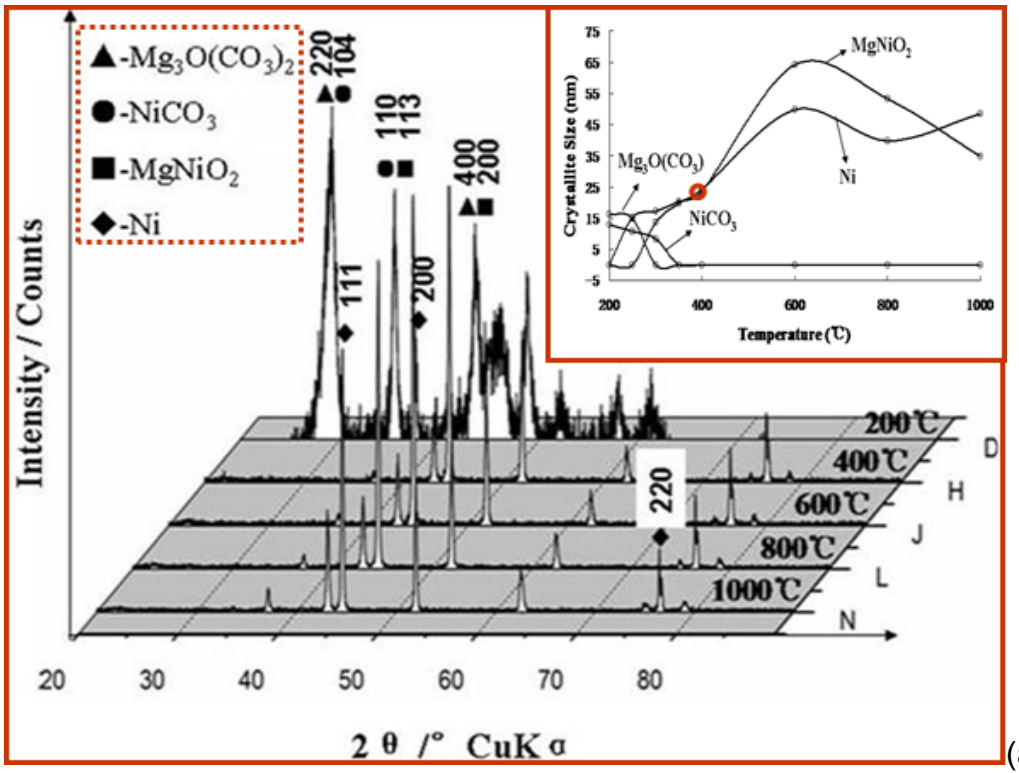

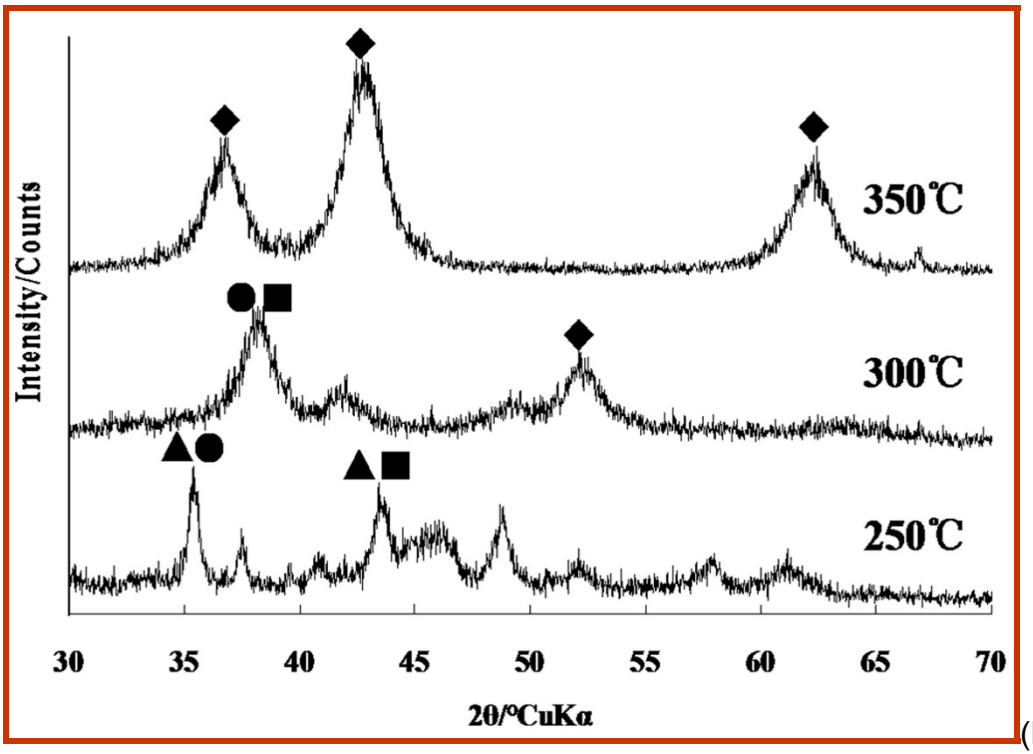

Fig. 3.1 (a) High temperature XRD pattern analysis of Ni powder formed process; (b) High temperature XRD pattern analysis of Ni powder formed process (250°C, 300°C and 350°C).

Table 3.1 The particle size of the crystalline phase in preparing Ni powder process by High temperature XRD				
Temperature [°C]	$Mg_3O(CO_3)_2$ [nm]	$NiCO_3$ [nm]	$MgNiO_2$ [nm]	Ni [nm]
200	16.338	12.874		
250	15.007	10.68	15.246	
300		8.359	17.230	13.673
350			20.336	19.881
400			23.496	24.316
600			64.335	49.904
800			53.356	39.886
1000			34.812	48.516

3.2.2 Preparation and refinement of Ni powder by electric furnace

The Ammonium oxalate [$(NH_4)_2C_2O_4 \cdot H_2O$] of 25g, 1.4mol/L $NiCl_2 \cdot 6H_2O$ and $MgCl_2 \cdot 4H_2O$ of a amount of 77g were used as starting materials for preparing Ni/MgO. In the present study, it was confirmed that the solute of the aqueous solution was completely dissolved at 50°C; aqueous solution mixed was stirred at rate of 300rpm for 2 hour. The next, aqueous solution stirred was filtered with the funnel and filter paper under the molar ratio of Mg: Ni (2:1) was prepared. Then the precursor was sintered at 10°C /min to 700°C by using electronic balance. $(NH_4)_2C_2O_4 \cdot H_2O$ was decomposed to CO and CO_2 under high temperature, in which CO can play a reductive role, the purpose of this experiment is to promote the generation of simple substance by chemical oxidation-reduction reaction, so that achieving the roles of high purity and

refined grain. According to a certain proportion promoted particles sufficient reaction. $NiCl_2 \cdot 6H_2O$ was reverted by $C_2O_4^{2-}$. In the powder prepared process, a small amount of $MgCl_2 \cdot 4H_2O$ was added because the oxidizing from Mg is much stronger than that of Ni. It made Ni be further reverted because Mg is active metal. The result consistent with high temperature X-ray diffraction result and the suitable temperature was 800°C. According to results from two kinds of equipments, it was confirmed that sufficient reaction was achieved by electric furnace. After that the black Ni/MgO sintered was formed. H_3BO_3 was added into Ni/MgO powder and was sintered under 800°C，900°C and 1000°C, respectively. The sintering process was analyzed by TG-DTA determine. Reaction equation of Ni powder as follows:

$$MgCl_2.6H_2O+(NH_4)_2C_2O_4 \rightarrow MgC_2O_4.mH_2O \downarrow +2NH_4Cl+(6+1-m)H_2O \quad (1)$$

$$MgC_2O_4.mH_2O \rightarrow MgO+CO\uparrow+CO_2\uparrow+mH_2O \quad (2)$$

$$NiCl_2.6H_2O + (NH_4)_2C_2O_4 \rightarrow NiC_2O_4.mH_2O \downarrow +2NH_4Cl+(6+1-m)H_2O \quad (3)$$

$$NiC_2O_4.mH_2O \rightarrow NiO+CO\uparrow+CO_2\uparrow+mH_2O \quad (4)$$

$$NiO+CO \rightarrow Ni+CO_2 \quad (5)$$

$$2MgO+B_2O_3 \rightarrow Mg_2B_2O_5 \quad (6)$$

Fig. 3.2 (a) shows the TG-DTA result for mixed powder. The curves show that the thermal development could be divided into three sections. The three sections of crystal water, CO and CO_2 release at 220°C and 400 °C; the endothermic peaks of MgO and NiO at 420°C are caused by thermal decomposition of $C_2O_4^{2-}$. The curve of weight remained stable was above 700°C.

Figure 3.2（b）shows crystal water lost at 100°C to generate B_2O_3. B_2O_3 and a small amount of elemental substance Mg react under 700°C to emerge exothermic peak of $Mg_2B_2O_5$. The curve has not changes above 800°C in the

figure. According to TG-DTA curves, the heat-treatment process was divided into three steps which included the volatilization of water and organic compounds.

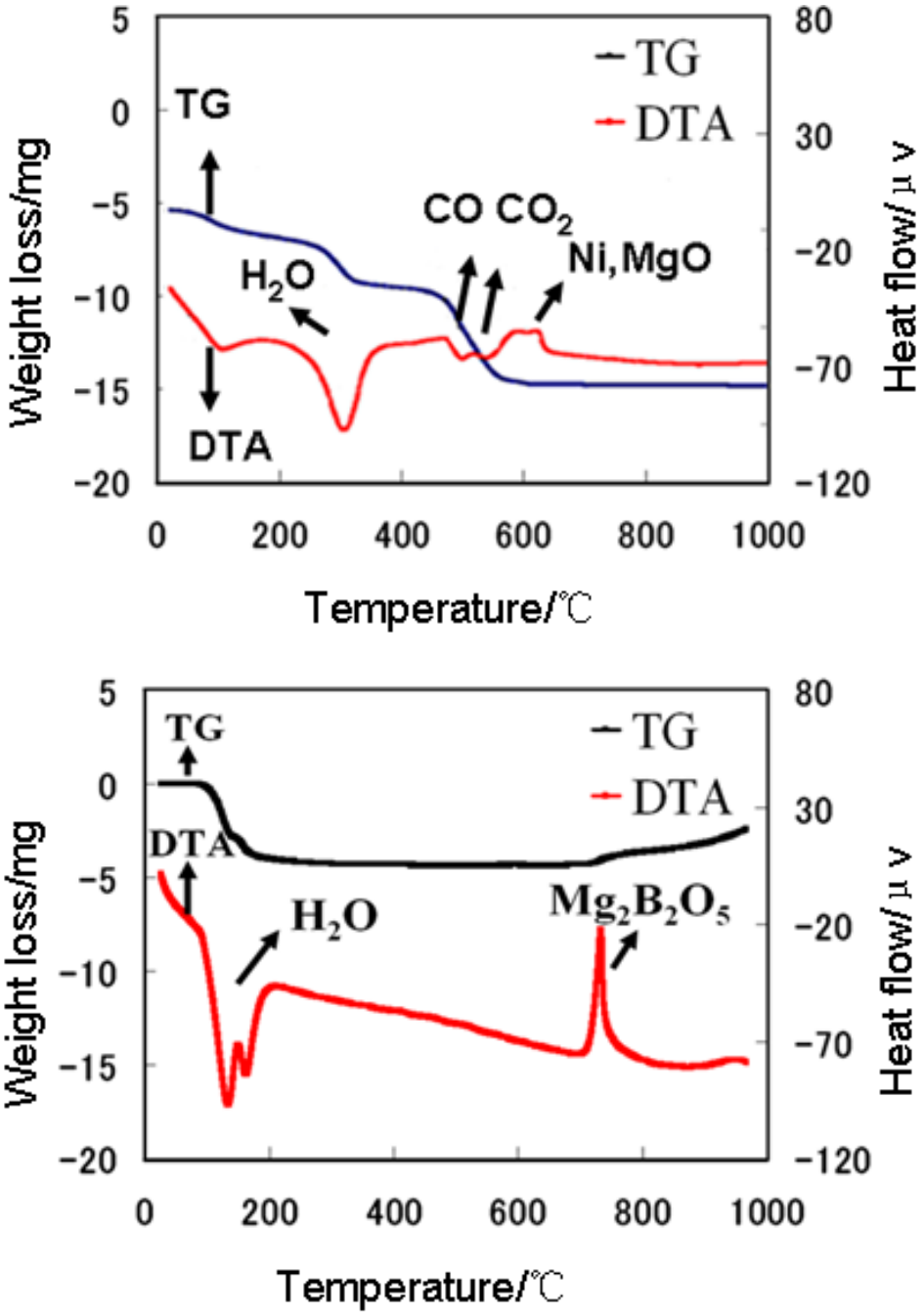

Fig. 3.2 TG-DTA image of thermal analysis (a) Mg-Ni powder sintered at 800°C (b) Mg-Ni added B powder sintered at 1000°C.

3.3 Experimental results and discussion

3.3.1 XRD pattern of generated phases

Fig. 3.3(a) shows MgC_2O_4 and NiC_2O_4 generated for the determination of the mixed powder. The result showed that the strength of the peaks was weak because the size of crystal grain prepared by co-precipitation elemental composition is complicated, so that the noise become more obviously and lead the strength to decline. In the detected process, a small amount of the impurities is also the mainly reason that affected the strength of the peaks. As shown in Fig. 3.3(b), With the conduct of the thermal decomposition, the oxalate are decomposed into CO and CO_2, and which make NiO be reverted Ni in sintering process of the powder under 700°C. The crystalline structure had not been changed after adding H_3BO_3 because the amount of adding H_3BO_3 was less cause the peak of $Mg_2B_2O_5$ was not detected out by X-ray scanning from 20℃ to 90°C. Elemental substance Ni is as the main characteristic peaks in the processes of the second sintering under 800°C, 900°C and 1000°C. It is result that the purity of Ni powder was relatively high and a small amount of impurities transformed into the gas from the electric furnace, such as Cl_2 produced with the heating temperature. According to above statement, experimental temperature of formed simple substance Ni powder is 700°C. The refined degree of the powder was further confirmed by SEM microstructure and EPMA distributed analysis.

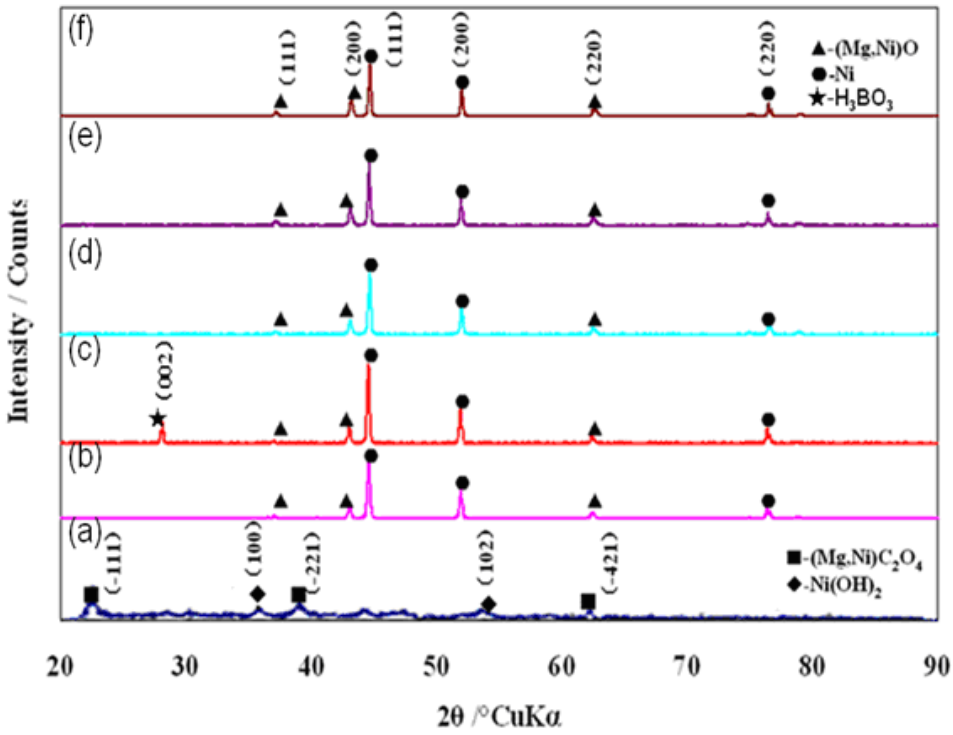

Fig. 3.3 XRD patterns analysis (a)Compound sintered at 700°C; (b) Ni/MgO powder; (c) powder added H_3BO_3 before sintering; (d) Ni/MgO added H_3BO_3 sintered at 800°C; (e) Ni/MgO added H_3BO_3 sintered 900°C; (f) Ni/MgO added H_3BO_3 sintered at 1000°C.

3.3.2 SEM microstructure analysis

The conclusions can be drawn according to SEM image. As shown in Fig. 3.4(a), the crystal grain is coarse and clear overlay phenomenon was observed. The larger sheet structure was exhibited. Figure 3.4(b) shows crystal grain is refined obviously in the process of the primary sintered because the reaction of oxide and CO. The size of the crystal grain became less than 2μm; it played a catalysis role for hydrogen absorption and desorption. As shown in Fig. 3.4(c), the crystal grain size of the mixed powder grinded after adding H_3BO_3 had not significant change. However, with the powder of H_3BO_3 added secondary sintering 800°C, grain is more refinement and uniform, and the size is about 1μm. The result shows that the most suitable temperature of secondary sintered is at 800°C in Figure 3.4(d).

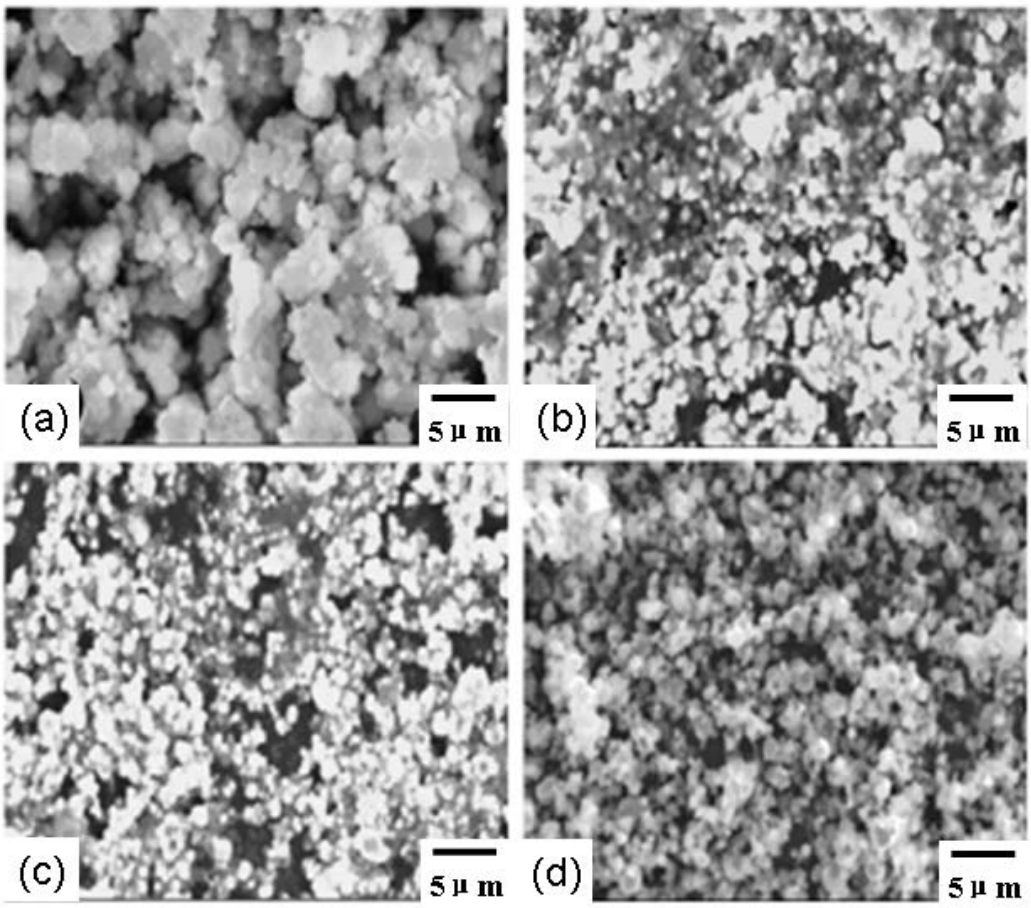

Fig. 3.4 SEM microstructure image (a)Mg-Ni precursor powder；(b) Mg-Ni powder sintered at 700°C；(c) Mg-Ni added B powder；(d) Mg-Ni added B sintered at 800°C.

3.3.3 TEM analyses of based experiment

In order to further confirm crystal orientation of Ni, the study made the calibration of the diffraction pattern basis on the original detection evaluation and calculated diffraction crystal face of Ni according to the lattice spacing. It is showed in Figure 3.5 that elemental substance Ni is used as the main characteristic peaks in the process of the second sintering and a small amount of MgO was proved. It is showed that the polycrystalline structure and the main crystalline phase is Ni in the range. Ni clusters formed regional is indicated in figure. The diffraction region is Ni (111) by phase identification and consistent with the XRD results. The result is that Ni element was prepared effectively.

The element and distribution in the selected region can be observed by EPMA analysis. In the process, elemental distribution status can be analyzed out clearly. The existing of element and the refinement degree were analyzed by the elemental uniformity in surface analysis and line analysis.

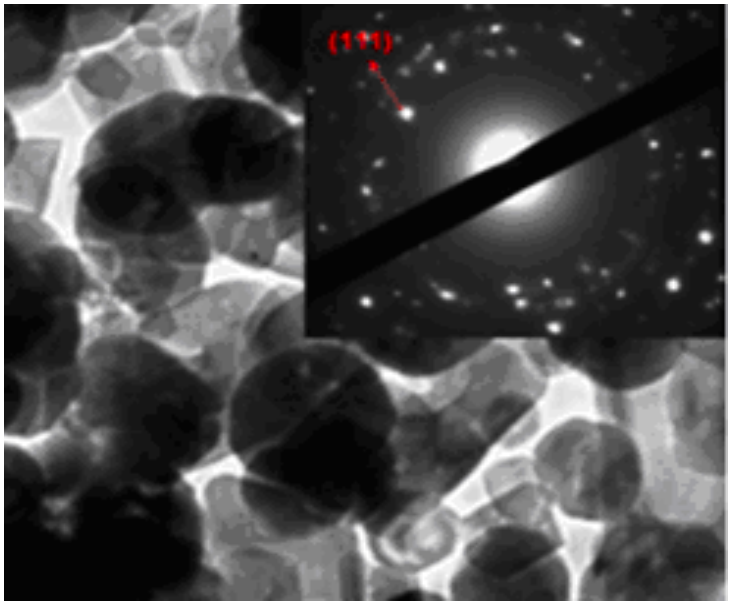

Fig. 3.5 TEM image of precursor power.

3.3.4 EPMA analysis of elemental distribution

As shown in Fig. 3.6(a), Mg, Ni, C and O elements are generated in the process which the precursor was prepared, it is indicated that the main resultant are MgC_2O_4 and NiC_2O_4. The line distributions of MgC_2O_4 and NiC_2O_4 are uniform, at the same position, Mg, Ni, C and O peaks simultaneously occur. Figure 3.6(b) shows that elements Mg and O generated in the sintered temperature 700°C, the main resultant are MgO and gain is grow up and is coarse, and the distribution of Ni is more uniform and the grain is more refinement. Elements Mg, Ni and O are generated in the preparation process of basis sample, elements Mg and O generated in the sintered process at 700°C, the main resultants are MgO and NiO. In accordance to the distribution of the Ni elements, the distribution of Ni element is uniform and the grain is refinement, which are analyzed to generate elemental substance Ni

powder. Complementary elements distributed of Mg and Ni elements are in the same position; the distribution of the part of element O and Mg were consistent. It is indicated that NiO was restored to simple substance Ni in the sintered process, so that MgO and Ni were observed. Figure 3.6(c) shows that Mg, B, and O elements are distributed for the grinding powder after adding H_3BO_3 and powder was refined obviously by SEM observation. The results show that the main resultant is MgO and grains grow up to refine. In accordance to the distribution of Ni, the distribution of Ni is more uniform and the grain is more refinement, and which are analyzed to generate elemental substance Ni. As secondary sintering carrying out, Mg, B and O elements are distributed. MgO and Ni particle is further uniform and refinement in Figure 3.6(d) obviously.

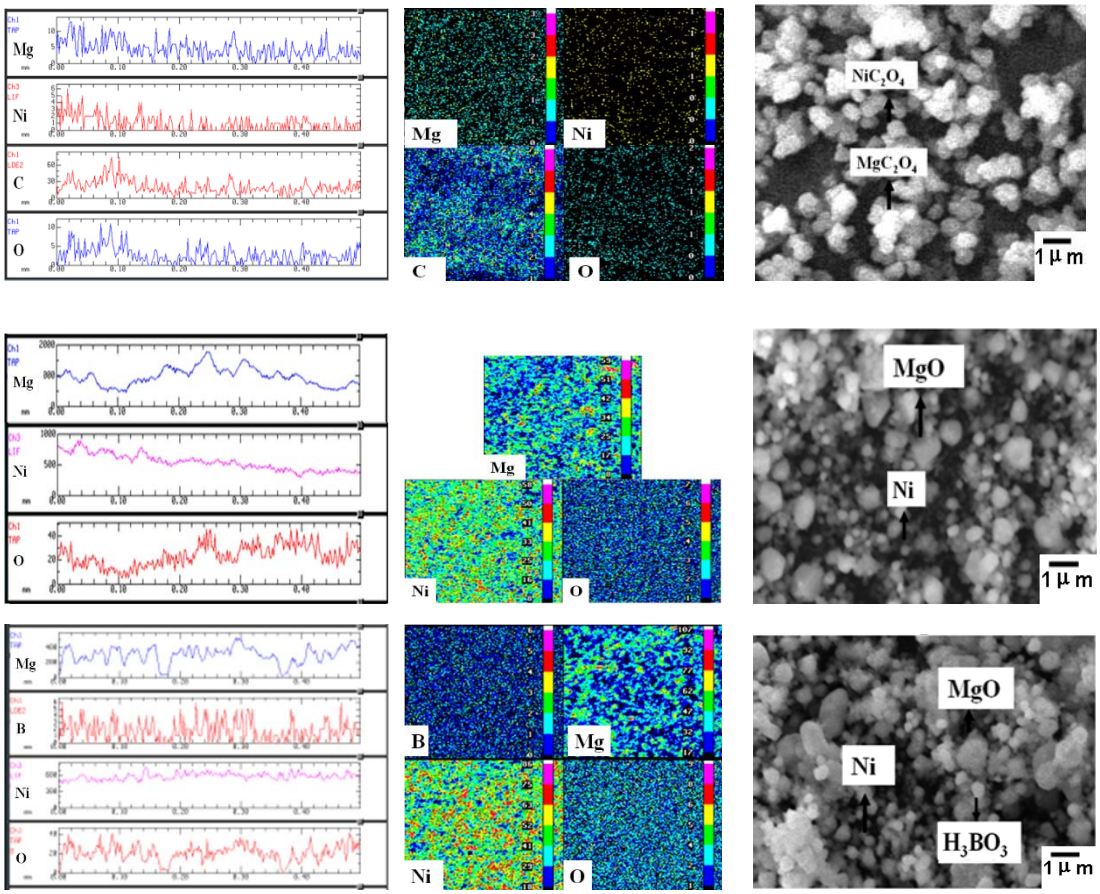

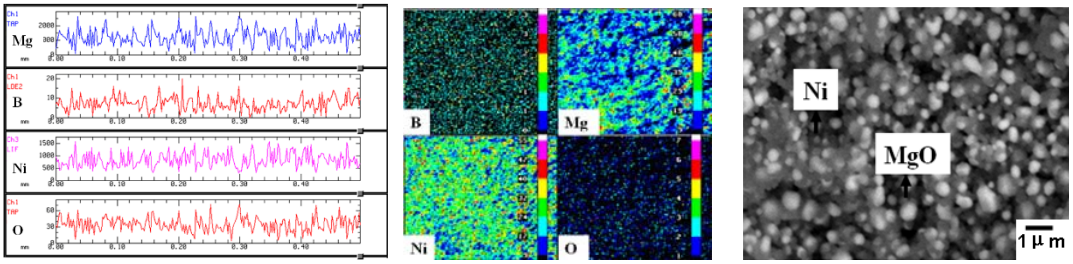

Fig .3.6 EPMA analysis image (a) Ni(MgO) precursor powder; (b) Ni(MgO) powder sintered at 700°C (c) Ni(MgO) added H_3BO_3 powder; (d) The powder sintered at 800°C.

3.3.5 XPS patterns analysis of the extent depth distribution

Full spectrum indicated the existence elements in the sample, what compounds were elemental compositions. The extend depth distribution analyzed as the change of sputtering to depth, observed elemental distribution from the surface of the sample to inside from inside and confirmed whether generated new compounds or alloys.

Figure 3.7(a) shows that B1s, Mg_{KLL}, O1s and Ni_{2p} peaks were observed by the analysis of full spectrum. Figure 3.7(b) shows that B_2O_3 is main characteristic peak. The sputtering depth distribution as shown in Figure 3.7(c), Mg_{KLL} and Mg_{2p} peaks were identified to MgO, and Mg2p peaks increased significantly as the increase of sputtering times. Figure 3.7(d) shows that Ni powder is produced at the time of generating NiO by the $Ni2p_{3/2}$ and $Ni2p_{1/2}$ peaks. According to sputtering depth distribution, $Ni2p_{3/2}$ $Ni2p_{1/2}$ peaks increased significantly. The amount of Ni is far more than NiO and is distributed in the internal. As shown in Fig. 3.7(e), 1s binding energy of metal oxides from 528eV to 531eV, O1s peaks shift to the right with the changes of sputter depth. It is result that Ni powders was prepared and get refinement effect, but the refined degree was tiny and did not generate simple substance and alloy phase can absorb hydrogen.

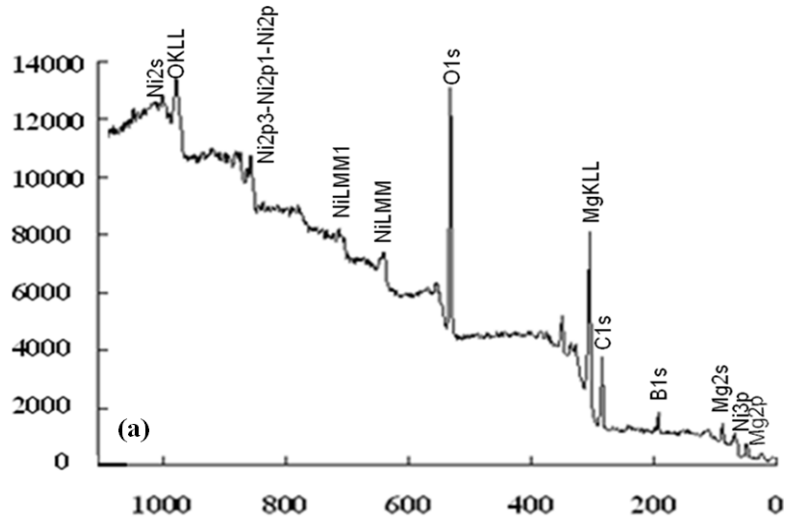
Ni2s
OKLL
Ni2p3-Ni2p1-Ni2p
NiLMM1
NiLMM
O1s
MgKLL
C1s
B1s
Mg2s
Ni3p
Mg2p
(a)

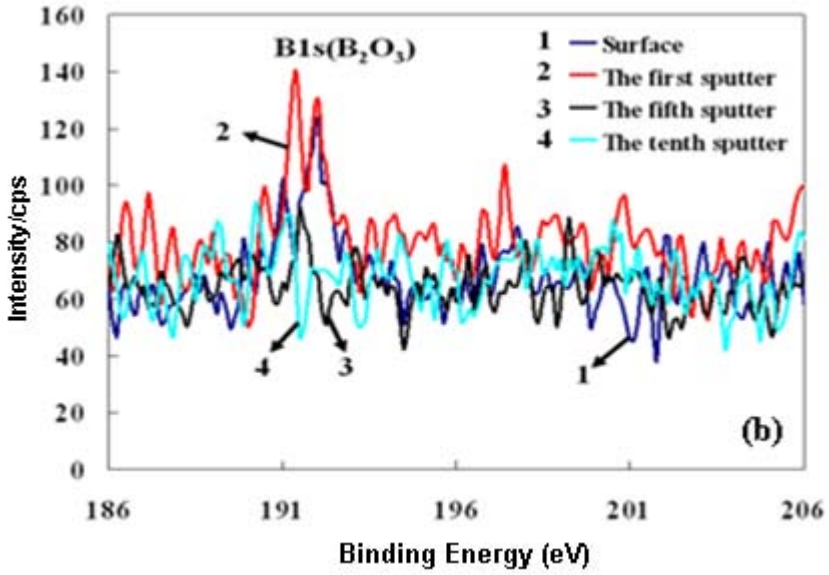
B1s(B_2O_3)
1 Surface
2 The first sputter
3 The fifth sputter
4 The tenth sputter
Intensity/cps
Binding Energy (eV)
(b)

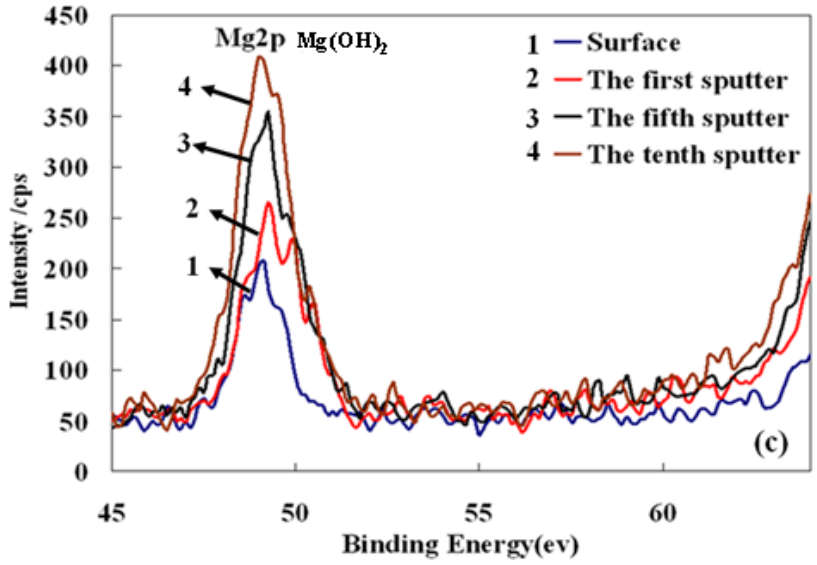
Mg2p Mg(OH)$_2$
1 Surface
2 The first sputter
3 The fifth sputter
4 The tenth sputter
Intensity /cps
Binding Energy(ev)
(c)

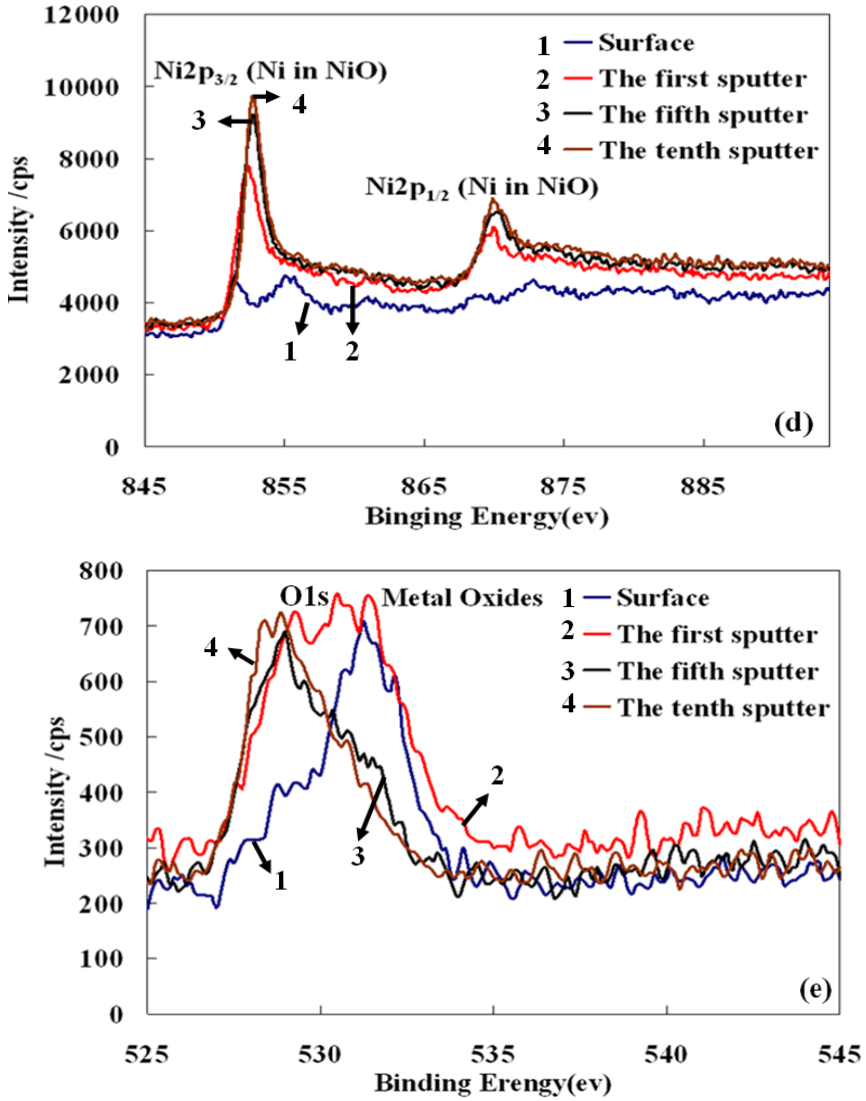

Fig . 3.7 XPS analysis: (a) Full spectrum of 800°C; (b) B1s depth distribution of MgO/Ni added B sintered at 800°C; (c) Mg2p depth distribution of MgO/Ni added B sintered at 800°C; (d) Ni2p depth distribution of Mg-Ni added B sintered at 800°C; (e) O1s depth distribution of Mg-Ni added B sintered at 800°C.

3.4 Concluding Remark

The purpose of this experiment is to prepare the precursor powder to form the simple substance or the alloy phase of hydrogen absorption and desorption by add other trace elemental or alloy hydrogen absorption and desorption phase.

The results show that oxalate was thermal decomposed completely to CO and CO_2 in the sintering process at 700°C, and a part of NiO was reverted directly to Ni because the reducibility of Ni is stronger than that of Mg. With the powder of H_3BO_3 added was the second sintered at 800°C, grain is more refinement and uniform, and the size is about 1μm. The most suitable temperature of the second sintered is under 800°C. The adding of H_3BO_3 promoted crystal grain refining. By the setting for temperature and the controlling for the sintered rate, simple substance Ni powder formed. According to above conclusions, Ni as catalytic phase can promote absorbing and desorbing hydrogen, but the adding H_3BO_3 did not produce a large effect on the crystal structure; there was only the granularity and refinement effect; there are not any promoting roles for the formation of the absorbed hydrogen phase. The next step of the experiment for the problems, other elements will be selected to form new alloy phases in sintering process by a new type sintered method, so that achieve the generation of a absorbed hydrogen phase.

References

[1] J Kim, J Ahn, et al, In situ transmission electron microscopy study on microstructural changes in NbF5-doped MgH_2 during dehydrogenation. Scr Mater 2010; 62: 701.

[2] X Yu, Y Guo, Z Yang, Synthesis of catalyzed magnesium hydride with low absorption/desorption temperature. Scr Mater 2009; 61: 469.

[3] C Milanese, A Girella, G Bruni, et al, Mg/Ni/Cu mixtures for hydrogen storage: a kinetic study. Intermetallics 2010; 18: 203-11.

[4] R Gremaud R, C Broedersz, A Borgschulte, et al, Hydrogenography of MgyNi1-yHx gradient thin films: interplay between the thermodynamics and kinetics of hydrogenation. Acta Mater 2010; 58: 658.

[5] C Aymonier, A Denis, Y Roig, M Iturbe, E Sellier, S Marre S, et al, Supported metal NPs on magnesium using SCFs for hydrogen storage: interface and interphase characterization. J Supercrit Fluid 2010; 53: 102.

[6] S Jin, J Shim, J Ahn, Y Cho, Improvement in hydrogen sorption kinetics of MgH2 with Nb hydride catalyst. Acta Mater 2007; 55: 5073.

[7] M Dornheim, S Doppiu, G Barkhordarian, U Boesenberg, T Klassen, O Gutfleisch, et al, Hydrogen storage in magnesium-based hydrides and hydride composites. Scr Mater 2007; 56: 841.

[8] M Song, S Kwon, D Mumm, S Hong, Development of Mg-oxide-Ni hydrogen-storage alloys by reactive mechanical grinding. Int J Hydrogen Energy 2007; 32: 3921.

[9] C Lin, C Wang, P Lee, H Lin, K Lin, The effect of Ti additions on the hydrogen absorption properties of mechanically alloyed Mg_2Ni powders. Mater Sci Eng A 2007; 449:1102.

[10] A Ebrahimi-Purkani, S Kashani-Bozorg, Nanocrystalline Mg_2Ni-based powders produced by high-energy ball milling and subsequent annealing. J Alloy Compd 2008; 456: 211.

[11] M Jurczyk, L Smardz, I Okonska, E Jankowska, M Nowak, K Smardz, Nanoscale Mg-based materials for hydrogen storage. Int J Hydrogen Energy 2008; 33: 374.

[12] F Gennari, M Esquivel, Structural characterization and hydrogen sorption properties of nanocrystalline Mg_2Ni. J Alloy Compd 2008; 459: 425.

[13] H Wang, S Chyou, S Wang, M Yang, C Hsu, H Tien, et al, Amorphous phase formation in intermetallic Mg_2Ni alloy synthesized by ethanol wet milling. J Alloy Compd 2009; 479: 330.

[14] S Ordonez, D Serafini, P Rojas, C Aguilar, M Santander, Thermal stability of amorphous $Mg_{50}Ni_{50}$ alloy produced by mechanical alloying. J Non-Cryst Solids 2010; 356:120.

[15] V Skripnyuk, E Buchman, E Rabkin, Y Estrin, M Popov, S Jorgensen, The effect of ball milling and equal channel angular pressing on the hydrogen absorption/desorption properties of Mg4.95 wt% Zn0.71 wt% Zr (ZK60) alloy. Acta

Mater 2004; 52: 405.

[16] V Skripnyuk, E Rabkin, Y Estrin, R Lapovok, Improving hydrogen storage properties of magnesium based alloys by equal channel angular pressing. Int J Hydrogen Energy 2009; 34:6320.

[17] V Skripnyuk, E Buchman, E Rabkin, Y Estrin, M Popov, S Jorgensen, The effect of equal channel angular pressing on hydrogen storage properties of a eutectic MgNi alloy. J Alloy Compd 2007; 436: 99.

[18] Y Kusadome, K Ikeda, Y Nakamori, S Orimo, Z Horita, Hydrogen storage capability of MgNi2 processed by high pressure torsion. Scr Mater 2007; 57: 751e3.

[19] K Jeon, A Theodore, C Wu, Enhanced hydrogen absorption kinetics for hydrogen storage using Mg flakes as compared to conventional spherical powders. J Power Sources 2008; 183: 693.

[20] J Qu, Y Wang, L Xie, J Zheng, Y Liu, X Li, Hydrogen absorption edesorption, optical transmission properties and annealing effect of Mg thin

films prepared by magnetron sputtering. Int J Hydrogen Energy 2009; 34: 1910.

[21] S Barcelo, M Rogers, C Grigoropoulos, S Mao, Hydrogen storage property of sandwiched magnesium hydride nanoparticle thin film. Int J Hydrogen Energy 2010; 35: 7232.

[22] M Tanniru, H Tien, F Ebrahimi, Study of the dehydrogenation behavior of magnesium hydride. Scr Mater 2010; 63: 58.

[23] A Neumaier, On the compa rison of H-matr ices with M -matrices [J] . Linear Alg ebr a Appl, 1986, 83: 135 - 141.

[24] A Berman, R Plemmons. Nonnegative matrices in the mathematical sciences [M] . New Yor k: Academic Press, 1979.

Chapter 4 Electrochemical properties/Actual capacity evaluation of Mg/Ni(MgO) and Mg/Ni(MgO)/Ti composites

4.1 Introduction

In the past few years, hydrogen storage, which had been widely used as negative electrode materials, has attracted much attention due to its several advantages, such as the high energy density, the durability against overcharge and over discharge [1, 2]. Recently, however, the rechargeable materials are encountering serious competition from Li-ion cells and other advanced cells with higher energy density. So it is urgent to develop some new-type electrode materials with higher activation capacity and lower cost in order to enhance the competition ability [3–5]. Fuel cell development is rapid. A metal hydride electrode was used primarily, for which the obvious reason was to replace expensive materials. Much of the research effort is still intended to improve the properties of this electrode material, such as corrosion resistance, rate-capability and ability hydrogen storage capacity [6, 7]. Yet, the gravimetric capacity is not expected to rise significantly because the intrinsic capacity is not much higher. It is known that Ti based alloys with high dynamic performance and excellent activation have been considered as new candidates for hydrogen storage applications. In the present work, it is the research purposes that electrochemical performance and absorption-desorption hydrogen performance were synthesized to prepare the electrode material of the absorption-desorption hydrogen [8].

The findings of our research work are that the substitution of Ti significantly improves the absorbed and desorbed kinetics and electrochemical performance [9]. Therefore, it is very desirable to investigate the influence on the hydrogen storage characteristics and electrochemical performance of Mg/Ni(MgO)/Ti prepared with a new sintering method.

The study basis on homemade Ni powder did the further research for the preparation of hydrogen storage materials. By a new type sintered method to study performance differences of hydrogen storage. The purpose is to generate absorbed hydrogen phase and catalytic phase can improve dynamics performance in the sintering process. The selection of element is crucial. It is showed that Ti alloy has good heat strength, low temperature toughness and fracture toughness; therefore, it had been widely applied in various fields, such as aircraft engine parts and rockets, missiles structure. Ti is also used as fuel, oxidizer tank and pressure vessel. Ti metal has excellent physical and chemical properties, good biocompatibility, low specific gravity and resistance corrosion [10–12]. The studies had shown that related the results had got corresponding development, but general method is ball milling method due to can effective increase surface area. There are some malpractices through application of the ball milling method [13]. The powder need to hold under a vacuum status and must use continuous milling to achieve hydrogen absorption and desorption cycles. In addition, the prepared powder by ball milling is not easy to save, no fixed shape to storage. Applications in various fields are limited [14].

The study broken traditional prepared method instead of cover method of a powder and an alloy to prepare hydrogen absorbing phase Mg_2Ni and catalytic phase NiTi that have excellent effect for hydrogen absorption and desorption, not only effectively increased the surface area of the sample, but also achieved the diffusion the powder to the alloy. Based on the formation of alloy, a part of simple substance was remained, so that the powder as medium make H atoms diffuse to the inner of alloy, dynamics performance of hydrogen absorption and desorption was improved.

The research mainly focused on two kinds of methods, one of methods was Ni powder directly was covered on pure Mg ingot; another method is simultaneously cover Ni powder and Ti powder on pure Mg ingot to conduct compare about the ability of hydrogen absorption and desorption for selecting

the most suitable test material between the both materials. The ability of hydrogen absorption and desorption was confirmed by electrochemical and the maximum voltage. In this study, adding a new element achieved the refinement purpose by repeatedly sintering; not only reach the refinement of powder, but also remain simple substance Mg based on generating new phase, which effectively offset the formed malpractices in sintering process.

4.2 Experimental methods by electronic balance

According to co-precipitation method prepared Ni(MgO) powder and adding Ti powder to form the new alloy phases made the sintered body had the specially layer structure. Through two kinds of methods diffused the powder to the surface and internal of pure Mg ingot. Ni powder directly covered on the surface of pure Mg to conduct sintering cause the formation of Mg_2Ni by using the first method; the second using method was conducted by Ni powder and Ti powder uniformly mixed according to certain percentage, the powders after mixing cover to pure Mg ingot, so that Mg_2Ni generated while resulting in catalytic phase NiTi. For the both materials, the ability of hydrogen absorption and desorption was detected and confirmed the more viable experimental direction to conduct a further study.

4.2.1 Preparation of Mg/Ni (MgO) composite by electric furnace

The basis sample powder Ni was sintered at 10°C /min to 700°C by using electronic balance. Ni/MgO sintered powder was added into under the molar ratio of Ni(MgO)：Mg =β：γ and was grinded for 2 hours and lay cover on the pure Mg ingot, the powder were permeated into pure Mg ingot in the form of doping was sintered under10°C /min to 700°C.

4.2.2 Preparation of Mg/Ni(MgO)/Ti composite by electric furnace

Ti was added into the sintering Ni(MgO) powder under the molar ratio of Ni(MgO)：Ti =β：γ and was grinded for 2 hours. The second, Ni(MgO) and Ti after grinding lay cover on the pure Mg ingot, the powder and the pure Mg ingot coverd were permeated into pure Mg ingot in the form of doping under the molar ratio of Mg: Ni: Ti（α:β:γ）and was sintered under10°C /min to 750°C.

4.3 Results and Discussions

4.3.1 Characterization of Mg/Ni(MgO) composite

Figure 4.1 shows that the composite continuous overlay each other during the sintering process, small particles of Ni(MgO) sintered powder was fully filled into the pure Mg ingot and the resulting alloy lattice has had defects and phase interface is increased constantly. It is indicated that Ni(MgO) permeated decreases the grain size below approximately 1.0 μm. Powder particles are relatively dense and the large particles still existed, Ni powder could permeate into the internal of Mg to form the depth diffusion of Mg_2Ni. It induced the formation of diffused layers and made the structure in the diffused layers loose. It helps to improve electrochemical performance. Uniform pitting is detected, so that promotes a uniform electrochemical reaction including the fact that voltage increases and the reaction rate becomes larger. It is the result that the effect on discharge is obvious.

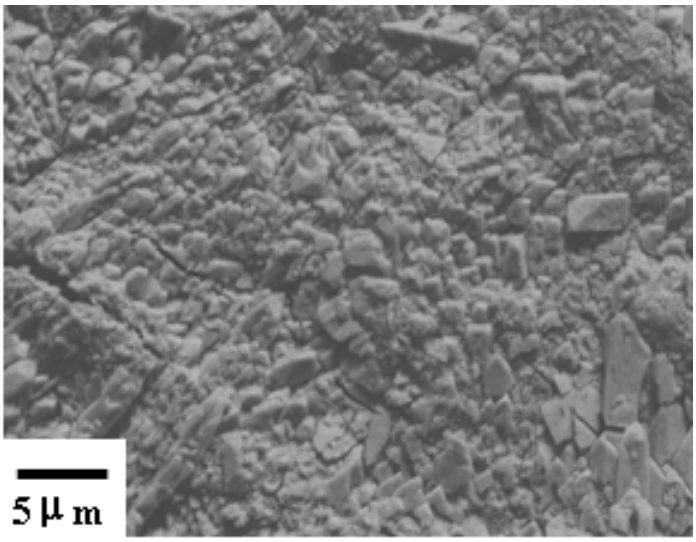

(a)

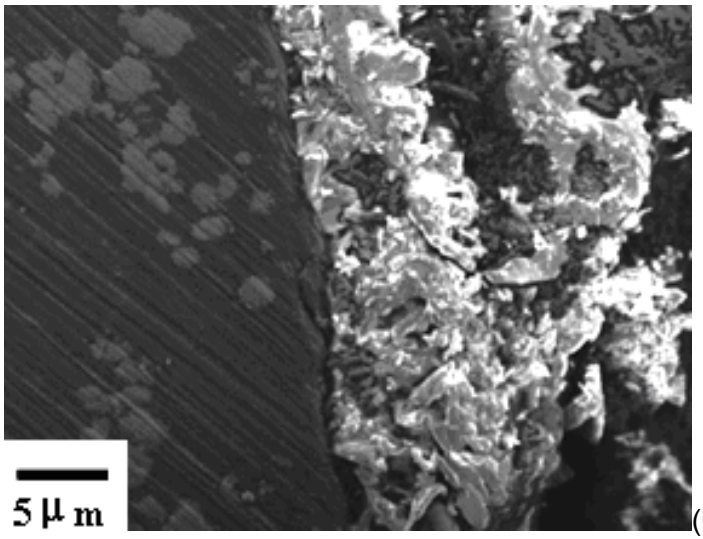

(b)

Fig.4.1 SEM section image (a) Mg/Ni(MgO) surface after corrosion; (b) Mg/Ni(MgO) section after corrosion.

As shown in Fig. 4.2, oxygen still exist in the composite, a small amount of MgO had been formed because prepared mixed powder process and oxidation in the second sintering lead to form a small amount of NiO again. According to distribution of the transition layer, amount of Mg_2Ni generated, but the structural features were not obvious. This phenomenon was caused is because some elemental Ni is oxidized and formed NiO, so that it made the reaction with Mg was not sufficient. The result indicated that the structure of the composite mainly produced as a simple substance. Mg, Ni and O elements are generated, it is showed that simple substance Mg and Ni elements are

stratified obviously in sections after the sintered process at 750°C, the main resultant are Mg and Ni and a small amount of MgO powder.

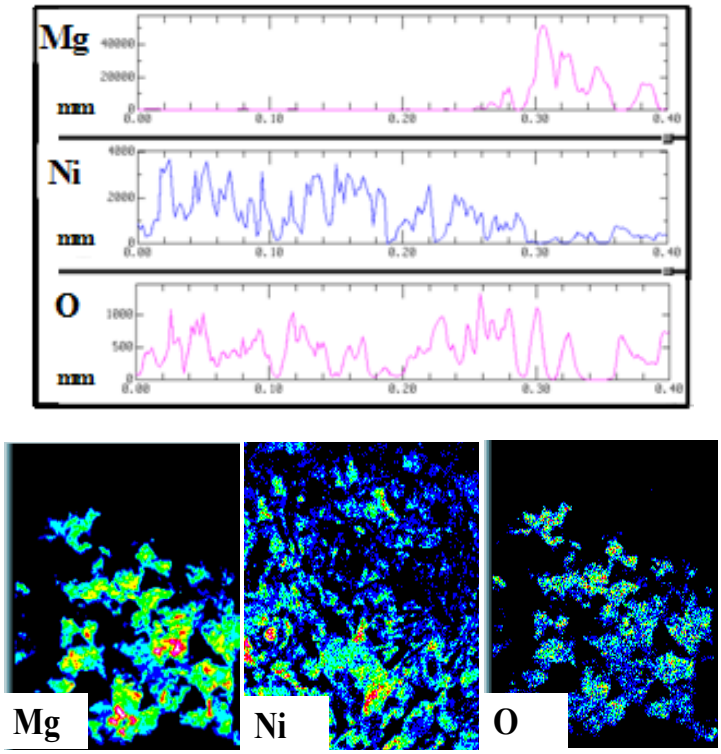

Fig. 4.2 EPMA section analysis of Mg/Ni(MgO).

As shown in Fig. 4.3, the results show that Ni was added in order to decrease the particle size of the crystallites. The composite consists of a multiple phases. The main phases are Mg, Ni and Mg_2Ni phases. The diffraction peaks of Mg and Mg_2Ni has a slight offset to low diffraction direction, it is indicated that the cell volume is increases significantly. The diffraction peaks of Ni has a slight offset to high diffraction direction, it is indicated that the cell volume is reduced significantly. Based on the above conclusions, the effect of doping was obviously.Mg_2Ni alloy phase were formed and the strength was high. Simple substance Ni and Mg as mainly phase existed on surface of the composite.

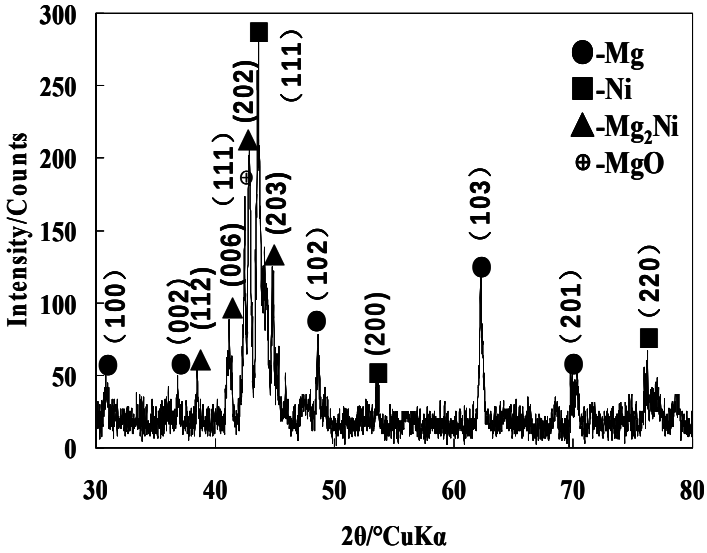

Fig. 4.3 XRD pattern of Mg/Ni(MgO).

The electron diffraction pattern reflects the crystal lattice spacing and reciprocal lattice configuration, relationship of diffraction pattern and the crystal structure was obtained by calculating. The specific standard process as shown in Figure 4.4, according to the formula, dhkl=Lλ/R, (Interplanar spacing d represent crystals characteristic; λ is electronic wavelength that represent the incident beam characteristics; θ is grazing angle that represent geometric relationship incident beam and crystal planes). Mg_2Ni phase generated in internal of composite. Mg_2Ni (P_6222) is hexagonal structure and the crystal grains distributed on interface, so that improve the effect of hydrogen absorption.

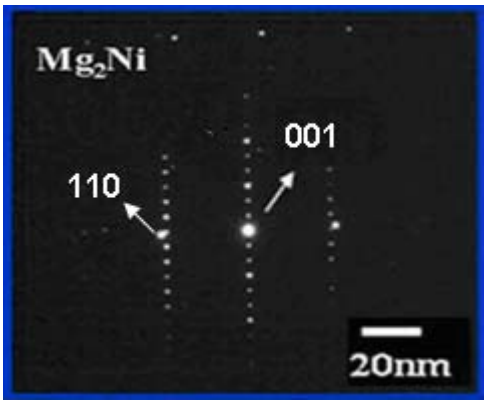

Fig. 4.4 TEM diffraction pattern and element distribution of Mg_2Ni.

As shown in Fig. 4.5, when the powder diffused into the inner of the alloy, the prepared method made the composite form multilayer diffusion layer, and the diffused layer had coherence; the powder diffused to upper and lower of the layers, so that effectively increase the surface of the powder in pure Mg ingot and achieved continuity of layer and layer.

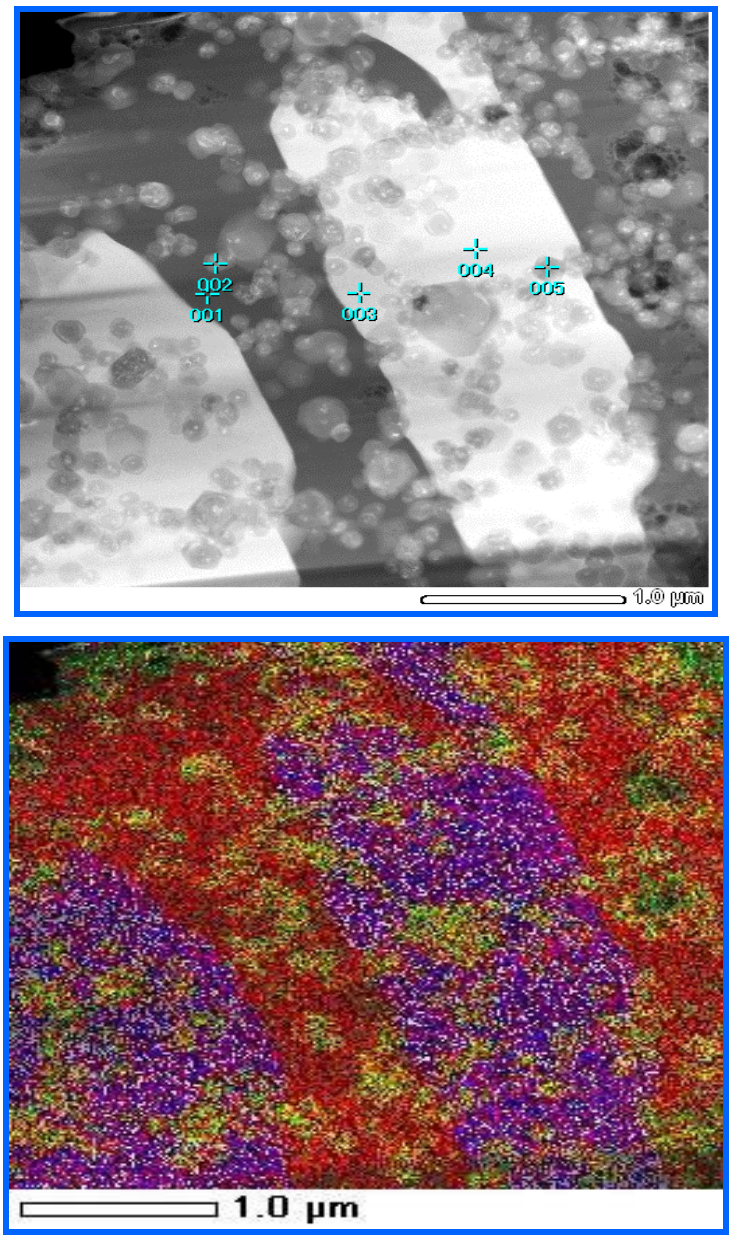

Fig. 4.5 SEM image and element distribution of Mg_2Ni.

As shown in Fig. 4.6, powder Ni diffused into the inner of pure Mg, the composite was prepared in form of multilayer diffusion layer, and the diffused layer had coherence; the powder could diffuse to upper and lower layers, so that effectively increase the surface of the powder in pure Mg ingot and

achieved continuity of layer and layer.

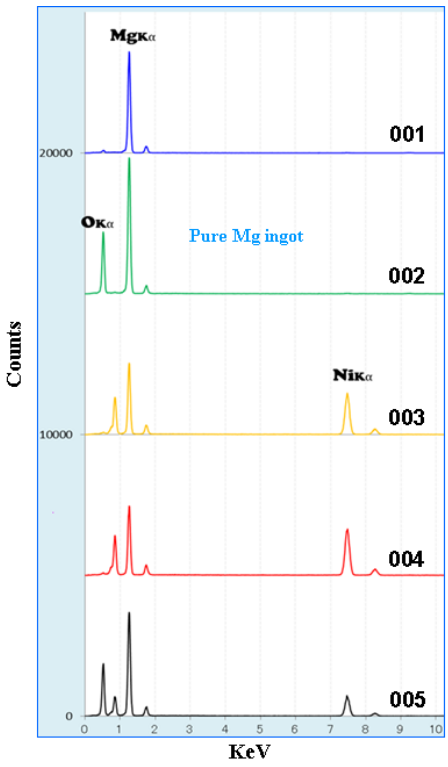

Fig. 4.6 EDS element distribution of 1st-5th hierarchical structure.

4.3.2 Characterization of Mg/Ni(MgO)/Ti composite

Mutual melted reaction had produced between the powder and pure Mg ingot. The powder in form of grains wrapped on a large particle Mg. it is indicated that Mg_2Ni/NiTi/Mg formed and the composite was loose and was foam status. The mold effect was relatively good because the existing of Ni. Ti trace adding on certain degree improved the toughness. Ni and Ti complement each other to form new type sintered body has specially structure.

The SEM images of Mg/Ni(MgO)/Ti are illustrated in Figure 4.7. Ni(MgO) and Ti powder permeated evenly fused into pure Mg ingot causes the refinement of grains. It is quite evident that the sintered body exhibits a typical dendritic structure. It is showed that pitting is more uniform and the structure is much richer obviously, and various sized particles exist in the range of less than 1μm. The large sized particles are still present in the composite. Surface

roughness significantly changed. Uniform apertures pitting is detected and the apertures pitting were small and distributed approximately uniformly. The small holes could be corrosion-proof because the structural type could block corrosive media from contacting the substrate, so that it promotes a uniform electrochemical reaction including the voltage increases and the reaction rate becomes larger. It is indicated that electrochemical properties was improved at room temperature.

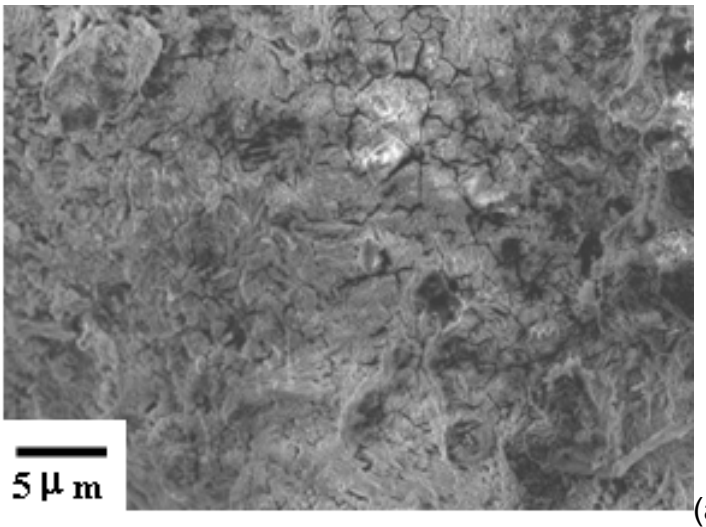

(a)

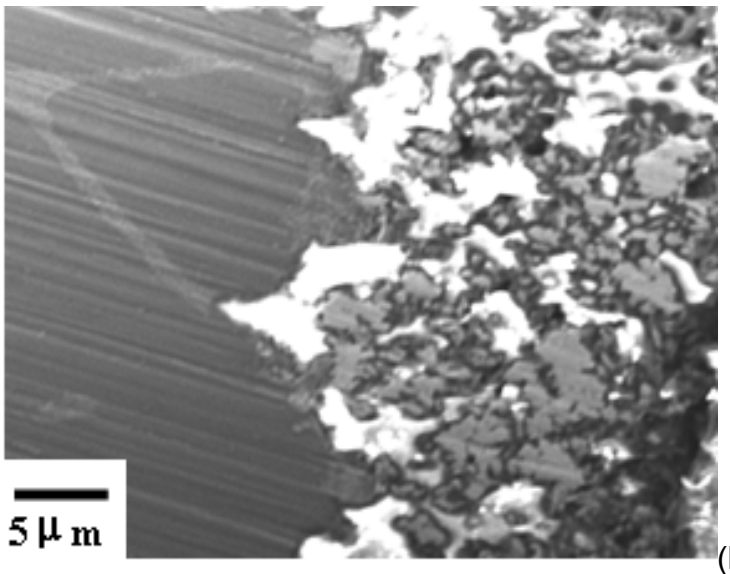

(b)

Fig. 4.7(a) SEM section image of Mg/Ni(MgO)/Ti before corrosion; (b) SEM section image of Mg/Ni/Ti/MgO after corrosion.

The adding of Ti effectively avoided the disadvantage easily oxidized during sintering. Although Ni and Ti were covered the surface of pure Mg ingot

after mixing, Ni and Ti formed NiTi alloy at first. But not reacted with Mg to form Mg_2Ni due to thermal expansion coefficient of the powder and the alloy has differences. NiTi alloy phase effectively inhibited the sample was oxidized again, at same time, absorbed hydrogen phase Mg_2Ni was formed due to directly contact with pure Mg ingot.

As shown in Fig.4.8, Mg, Ni, Ti and O elements are generated. It had shown that Mg, Ni and Ti elements are stratified on section after the sintered process of 750°C, the main resultants are Mg, Ni, Ti and a small amount of MgO. The most important is the formation of NiTi phase because the peaks of Ni phase and Ti phase appear at the same position.

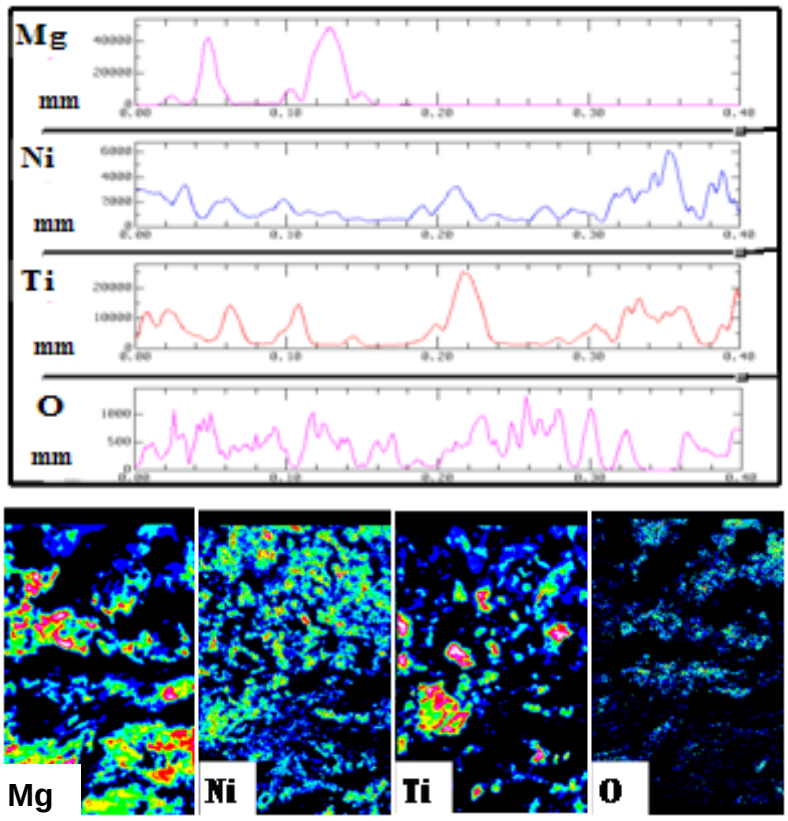

Fig. 4.8 EPMA section analysis of Mg/Ni(MgO)/Ti.

This result is the XRD observations depicted in Figure 4.9. It shows that Mg, Ti and Ni are generated after forming composite. The crystalline structure has not been changed after the powder was sintered. Elemental substance Ni is used as the main characteristic peaks. A part of diffraction peaks of Mg_2Ni disappear because Ti leads to the stress increases and the size of grains is

reduced constantly. Thereby Ni and Ti in the form of simple substance is used as main phases existed is permeated into the pure Mg ingot and a part of NiTi phase was formed. This phenomenon may be attributed to the fact that the amount of the Mg, Ni, Ti and NiTi phases are very strong, therefore, crystal phases is able to be detected by the XRD observation. The result is consistent with that of EPMA analysis.

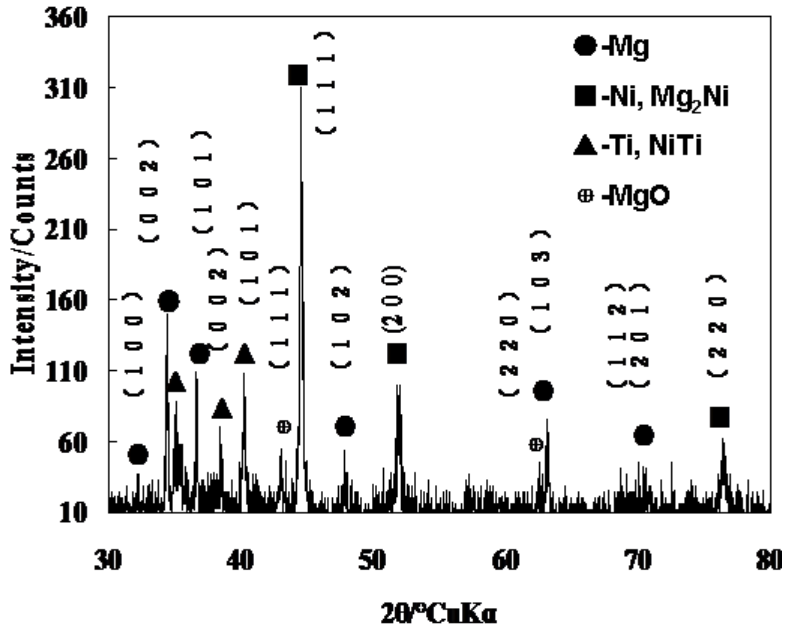

Fig. 4.9 XRD pattern of Mg/Ni/Ti sintered body.

NiTi (Pm3m) phase formed in inner of the composite. Mg_2Ni (P_6222) is hexagonal structure and the crystal grains distributed on interface, so that improve the effect of hydrogen absorption. As shown in Fig. 4.10, Mg_2Ni and NiTi alloy phases of transition layer were observed. It is indicated the powder and the metal produced mutually diffusion and formed multilayer structure. The transition interfaces of diffusion layers are very obvious and Mg_2Ni and NiTi alloy exist in the each diffusion layer due to NiTi and Ni diffused into pure Mg ingot. The formed Mg_2Ni distributed on the surface and a small amount distributed in the inner, so that improved the dynamic performance. NiTi phase in the internal of the sintered body played catalytic role made hydrogen absorption not only stay on the surface of sintered body, but also made H atom diffused in the internal and played important role which could effectively

increase the surface. The electrode material performance was improved and further was confirmed by the capacity determination of hydrogen absorption-desorption under molded sintered body status. It is results that hydrogen absorption phase and catalytic phase throughout the entire composite, so that promoted the diffusion of H atom to inner and improved the kinetics performance. The activated ability improved the reversible reaction was more intense. The generation for the development and application of new electrode material has a crucial signification.

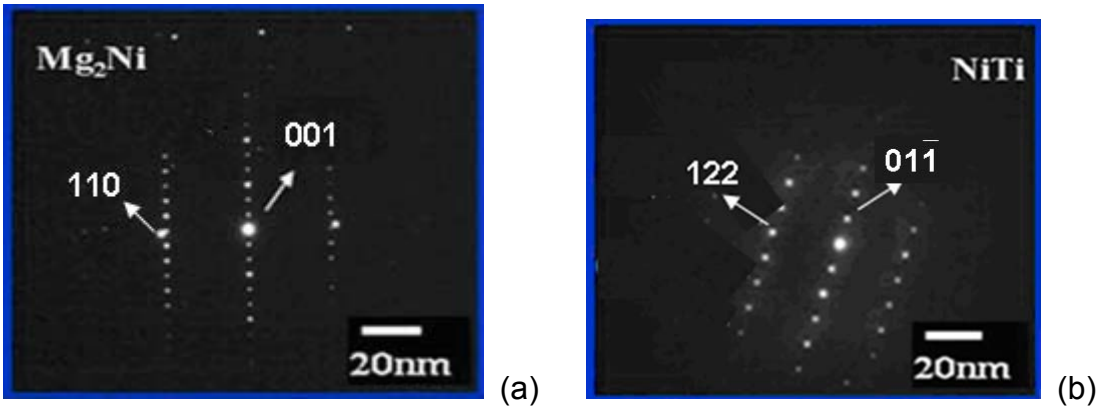

Fig. 4.10 TEM diffraction pattern and element distribution (a) Mg_2Ni; (b) NiTi.

Sampling was conducted for the sample, the position of sampling was diffused layer constituted of layers. According to distribution of element, the second mixing of NiTi powder and Ni was used to conduce sintering, Ni powder repeatedly sintering made the crystal grain completely refinement and formed NiTi alloy at first. But adding again Ni powder could more fully contact with pure Mg ingot, so that formed fully diffusion due to Mg_2Ni was generated. As shown in Fig. 4.11, when the powder diffused into the inner of the alloy, superimposed prepared method made the composite form multilayer diffusion layer, and the diffused layer has coherence; the powder could diffuse to upper and lower layers, so that effectively increase the surface of the powder in pure Mg ingot and achieved continuity of layer and layer.

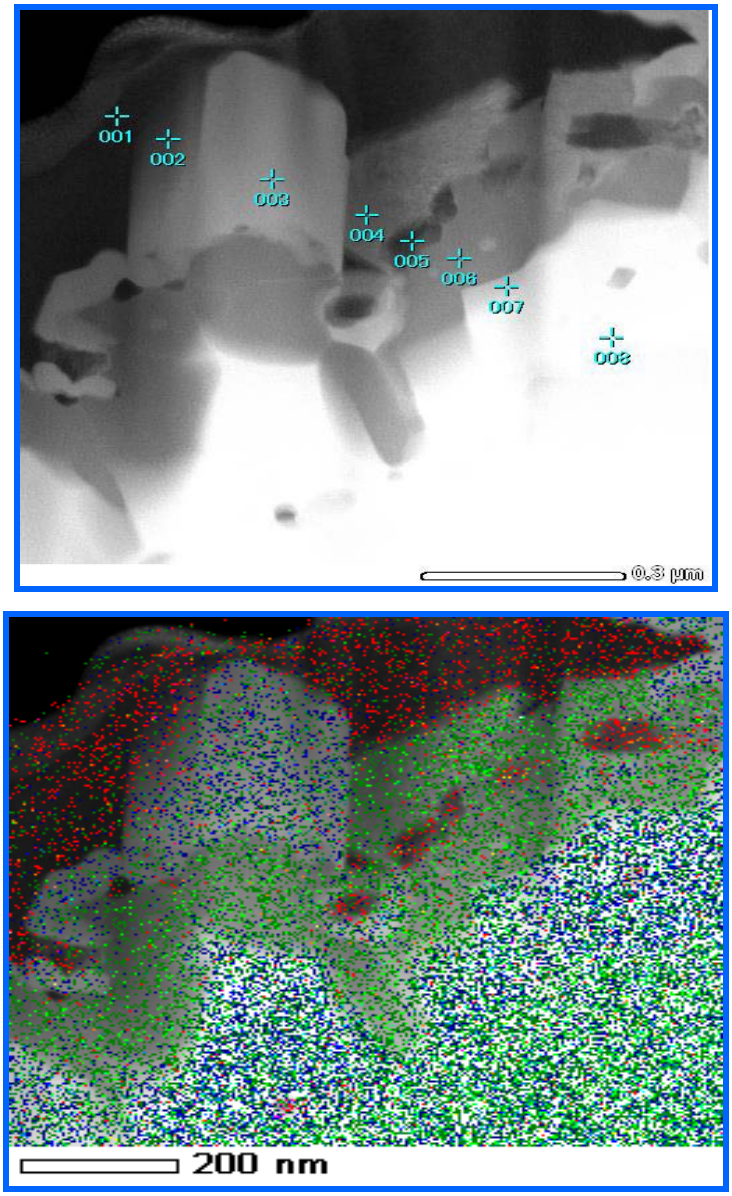

Fig. 4.11 SEM diffraction image and element distribution of Mg_2Ni and NiTi.

According to the analysis of EDS strength in Fig. 4.12, Ti powder and Ni powder diffused into the internal of pure Mg ingot with diffused depth changes and the strength gradually change because the generation of new alloy phase Mg_2Ni and NiTi. The strength of Mg decreased with extended depth. It is showed that Mg mainly distributed on the surface and a small amount of Mg_2Ni formed by the direct contact of Ni powder and pure Mg ingot directly diffused into the inner. As shown in Fig. 4.12, the simple substance Mg was mainly distributed in the first layer and a small amount of NiTi and Mg_2Ni existed. As shown in the second layer, the strength of Mg was significantly reduced and

that of Ni and Ti has increased. The result is that NiTi phase increased and diffused into the internal. As shown in third layer, the strength of Mg significantly reduced and NiTi formed deep diffusion. As shown in fourth layer, the strengths of Mg and Ni had been reduced, but the strength of Ti had a bit increase. It is shown that Ti replaced Ni in Mg_2Ni and formed NiTi alloy phase which diffused into the pure Mg ingot and the diffusion had closed to the second diffused layer. The fifth layer was shown that the strength of Mg was enhanced and the strengths of Ni and Ti reduced obviously. The simple substance Mg was mainly phase and a small amount of Mg_2Ni and NiTi appeared. It is indicated that the fifth layer is the second diffused layer. As shown in sixth layer, the strength of Mg significantly reduced and that of Ni and Ti has increased; NiTi phase has increased and diffused into the internal of the second superimposed layer. In the seventh and eighth layer, Mg peak had disappeared and NiTi formed deep diffusion. The diffused layers could be distinguished obviously. The special layered structure has improved the hydrogen storage properties. Mg_2Ni as an absorb phase formed the surface of each layer and NiTi as a catalytic material being distributed into the the inner of each layer. Both alloy phase improved H atoms surface absorption and diffusion to the inner to produce hydride.

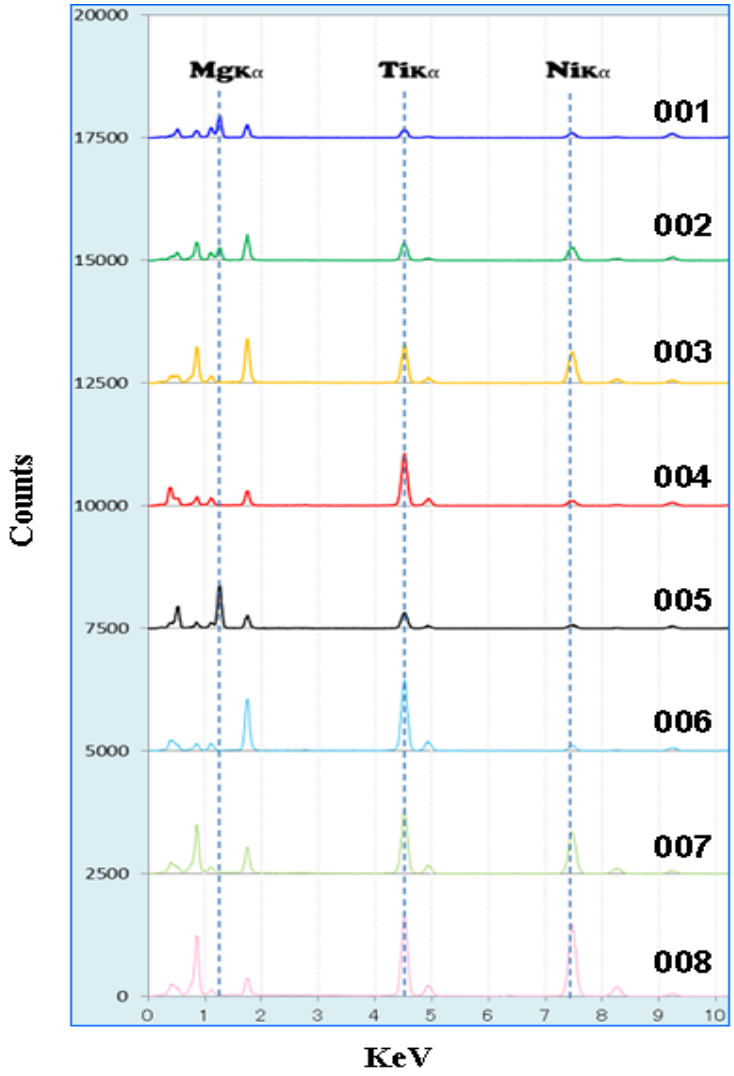

Fig. 4.12 EDS element distribution of 1st-8th hierarchical structure.

4.3.3 Voltage determination by electrochemistry

The study applied electrochemical to detect the performance. The potential voltage and current were analyzed to calculate hydrogen absorption and desorption properties.

The electrochemical corrosion experiment about basis sample, Mg/Ni(MgO) and Mg/Ni(MgO)/Ti composites had been performed for 60 minutes and their respective morphology was observed. As shown in Fig. 4.13, Mg/Ni(MgO) and Mg/Ni(MgO)/Ti were compared. Figure 4.13(a) shows that Mg/Ni(MgO) sintered body stability becomes better. Figure 4.13(b) shows that the voltage of Mg/Ni(MgO)/Ti sintered body is the highest and the stability

become best. The results indicate that the hydrogen evolution reaction over positive potential of Ni(MgO) has been increased; the hydrogen depolarization was slowing down, therefore the self-corrosion rate was cut down, the utilization of anode was enhanced. It is shown that Mg/Ni(MgO)/Ti sintered body has good electrochemistry performance. For the sintered body, starting voltage reached to a maximum of -0.92V, it is indicated that the sample has the large potential to effectively absorb and release hydrogen. In order to further confirm the dynamic performance of the material, cyclic voltammeter was used to calculate the amount of hydrogen absorption and desorption and the result was theoretical value for the ability.

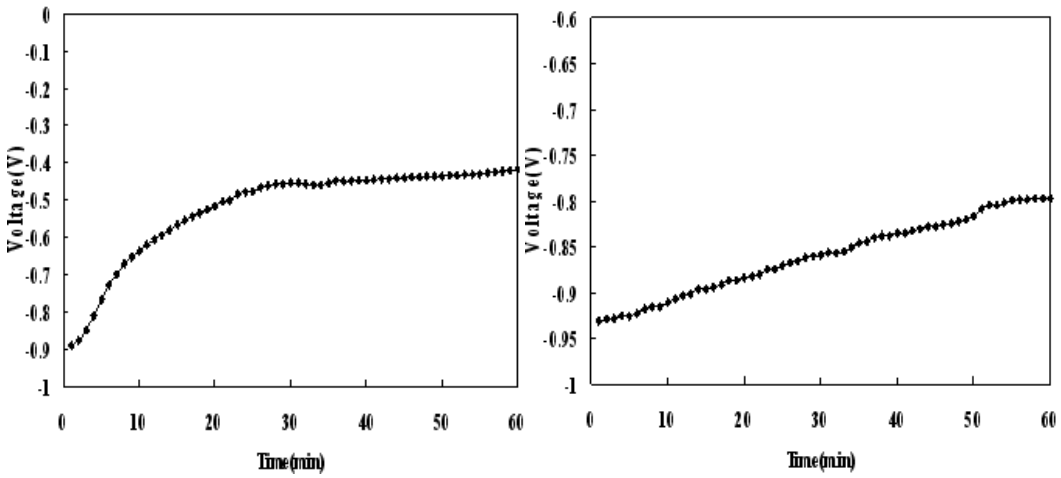

(a) (b)

Fig. 4.13 Voltage determination (a) Mg/Ni(MgO); (b) Mg/Ni(MgO)/Ti sintered body.

4.3.4 Determination for the ability of absorption-desorption hydrogen by cyclic voltammeter

In the detection process, once hydrogen atoms are absorbed, they can occupy the sites in the crystal lattice as shown in Fig. 4.14(a) and Fig. 4.14(b). Whether hydrogen is absorbed or desorbed depends on the energy. This energy depends upon the hydride-forming material in MHx the hydrogen atoms occupy the sites.

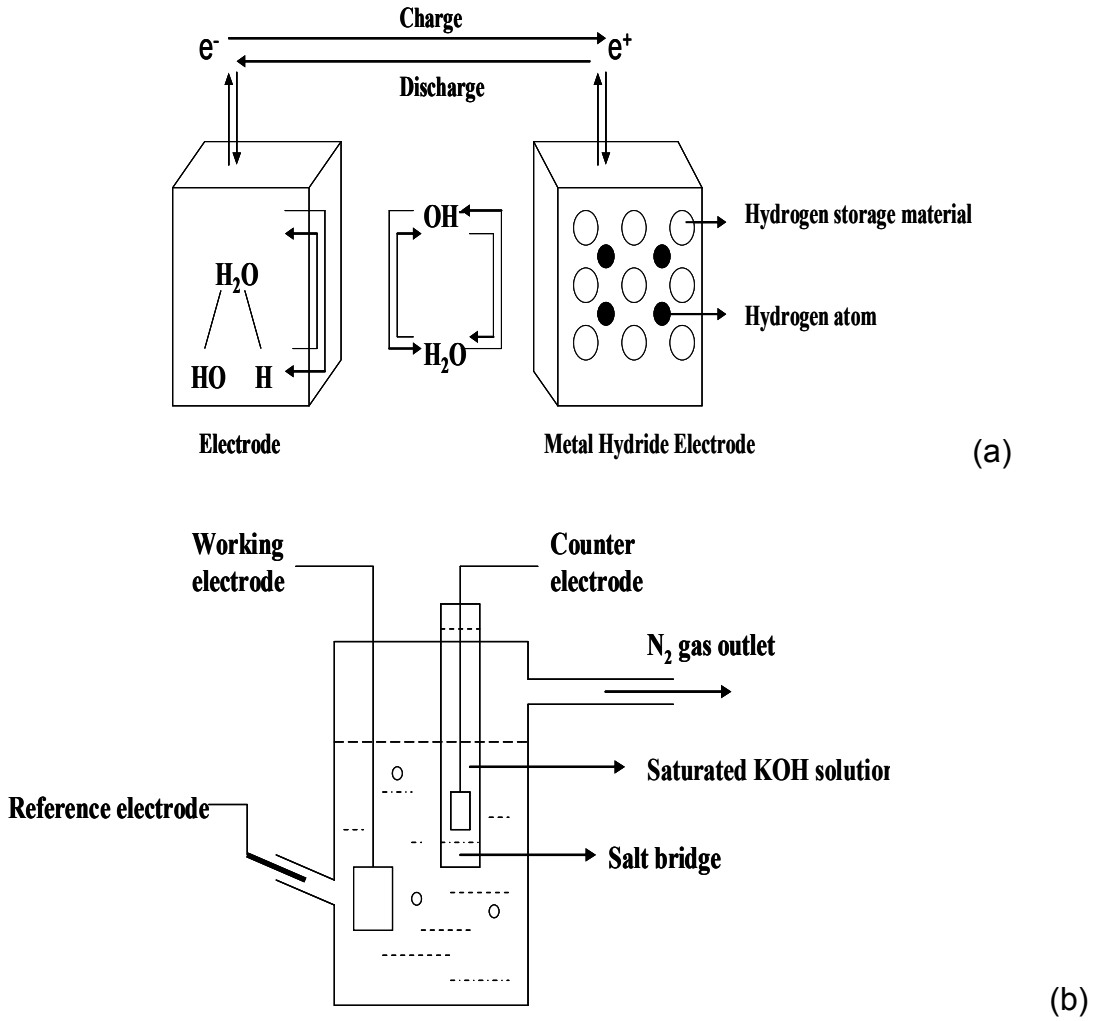

Fig. 4.14(a) Schematic of electrochemical method; (b) Apparatus of working.

(a) Electrochemical evaluation of Mg/Ni(MgO)

As shown in Fig. 4.15(a), Mg/Ni(MgO) composite in neutral solution produced obviously oxidation and reduction, in which oxidized reaction showed unstable state in one cycle process. After absorbing hydrogen, dehydrogenation peak was obvious and compared to CV curve before absorbing hydrogen the position of reduction peak was more negative. It is showed that the capacity of hydrogen absorption was small when reduction produced, so that H in the alloy directly diffused into the reacted center of electrode surface and adsorbed on the surface of electrode to generate H_2O. Oxide layer was broken lead to the formation of holes and the increase of

corrosive because Mg_2Ni partial dissolution; the negative current was increased significantly. After adding H_2O and absorbing hydrogen, the curve became more stable; restored peak became weaker obviously, the reason was the formation of $Mg(OH)_2$ by the reaction between pure Mg and H_2O. The generation of the passivation layer serious affected reducing intensity. As shown in Fig. 4.15(b), oxidized and reductive reaction became stable and the reaction was obviously. The oxidized current reached to 50mA; the reductive current was -50mA. After absorbing hydrogen, the electrolysis of water promoted significantly the current; the potential window in reduction side expanded and moved to negative direction. The electro-catalytic activity of the electrode was affected because absorbing hydrogen formed Mg_2NiH and NiTiH phases. The phenomenon promoted H reaction in oxidation and reduction and affected electrode transfer in electrode reaction, the potential window was expanded and the current was enhanced obviously compared to CV curve before absorbing hydrogen. When Mg_2NiH depend on itself catalytic reacted with H_2O, electrolysis was promoted, so that improved significantly the dissolution of the alloy and reduced the corrosive of the specimen, so that increased reduction current.

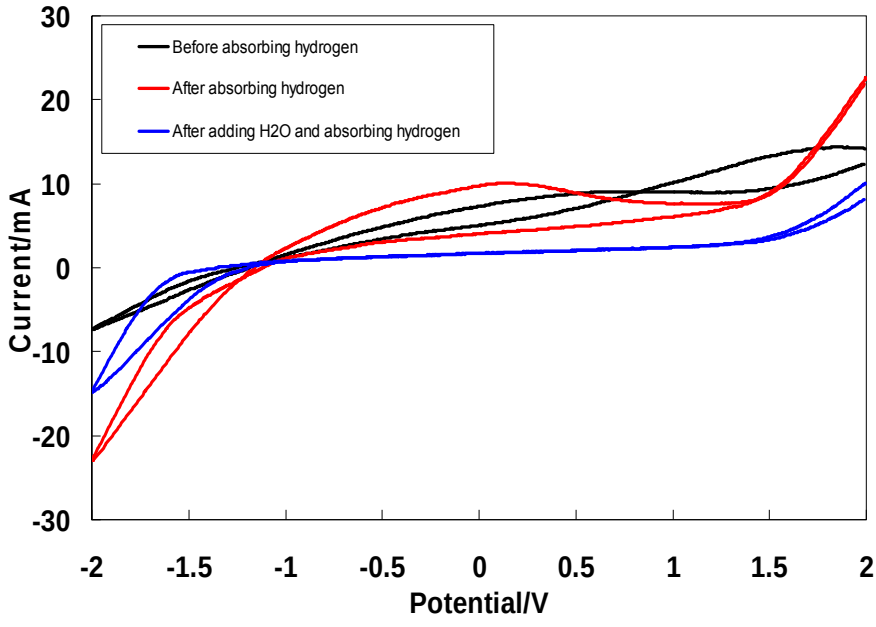

(a)

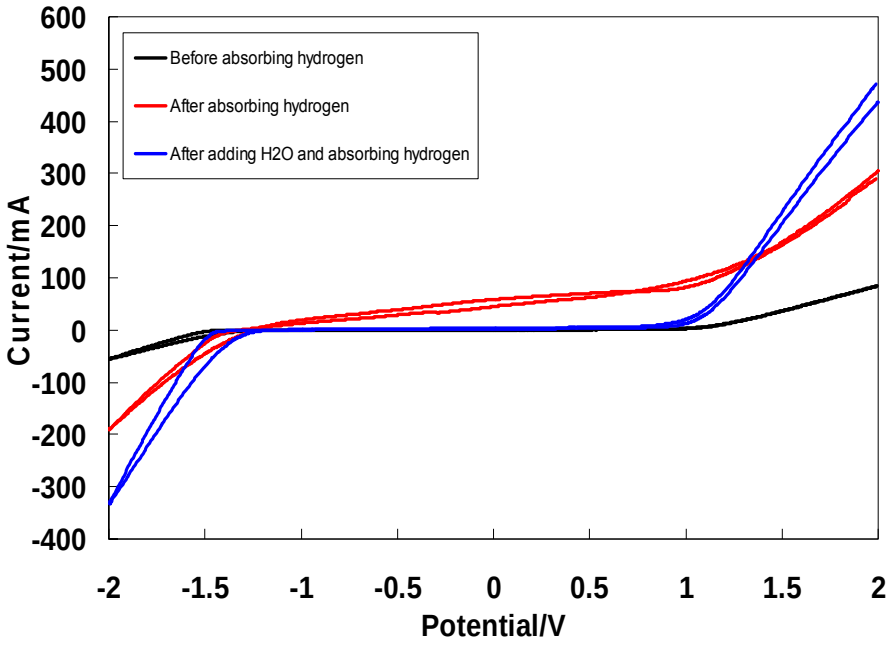

(b)

Fig. 4.15 Oxidation/Reduction of Mg/Ni(MgO) (a) Neutral solution(PH7); (b) Alkaline solution(KOH).

(b) Electrochemical evaluation of Mg/Ni(MgO)/Ti

As shown in Fig. 4.16(a), Mg/Ni(MgO)/Ti composite emerged obvious reducibility and the stability was well. In cycle process, closed state was achieved in the smaller range. It is showed that the adding of Ti for oxidized and reductive reaction played promoted role. After absorbing hydrogen, dehydrogenation peaks was obvious and compared to CV curve before absorbing hydrogen the position of reduction peak was more negative. It is showed that the capacity of hydrogen absorption was small when reduction produced, so that H in the alloy directly diffused into the reacted center of electrode surface and adsorbed on the surface of electrode to generate H_2O. Oxide layer was broken lead to the formation of holes and the increase of corrosive because Mg_2Ni partial dissolution through the existing of MgO; negative current was increased significantly. In the alkaline solution, the formation of Mg_2NiH hindered Mg_2Ni to produce partially dissolution and made the porous structure of the surface of the specimen be improved; the oxygen

produced positive electrode did not easy to react with alkaline solution to generate OH^-, so that reduced reduction current. When adding H_2O and absorbing hydrogen, there is water on the surface of the specimen while formed hydroxide. To use the features of the absorption had positively charged, the directly electrochemistry was achieved. In which the main hydroxide was $Mg(OH)_2$. The results shown the hydroxide could significantly increase the current of the peaks to generate stable hydroxide film which had catalytic oxidized role for the surface nature of the electrolysis. The hydroxide only consumed H^+ in solution; PH value of the solution rapidly increased. In the electrolysis process, cathode became obviously alkaline to improve the density of the current was higher. As shown in Fig. 4.16(b), when the specimen was detected in alkaline solution, the cycle reaction did not produce obvious fluctuations. After absorbing hydrogen, Mg_2NiH and NiTiH could damage oxide layer effectively, so that the dissolution and corrosive of the alloy were enhanced significantly, the reduced current was increased. The current of oxidation and reduction was reduced when adding H_2O and absorbing hydrogen. The curve became more stable; the formation of NiTiH played the protective effect for damaging passivation layer, so that reduced the restored current. The generation of the passivation layer serious affected current density.

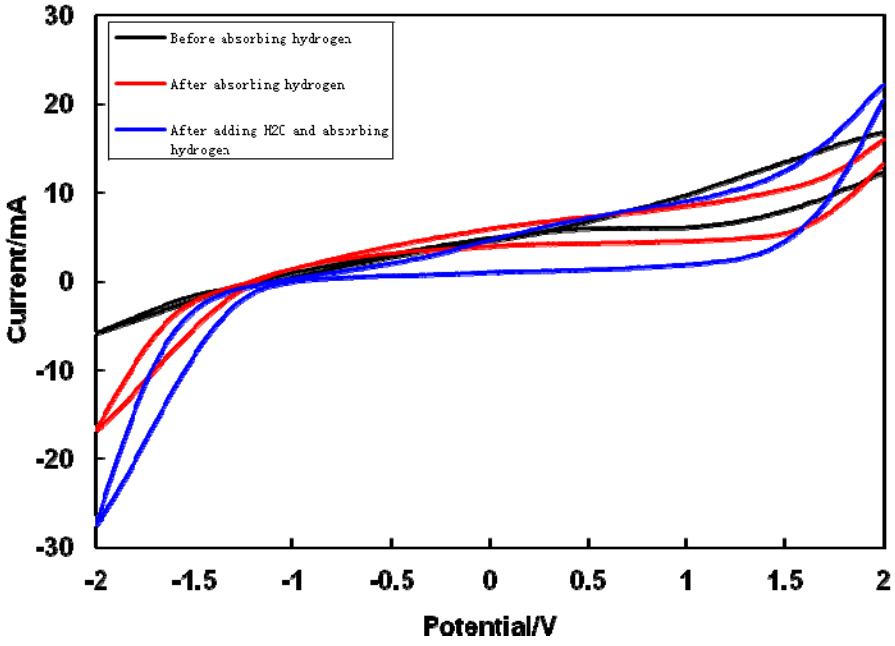

(a)

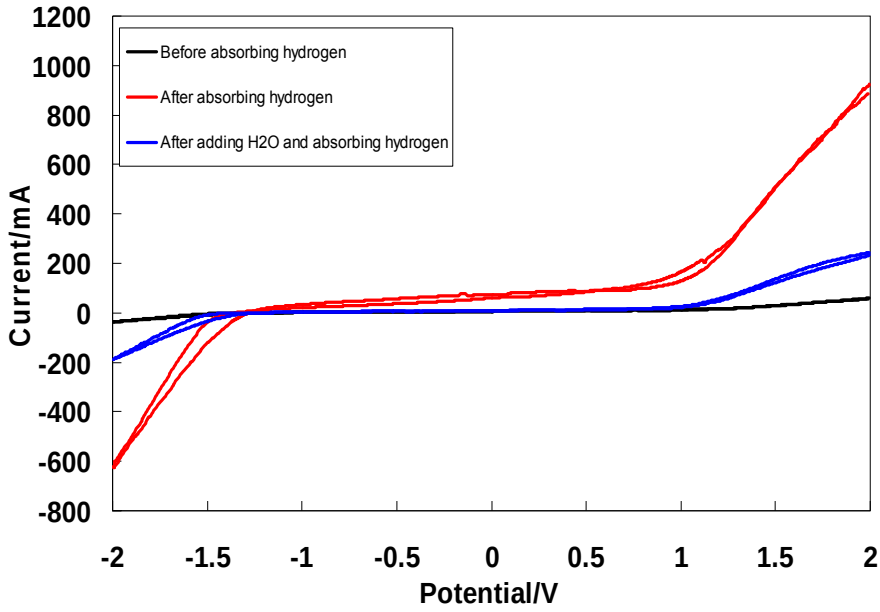

(b)

Fig. 4.16 Oxidation/Reduction of Mg/Ni(MgO)/Ti (a) Neutral solution(PH7); (b) Alkaline solution(KOH).

As shown in the Fig. 4.17(a), the cyclic voltammeter of sintered body Mg/Ni(MgO) electrodes in potential region between 0 and -1.2V vs. Ag/AgCl at the scanning rate of 50mV/s. Obviously, during a single cyclic voltammeter experiment, a metal hydride electrode are second oxidized on a forward scan form -1.2 to 0 V. The symmetry happened in anodic and cathodic branch indicates that the metal hydride electrode is a totally reversible system. The

results revealed that generate Mg/Ni(MgO) sintered body in form of penetration can reversibly absorb and desorb hydrogen, whereas Mg/Ni(MgO) absorb appreciable amount. As shown in the Fig. 4.17(b), the cyclic voltammeter of sintered body Mg/Ni(MgO)/Ti electrodes in potential region between 0 and -1.2V vs. Ag/Agcl at the scanning rate of 50mV/s. And during a single cyclic voltammeter experiment, metal hydride electrode is second oxidized on a forward scan form -1.2 to 0 V. The symmetry happened in anodic and cathodic branch indicates the metal hydride electrode is a totally reversible system. It was shown that the ability of excellent sorption kinetics was revealed again. The Mg/Ni(MgO)/Ti revealed excellent kinetic properties and the highest hydrogen absorption capacity is 6.0 wt%. However, Ti being employed as hydrogen storage medium reveals excellent sorption kinetics due to Ti limits the gravimetric capacity loss by substituting a heavier element became a very important factor. The quality hydrogen storage capacity of hydrogen storage material (H/M) is w%, according to the formula (1):

$$W\ \%=(Cmax-C)360*MH/NA*e=3.7606*10^{-3}*(Cmax-C) \quad (1)$$

Cmax is the maximum discharge capacity of alloy electrodes; M_H is relative atomic mass (1.0079); N_A is avogadro constant ($6.0221367*10^{23}mol^{-1}$); e is electron charge ($1.60217733*10^{-19}$). The capacitance C is converted to charge capacity (Cmax-C). Elemental Mg and Ni appeared in the Mg/Ni(MgO) sintered body formed and contain mainly Mg_2Ni alloy phase. In which Mg and Mg_2Ni formed reversible oxidized and reductive peaks, but Ni did not form reversible reaction. The ability of hydrogen absorption and hydrogen desorption of Mg/Ni reached to 6% and 0.4% under room temperature**.** The Mg/Ni(MgO) sintered body was modified to the peak current of oxidized peak become larger by adding Ti, so that electrode for the rate of hydrogenated charging and discharge was increased and The electrochemical reaction of the hydrogen can be more easily carried out. Adding Ti into Mg / Ni after modified improved the electro-catalytic activity of the electrode. The amount of hydrogen storage

alloy is greater, the area of the anode electrode peak on the cyclic voltammeter curve is greater and the current of oxidized peak of hydrogen become larger. The area of oxidized peak for the sintered body of Mg/Ni(MgO)/Ti is larger than that of Mg/Ni composite. It is indicated that the discharge capacity of Mg/Ni/Ti sintered body is higher than that of Mg/Ni. The ability of hydrogen absorption and hydrogen desorption of Mg/Ni/Ti reached to 6% and 2% under room temperature.

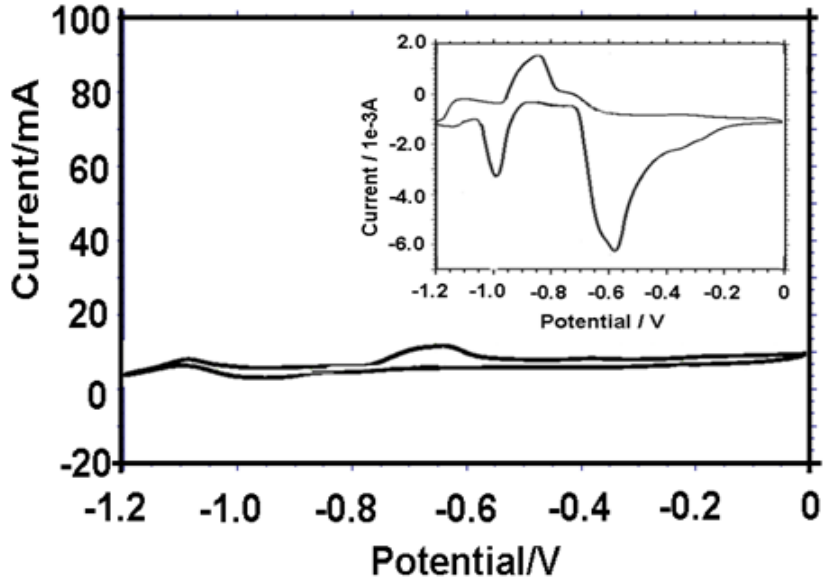

(a)

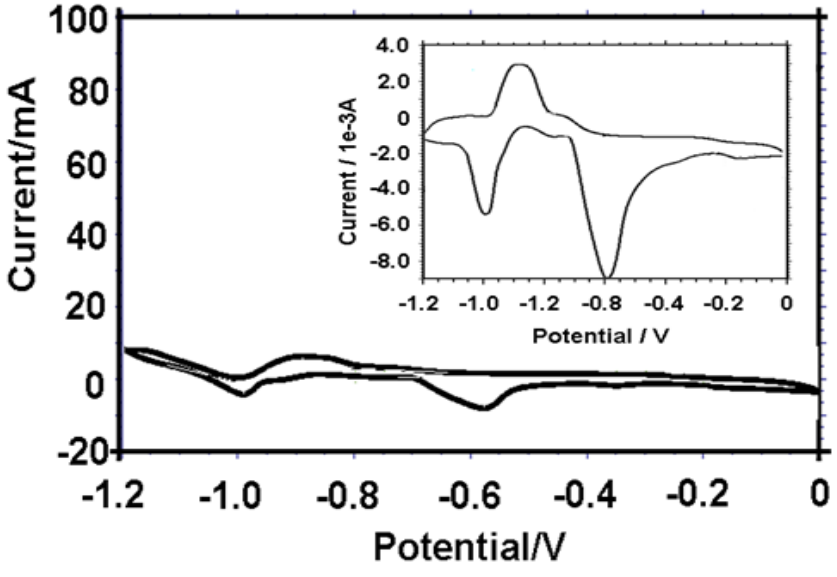

(b)

Fig. 4.17 Oxidization/Reduction of a small range (a) Mg/Ni(MgO); (b) Mg/Ni(MgO)/Ti.

The electrochemical properties and H-storage properties for Mg/Ni(MgO)

and Mg/Ni(MgO)/Ti were examined. The results obtained are summarized as follows:

Ti as transition metals is most promising would be exceptionally suitable because has a reasonably high gravimetric capacity to improve electrochemical properties and ability of absorbing-desorption hydrogen with the new method of penetration and sintering. The addition of Ti not only enhanced uniformity and refinement maximum and effective, but also generated NiTi alloy phase and improved electrochemical properties that the voltage increases and the reaction rate about the ability of hydrogen absorption and desorption kinetics becomes larger. The novel point of the experiment is catalytic phase formed based on Mg_2Ni phase was generated. Therefore, the catalytic effect should be characterized by the further analyses in future works.

In the above experiment, the ability of new type sintered body for hydrogen absorption and desorption had been confirmed and further proved the capacity of Mg/Ni(MgO)/Ti was worthy of discussion.

4.3.5 Capacity evaluation of hydrogen absorption/desorption for Mg/Ni(MgO)/Ti

(a) Qualitative synthesized analysis from 400 °C to 250°C

According to determining of a temperature at about 250°C, the study adjusting the temperature from 400°C to 250°C in order to confirmed what is the key factor helped hydrogen absorption and desorption. The PCT curve detected respectively the effects on the hydrogen storage capacity under the temperature and the pressure. The different detected conditions of hydrogen absorption and desorption were selected and in which the actual capacity for the composite were further confirmed. As shown in Fig. 4.18(a), the activation process was longer under certain pressure at keeping temperature for 30°C; at

beginning of the first hour when the temperature was heated to 400°C and the H_2 pressure was adjusted to 1MPa, the rate of hydrogen absorption and desorption rapidly increase. After keeping 30min, molar ratio of hydrogen absorption was 0.18. In the period, the temperature and H_2 pressure were as a switch. When keeping for 400°C, hydrogen absorption rate became to slow, but still showed a gradually increased trend. The rapid increasing of temperature could improve the performance of hydrogen storage. In the process, the sintered body achieved rapid activated process during the induction period when keeping the temperature and H_2 pressure. For the composite, the results showed that the composite could effective absorbing and releasing hydrogen with extending time and could achieve the physical adsorption and desorption on the surface; when only H_2 pressure was adjusted, the first cycle of hydrogen absorption and desorption was completed. It is indicated that H_2 pressure as main switch played a key role in the activated process. As shown in Fig. 4.18(b), in the red box marked area, the rate and the capacity of hydrogen absorption and desorption under different conditions were discussed in detail. For the composite, the changes of the temperature and H_2 pressure for the hydrogen absorption and desorption has a certain thermodynamics effect, Soaring increase the temperatures and H_2 pressure help to improve hydrogen absorption to product, For the purposes of this experiment, the composite achieved effective absorption and desorption with the changing of the temperature and H_2 pressure. Before the second cycle of hydrogen absorption and desorption, the temperature and H_2 pressure improved the increasing of hydrogen absorption, but simply temperature change for the effect of hydrogen absorption was not obviously under a constant H_2 pressure. As shown in Fig. 4.18(c), the capacity of hydrogen absorption was significant increase and up to 125mg about 0.68 under 4.5MPa and achieved to the saturation value. With the increasing of H_2 pressure, the hydrogen desorption process started, the actual capacity of hydrogen desorption is up to 0.38, so that achieved purpose that the surface area was

increased in internal of composite. The diffused layers existed as a catalyst layer, in which large Mg grain and Mg_2Ni phase generated existed as the substrate of hydrogen absorption and hydrogen desorption and NiTi catalytic phase distributed in each diffused layers. According to above results, it is a curial role that H_2 pressure as the switch of hydrogen absorption and desorption was confirmed. In the adjusting process from 440°C to 250°C, the large amount of hydrogen absorption and desorption had been achieved, but the rate of hydrogen absorption and desorption was not improved.

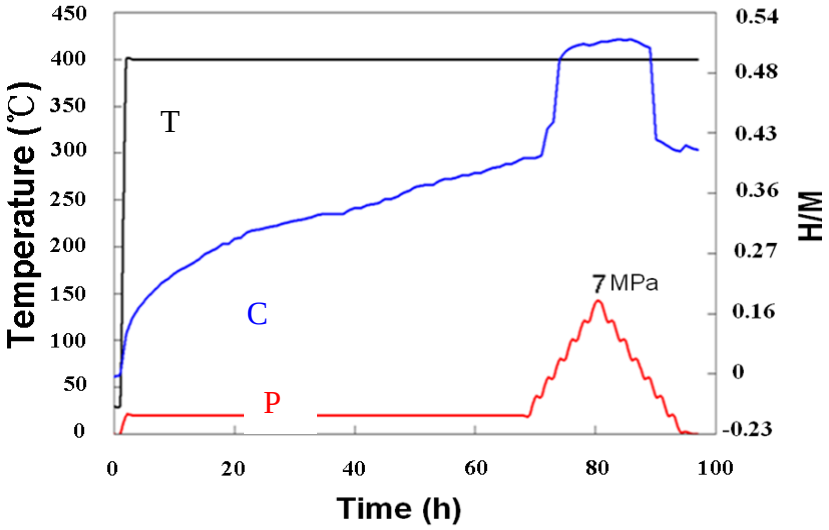

(a)

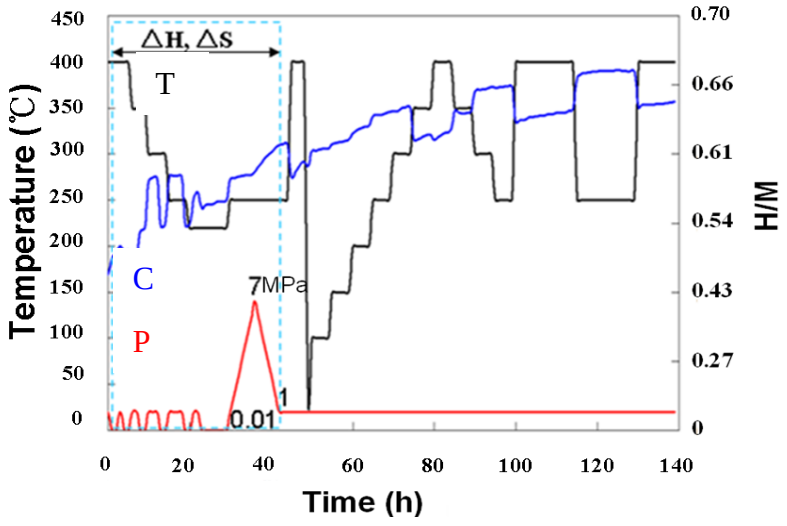

(b)

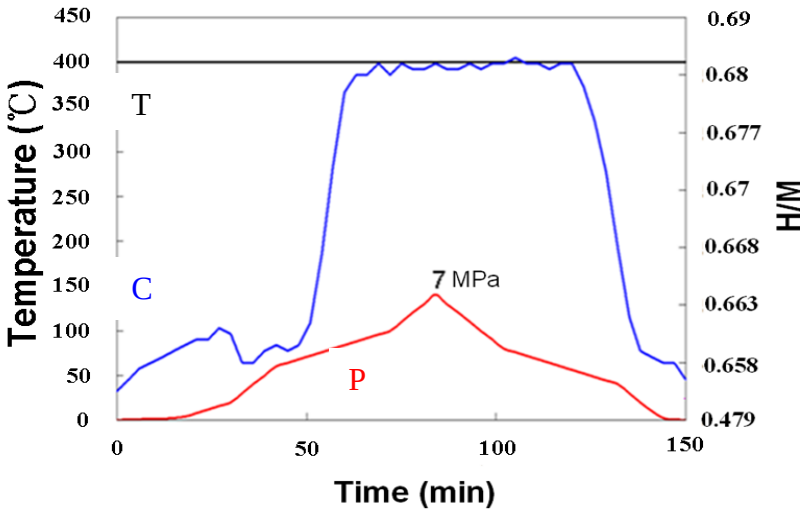

(c)

Fig. 4.18 (a) PCT curves on surface absorption from room to 400°C by gradually adjusting H pressure; (b) PCT curves of H diffusing to inner of the sintered by adjusting H_2 pressure and temperature different time; (c) PCT curves under constant temperature 400°C and different H_2 pressure from 0.01MPa to 7MPa.

(b) Qualitative separately analysis under different H_2 pressure and temperature

In order to further determine the most suitable experimental conditions, the study for the composite conducted qualitative determinations of each stages. In which the determined time of each process was long in order to confirm the stability of the sample and the saturation level in hydrogen absorption and desorption process.

As shown in Fig. 4.19, based on the above basis experiment, the PCT curve detected respectively the effects on the hydrogen storage capacity under the temperature and the pressure. The temperature was set from 400℃ to 250℃ based on the analysis from XRD results. The different detected conditions of hydrogen absorption and desorption were selected and in which the qualitative and quantitative analysis for the composite were further confirmed. The induction period activation process was longer under certain pressure at keeping temperature for 30°C; at beginning of the first hour, the activation effect had been not obviously improved. When the temperature heated up to 400°C and H_2 pressure to 1MPa, the rate of hydrogen absorption and desorption rapidly increase. After keeping 30min, molar ratio is 0.18. Under keeping for 400°C and H_2 pressure, Hydrogen absorption rate become to slow, but still show a gradually increased trend. It is shown that the amount of hydrogen absorption gradually reach saturation. The activated effect had been completed and will start the first cycle of hydrogen absorption and desorption. In the process, the sintered body achieved rapid activated process during the induction period under keeping of the temperature and H_2 pressure. For the composite, the efficient surface physical adsorption was achieved. The experimental purpose is to observe the hydrogen absorption and desorption rate only depend on the extension of time.

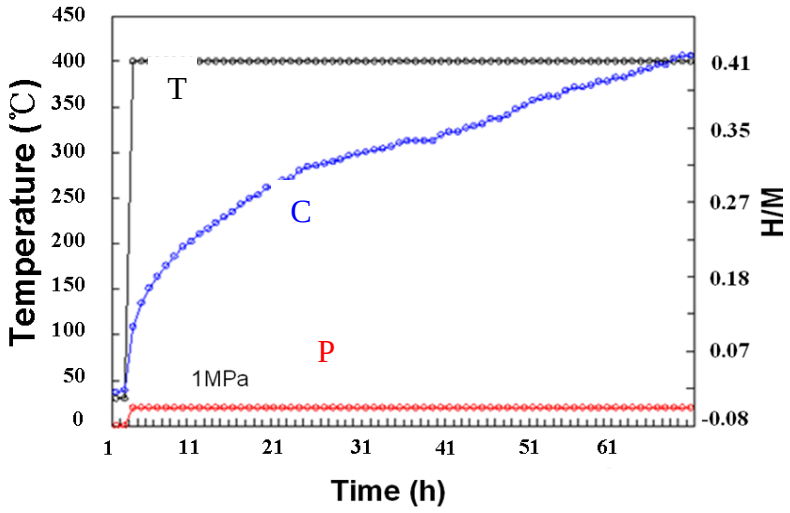

Fig. 4.19 Capacity of absorbing hydrogen from room temperature 30°C to 400°C when adjusting H_2 pressure from 0.01MPa to 1MPa.

The experimental purpose for this cycle process is to analysis saturation level and the rate completed once time hydrogen absorption and desorption only depend on the extension of time. As shown in Fig. 4.20, the hydrogen pressure is gradually increased under keeping the temperature at 400 °C, in which the hydrogen pressure was add from 3MPa to 4MPa after holding about 1 hour, hydrogen absorption rate was significantly improved, and the amount of hydrogen absorption and desorption was further increase. With the increasing of H_2 pressure, the absorption rate trend to slow. It is shown that the changes of H_2 pressure play the importance role for the thermodynamic performance. When H_2 pressure was down to 4MPa, the amount and the rate of hydrogen absorption and desorption had been improved. A single hydrogen pressure change can achieve the physical adsorption on surface. When reach saturation state, the hydrogen pressure for release hydrogen was studied under constant temperature condition. When the hydrogen pressure at 3MPa, hydrogen began release; the hydrogen pressure lower to 2MPa, the hydrogen desorption rate is rapidly increasing, the amount of hydrogen reached 0.31

within 1 hour. It is indicated that the rate and the hydrogen of desorption get obviously improvement during short time when the H_2 pressure was down to 2MPa.

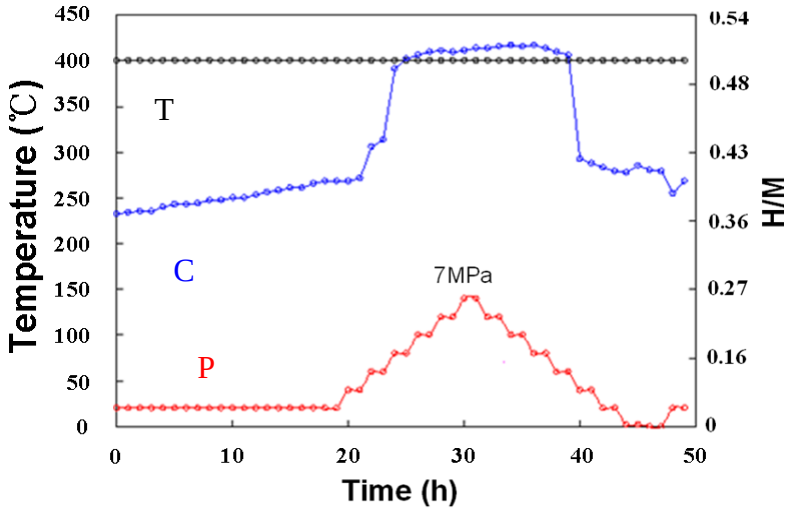

Fig. 4.20 Capacity of absorbing and desorbing hydrogen under constant temperature 400°C when adjusting H_2 pressure from 1MPa to 7MPa.

In order to confirm a key factor, the determination conditions were set under different temperature and H_2 pressure at the same time. The result showed that the capacity of hydrogen absorption and desorption was consistent with the changing of H_2 pressure. As shown in Fig. 4.21, the hydrogen absorption curve appeared the trend to rise with the adjusting pace of H_2 pressure. In the increasing of the hydrogen absorption process, the temperature had produced less impact. The experiment process was divided into the different stages and the holding time for each platforms of hydrogen absorption and desorption was extended to evaluate the rate and saturation degree, a small amount of H_2 released when the temperature was down to 350 °C and 1MPa, after keeping about 1 hour hydrogen absorption amount increased again. When the temperature was lowered to 300 °C and 1MPa and the hydrogen desorption process does not appear immediately, but kept for 2 hours, the desorption start and the rate was faster. The hydrogen desorption process was completed rapidly in about 30min. The temperature is down to 250°C and 1MPa, the hydrogen absorption rate was fastest, after holding time

to stable, the temperature down to 220 °C 1MPa, hydrogen absorption started and been holding for a certain time, the desorption started and reach to steady. The hydrogen absorption and desorption processes was accompanied during the four time cycles, the results show that when the temperature is lowered to 250°C, it fastest hydrogen absorption, quickly reaches saturation in a relatively short period of time to achieve the discharge of hydrogen. The rate of hydrogen absorption was fastest and rapid reach to saturation when the temperature was down to 250°C, so that achieved hydrogen desorption in the short time.

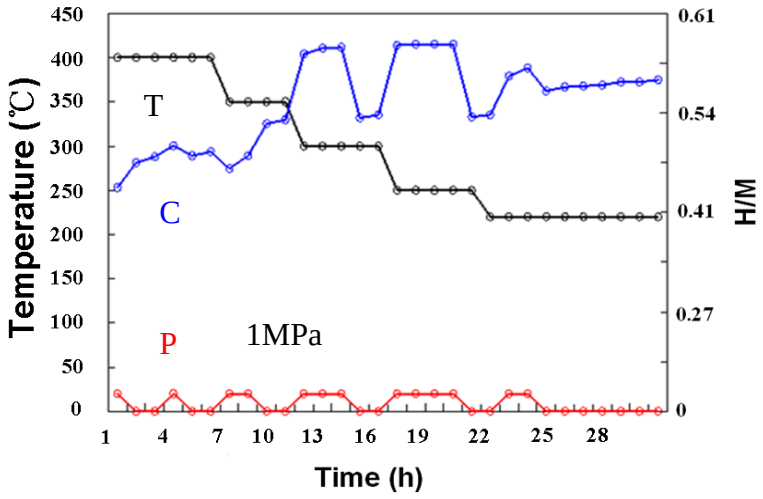

Fig. 4.21 Capacity of absorbing and desorbing hydrogen under different temperature when adjusting H_2 pressure between 0.01MPa to 1MPa.

As shown in Fig. 4.22, according to rapid absorb and release hydrogen at 250°C, thereby, the rate and a amount of hydrogen absorption for keeping 250°C was further discussed under adjusting H_2 pressure. The amount of hydrogen absorption although increased, but the hydrogen absorption rate is extremely slow in the substantial change of hydrogen pressure. In the first cycle process, the hydrogen desorption process produced within 1 hour. With

the ending of the first cycle, the temperature was changed under constant H_2 pressure, the second cycle appeared; but the result compared to that of the first cycle the amount of hydrogen absorption and desorption obviously less. It is shown that depend on the change of the temperature did not well improved. For this study, the key helped generate hydrogen absorption and desorption processes are the changes H_2 pressure, but the changes of the temperature would have a greater affect on the hydrogen absorption and desorption and accompanied the temperature change to had greater promoting role.

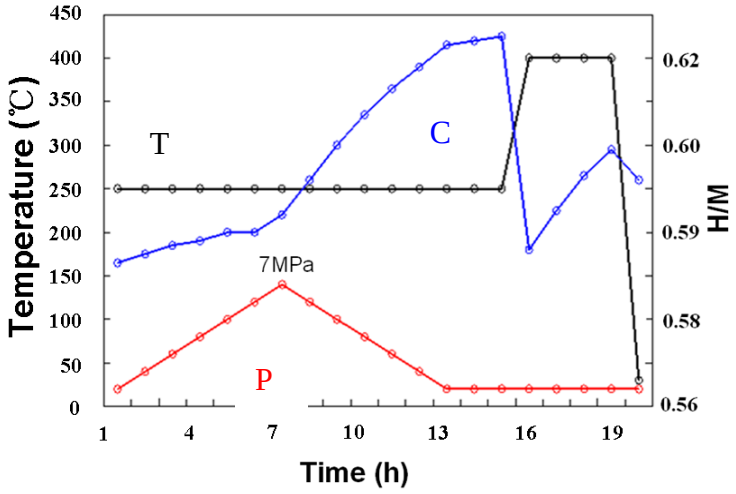

Fig. 4.22 Capacity of absorbing and desorbing hydrogen when adjusting temperature (from 250°C to room temperature) and H_2 pressure (from 1MPa to 7Mpa) at different times.

In order to verify the role of H_2 pressure as key factor, the determination was conducted under constant H_2 pressure and adjusting the temperature. As shown in Fig. 4.23, under constant hydrogen pressure conditions, the rate and

the amount of the hydrogen absorption was no significant improvement with gradually changing the temperature. The significant desorption plateau appear nearby 300°C. It is showed that the effect on heating temperature for the

hydrogen absorption was not very obvious, and to greater improve thermodynamic performance of hydrogen desorption is need to further improve.

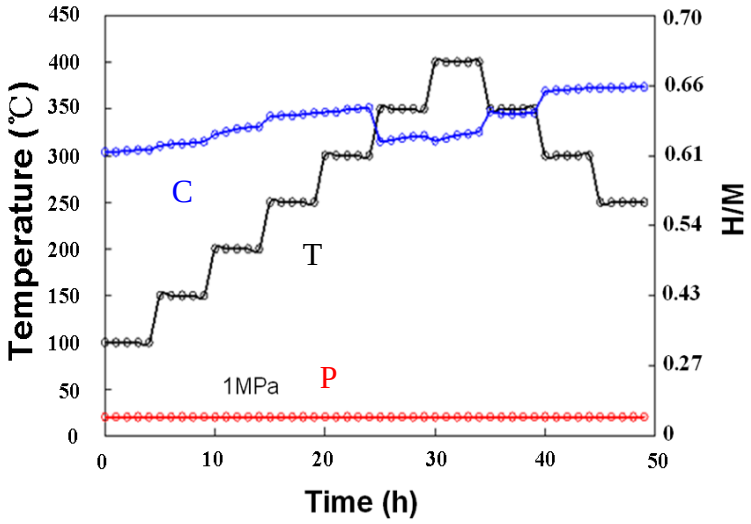

Fig. 4.23 Capacity of absorbing and desorbing hydrogen under constant H_2 pressure 1MPa when adjusting temperature from 100 °C to 400 °C.

When continuously keeping constant H_2 pressure, a cycle of hydrogen absorption and desorption was achieved, but the capacity of hydrogen absorption and desorption was less. According to above conclusions, the effect was obvious by changing H_2 pressure to promote hydrogen absorption and desorption thermodynamics; as shown in Fig. 4.24, to keep the constant H_2 pressure and changed measured temperature, the hydrogen absorption rate was relatively slow while keeping 400 °C and a small amount of hydrogen absorption increased. It is indicated that a constant hydrogen pressure and temperature for the hydrogen absorption rate and the improvement of the hydrogen storage capacity were not obvious, only by extending time could achieve a small amount of hydrogen absorption and desorption. With the temperature decreasing, the hydrogen absorption and desorption was completed in 30min. But the amount of hydrogen absorption and desorption

was only 0.38. The adjusting H_2 pressure for hydrogen absorption and desorption played a very significant role.

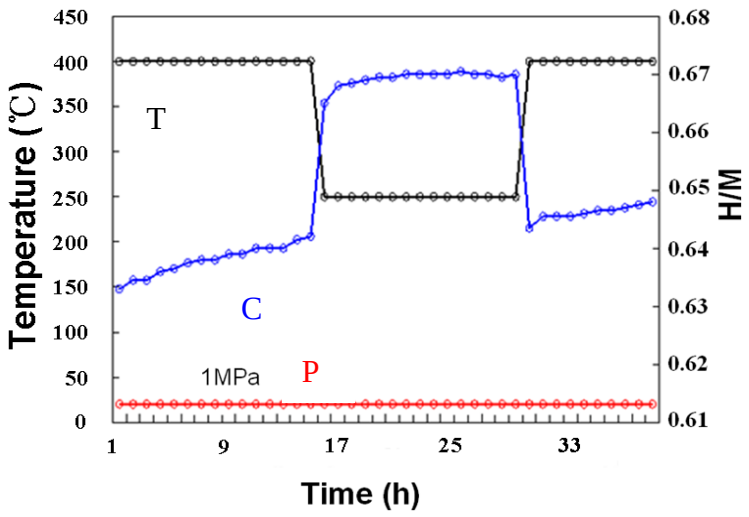

Fig. 4.24 Capacity of absorbing and desorbing hydrogen under constant H_2 pressure 1MPa when adjusting temperature from 400 °C to 250 °C.

The verification was conducted again to prove the important effect under constant temperature when adjusting H_2 pressure. In which the capacity of hydrogen absorption and desorption was consistent with the changing of H_2 pressure. But the capacity of hydrogen absorption and desorption was less because the value reached to saturation. As shown in Fig. 4.25, when the temperature is constant, hydrogen absorption rate relatively slow with the change of hydrogen pressure, less hydrogen absorption capacity was obtained, only according indefinite to extent about time to achieve a small amount of hydrogen absorption and desorption. The tendency of hydrogen absorption and desorption was consistent with the change of H_2 pressure. It is indicated that an amount of hydrogen absorption and desorption after several cycles reach to 0.68 and 0.14.

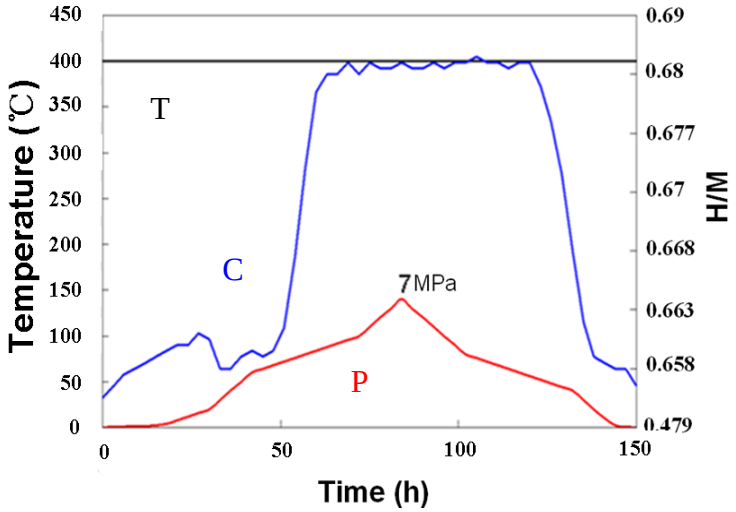

Fig. 4.25 Capacity of absorbing and desorbing hydrogen under constant temperature 400 °C when adjusting H_2 pressure from 0.01MPa to 7MPa.

4.4 Defects and discussion

For the above analysis, the effect of H_2 pressure to the sample was obviously and the temperature also has a little affects. The determinations of this experiment were conducted most under constant temperature and H_2 pressure, and simple depend on the extending time to reach saturation, so that detected the performance of hydrogen absorption and desorption. It is shown that the amounts of hydrogen absorption exceed 0.66 and the result breaking the previous amount for hydrogen storage alloy. But the rate of hydrogen absorption and desorption contrasted to the powder prepared by milling boll method become longer. It is consider that MgO may produce negative affect to the specimen, although MgO can play a absorbent role, but easy to react with H_2O form $Mg(OH)_2$ hydroxide. The hydroxide would serious impact the capacity and the rate of hydrogen absorption and desorption.

4.5 Concluding Remark

Mg_2Ni/NiTi/Mg sintered body that had the good performance of absorbing-desorption hydrogen were prepared and was detected under different condition of the temperature and H_2 pressure. It is result that the most suitable determined temperature was 250°C. For the composite, the switch of hydrogen absorption and desorption was to adjust H_2 pressure. The new method was used to prepare a specific sintered body material which had a large surface area and has a special layered structure by a superposed method. NiTi as catalytic phase and Mg_2Ni as hydrogen absorption phase improved the hydrating thermodynamics performance. After several cycles, the amount of actual hydrogen absorption-desorption was 0.68 and 0.14 under different conditions of H_2 pressure and the temperature. Therefore, the using of theoretical calculations and PCT curves under the different temperature and H_2 pressure were the powerful evidence that effectively absorbed hydrogen and specifically for releasing hydrogen could be achieved for a composite. But there are still great malpractices that the rate was slow and difficult to conduct activation.

In this paper, applying thermodynamic parameters calculation to confirm the temperature range was nearly 250°C. The experimental purpose was to achieve rapidly absorbing and desorbing for the block and to reach a greater amount of hydrogen absorption and desorption. The determination would be adjusted by confirmed temperature range and activated conditions help to absorb and desorb hydrogen. MgO obviously affected the rate of hydrogen absorption. The determination would be reconsidered to detect once again under no MgO condition. The detected condition was adjusted under 250°C up and down and changing H_2 pressure as the key factor under the different temperature conditions to detect the actual amount and the rate.

References

[1] W. Doenitz, R. Schmidberger, E. Steinheil and R. Streicher, Hydrogen production by high temperature electrolysis of water vapour, Int. J. Hydrogen Energy 1998, 5, 55-63.

[2] H. Gaffron, J.J. Rubin, Fermentative and photochemical production of hydrogen in algae, J.Gen. Physiol. 1942, 26, 219-240.

[3] D. H. Wang, Y. C. Luo, R. X. Yan, F. L. Zhang, L Kang, Phase structure and electrochemical properties of $La_{0.67}Mg_{0.33}Ni_{3.0-x}$ Co_x (x=0.0, 0.25, 0.5, 0.75) hydrogen storage alloys. J. Alloys Compd., 2006, 413: 193.

[4] Y. X. Liu, L. Q. Xu, W. Q. Jiang, G. X. Li, W. L. Wei, J Guo, Effect of substituting Al for Co on the hydrogen-storage performance of $La_{0.7}Mg_{0.3}Ni_{2.6}AlxCo_{0.5-x}$ (x=0.0–0.3) alloys. Int. J. Hydrogen Energy, 2009, 34: 2986.

[5] L Jiang, G. X. Li, L. Q. Xu, W. Q. Jiang, Z. Q. Lan, J Guo, Effect of substituting Mn for Ni on the hydrogen storage and electrochemical properties of $ReNi_{2.6-x}MnxCo_{0.9}$ alloys. Int. J. Hydrogen Energy, 2010, 35: 204.

[6] O. Arnaud, P. Barbic, P. Bernard, A. Bouvier, B. Knosp, B. Riegel and M. Wohlfahrt-Mehrens, Study of the corrosion resistance of Cr, Zr, Y doped AB5 type alloys in KOH, J. Alloys Compd. 2002, 330-332, 262-267.

[7] A. Singh, B.K. Singh, D.J. Davidson and O.N. Srivastava, Studies on improvement of hydrogenstorage capacity of AB5 type: =$MmNi_{4.6}Fe_{0.4}$ alloy, Int. J. Hydrogen Energy 2004, 29, 1151-1156.

[8]. Y. S. Myoung Youp Song, Hydrogen Storage Properties of a Ni, Fe and Ti-Added Mg-Based Alloy. Met. Mater. Int., Vol. 18, No. 2, pp. 279~286 2012.

[9]. M. Pozzo, D. Alfè, A. Amieiro, S. French, A. Pratt, Hydrogen dissociation and diffusion on Ni- and Ti-doped Mg(0001) surfaces. J. Chem. Phys. 128, 094703(2008).

[10] L Schlapbach, A Züttel, Hydogen-Storage Matcrials for Mobile Application, Journal of Nature, Vol. 414,353-358.

[11] M. V. Simičić, M. Zdujić, R. Dimitrijević, L. Niko-lić-Bujanović, N. H. Popović, Hydrogen Absorption and Electrochemical Properties of Mg_2Ni-Type Alloys Synthesized by Mechanical Alloying, Journal of Power Sources, Vol. 158, 730-734.

[12] A. Ebrahimi-Purkani, S. F. Kashani-Bozorg, Nano-crystalline Mg2Ni-Based Powders Produced by High-Energy Ball Milling and Subsequent Annealing, Journal of Alloys and Compounds, Vol. 456, 211-215.

[13] D. Kyoi, T. Sakai, N. Kitamura, A. Ueda and S. Tanase, Synthesis of FCC Mg–Ta Hydrides Using GPa Hydro-gen Pressure Method and Their Hydrogen-Desorption Properties, Journal of Alloys and Compounds, Vol. 463, 306-310.

[14] J. L. Bobet, E Akiba, B Darriet, Study of Mg-M (M=Co, Ni and Fe) Mixture Elaborated by Reactive Mechanical Alloying: Hydrogen Sorption Properties, International Journal of Hydrogen Energy, 2001, 26, 493-501.

[15] N Takeichi, K Tanaka, H Tanaka, T.T. Ueda, Y Kamiya, M Tsukahara, et al, Hydrogen storage properties of Mg/Cu and Mg/Pd laminate composites and metallographic structure. J Alloys Compd 2007; 446: 543.

[16] S Orimo, H Fujii, Effects of nanometer-scale structure on hydriding properties of Mg-Ni alloys: a review. Intermetallics 1998; 6: 185.

[17] E Berube, G Radtke, M Dresselhaus, G Chen, Size effects on the hydrogen storage properties of nanostructured metal hydrides: a review. Int J Energy Res 2007; 31: 637.

[18] M Jurczyk, L Smardz, I Okonska, E Jankowska, M Nowak, K Smardz, Nanoscale Mg-based materials for hydrogen storage. Int J Hydrogen Energy 2008; 33: 374.

[19] H. Y. Shao, Y. T. Wang, H.R. Xu, X.G. Li, Preparation and hydrogen storage properties of nanostructured Mg_2Cu alloy. J Solid State Chem 2005;

178: 2211.

[20] J. P. Lei, X. L. Dong, X. G. Zhu, et al, Formation and characterization of intermetallic Fe-Sn nanoparticles synthesized by an arc discharge method. Intermetallics 2007; 15: 1589.

[21] L David, B. F. Sandrine, F Laurent, Patrick A, Development of a volumetric method-experimental test bench for hydrogen storage characterization. Int J Hydrogen Energy 2007; 32: 1846.

[22] Zhou SH, Wang Y, Shi FG, Sommer F, Chen LQ, Liu ZK, et al. Modeling of thermodynamic properties and phase equilibria for the Cu-Mg binary system. JPEDAV 2007; 28: 158.

[23] Frederick MJ, Goswami R, Ramanath G. Sequence of Mg segregation, grain growth, and interfacial MgO formation in Cu-Mg alloy films on SiO_2 during vacuum annealing. J Appl Phys 2003; 93: 5966.

[24] Andreasen A, et al. Dehydrogenation kinetics of air-exposed MgH_2/Mg_2Cu and $MgH_2/MgCu_2$ studied with in situ X-ray powder diffraction. Appl Phys A 2006; 82: 515.

Chapter 5 Electrochemical properties/Actual capacity evaluation of Mg/Ni/Ti composite

5.1 Introduction

Widely used method is to use ball milling method to prepare a powder, a powder has high absorbing and desorbing hydrogen capacity; the rate had also been grater improved through various processes and adding catalytic elements [1-3]. But there are still lots of deficiencies, for example, easy to chalk; not easy to save and carry and a cycle of hydrogen absorption and desorption was achieved under constantly ball milling. For produced negative factors from absorbing and desorbing hydrogen, many researchers from domestic and foreign had a large number of experiments to improve kinetic and thermodynamic properties [4-7]. Alloy preparation had been attended. The amount of traditional AB_5, AB_2 and AB hydrogen storage materials are less than 2%, the result limited the actual application of hydrogen storage materials. Therefore, high capacity hydrogen storage materials had been a focus in various fields. In the present, for a alloy, more attention was V-based solid solution hydrogen storage alloy; The theoretical amount of hydrogen storage of VH_2 was up to 3.8%, but the activated properties was poor lead to limit the widely application. The relative alloy had been further studied [8, 9]. The amount of hydrogen absorption and desorption after homogenization heat treatment could be raised to 2%. It had been one of research hotspots. But the study on the affects from temperature and H_2 pressure to hydrogen absorption and desorption is not sufficient [10-13].

5.2 Experimental methods by electronic balance

According to co-precipitation method prepared Ni powder and adding Ti powder to form the new alloy phases made the composite had the specially

layer structure. Ni powder and Ti powder uniformly were mixed according to certain percentage, the powders after mixing cover to pure Mg ingot, so that Mg_2Ni generated while resulting in catalytic phase NiTi. The ability and capacity of hydrogen absorption and desorption were detected by confirmed the most viable detected condition to conduct a further study.

5.2.1 Preparation of Mg/Ni/Ti sintered body by electric furnace

Ti was added into the sintering Ni powder under the molar ratio of Ni：Ti =β：γ and was grinded for 2 hours. The second, Ni and Ti after grinding lay cover on the pure Mg ingot, the powder and the pure Mg ingot covered were permeated into pure Mg ingot in the form of doping under the molar ratio of Mg: Ni: Ti（α:β:γ）and was sintered under10°C /min to 750°C.

5.3 Results and Discussions

5.3.1 Characterization of Mg/Ni/Ti composite

As shown in Fig. 5.1, the composite continuous overlay each other during the sintering process, small particles of Ni and Ti powder were fully filled into the pure Mg ingot and the resulting alloy lattice has had defects and phase interface is increased constantly. It is indicated that the grain size below approximately 1.0μm. Powder particles are relatively dense and the large particles still existing, NiTi powder could permeate into the internal of Mg to form diffused layers and made the structure in the diffused layers loose.

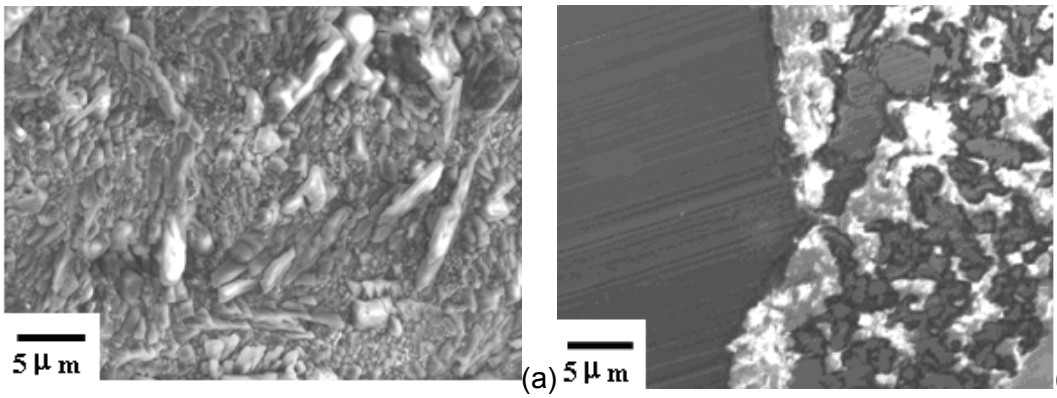

(a) (b)

Fig. 5.1 SEM section image (a) Mg/Ni/Ti surface after corrosion; (b) Mg/Ni/Ti section after corrosion.

As shown in Fig.5.2, according to distribution of the transition layer, Mg_2Ni generated on the surface and structural features were obvious. NiTi generated

in internal of the composite. This phenomenon was caused because Mg_2Ni form at first, with diffusion into the inner, Ti and Mg_2Ni reacted form NiTi alloy phase. The distribution of Mg, Ni and Ti elements are shown clearly, it is showed that the peaks of Mg and Ni elements are in the same position and distributed on the surface; the peaks of Ni and Ti elements distributed in same position of the inner.

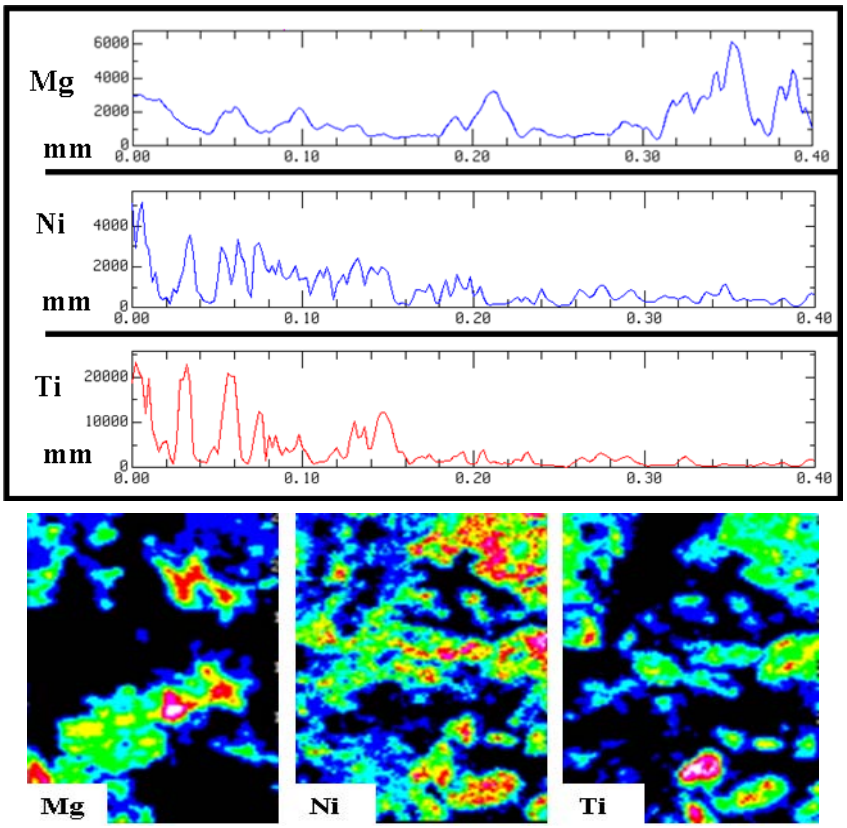

Fig. 5.2 EPMA section analysis of Mg/Ni/Ti.

As shown in Fig. 5.3, Mg_2Ni and NiTi phases generated in each diffused layer because of the powder and the metal produced mutually diffusion and formed multilayer structure. According to equation:

$$d_{hkl} \times r_{hkl} = L\lambda \quad (1)$$

d_{hkl} is interplanar spacing, r_{hkl} is radius of the diffraction spots, L is camera constant, λis x-ray wavelength. Mg_2Ni (P6222) is a hexagonal structure and d (203)=2.012Å; d(110)=2.610Å. The crystal grains distributed on the interface, resulting in the improvement of the effect on hydrogen absorption; NiTi (Pm3m) phase formed in the inner of the sintered body and d (110) =2.1116 Å,

d (200) =1.487Å, d (211) =1.218 Å. Its face-centered cubic structure helps to promote hydrogen absorption and desorption as catalytic phase; Mg_2Ni distributed on the surface of the sintered body and a small amount distributed in the inner, which improved the absorbed hydrogen ability. But only absorbed phase Mg_2Ni did not promote the improvement of hydrogen storage properties. Therefore, catalytic phase NiTi as a medium could speed up the absorption/desorption rate and make H atoms diffused into the internal of the sintered body. NiTi phase not only stays on the surface of the composite, but also could effectively increase the surface area because the mixed Ni and Ti powder conducting reaction with pure Mg ingot in sintering process, resulting in the hydrogen absorption phase and catalytic phase throughout the entire sintered body, and effective promoted the diffusion of H atom to the inner and improved the amount of hydrogen absorption/desorption for the sintered body. Lattice deformation was formed due to the great difference in thermal expansion coefficients of the powder and pure Mg ingot to provide a beneficial channel for H atoms diffusing into the internal of the sintered body.

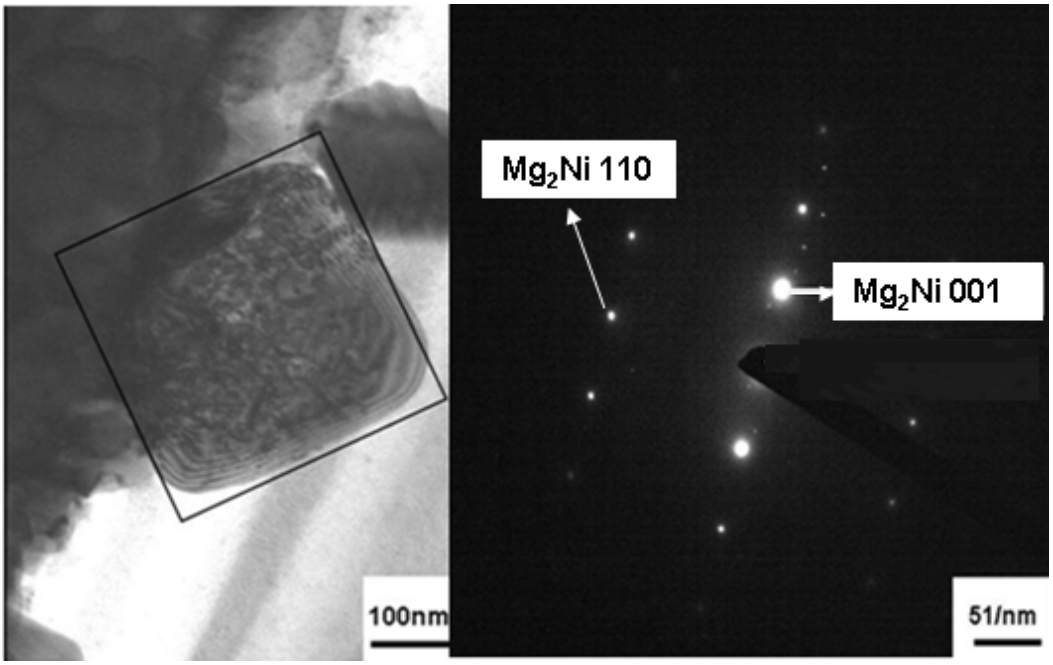

(a)

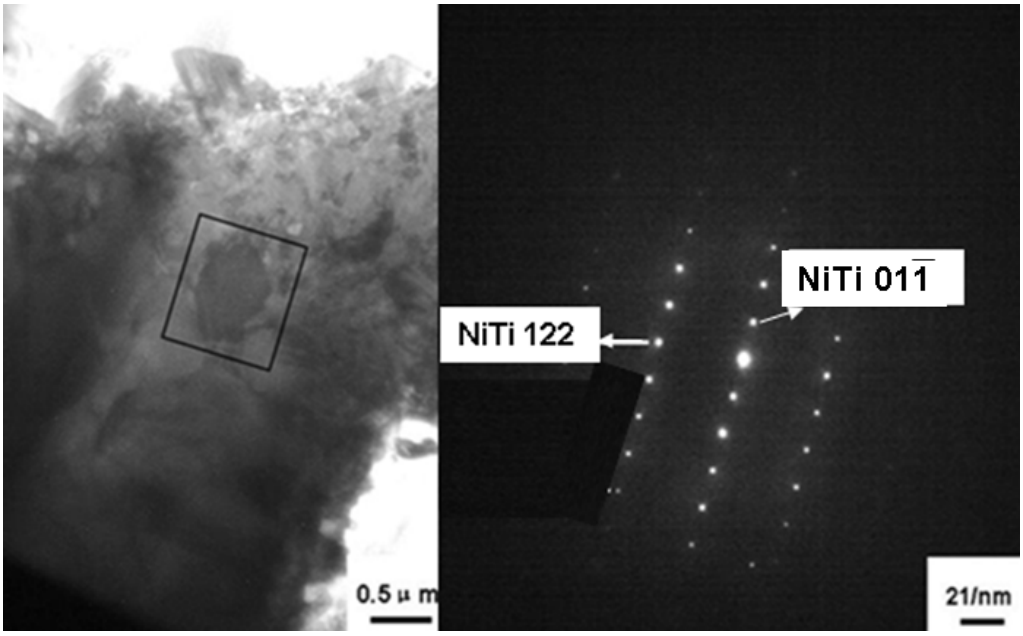

(b)

Fig. 5.3 TEM micrograph of alloy phases (a) Mg_2Ni;(b) NiTi.

5.3.2 Determination for the ability of absorption-desorption hydrogen by cyclic voltammeter

As shown in Fig. 5.4(a), Mg/Ni/Ti in neutral solution emerged obvious oxidized and reductive properties, good stability and closed state in small detected range. It is showed that the adding of Ti promoted the formation of NiTi alloy phase and diffused into the internal of the composite, so that play catalytic role to improve oxidized and reductive reaction. After absorbing hydrogen, there is not oxide layer on the surface due to no the adding of MgO, the reaction rate speed the current of oxidation and reduction. Under Mg_2NiH and NiTiH autocatalytic role, the ions in solution too late to diffuse on the surface of electrode to conduct supplementary; caused the concentration of the ions reduced nearby the surface of electrode and made electrode potential deviated pre-equilibrium potential compared to that before absorbing hydrogen, so that reduction current obviously increased. After adding H_2O and absorbing hydrogen, a certain fluctuation appeared on CV curve; the curve was more vertical. It is showed that a large amount of oxide layer formed on the surface of specimen, so that affected the good catalytic activity. Hydroxide electrode

was surface control rather than diffused process. As shown in Fig. 5.4(b), when the electrolyte was alkaline solution KOH, oxidized and reductive reaction became intense and there were not obvious fluctuations. The oxidized current reached to 800mA, the reductive current reached to -600mA. Reducibility was significantly increase lead to the ability of hydrogen absorption and desorption was obviously improved. After absorbing hydrogen, with voltage increasing, speed reach to decomposition voltage of the metal hydride; the capacity of hydrogen absorption was large, compared with the specimen before absorbing hydrogen, the potential window range of oxidation and reduction became to narrow and the current decreased. After adding H_2O and absorbing hydrogen, there was a clear reduction peak, it indicated that release hydrogen was obviously. Mg_2Ni and NiTi phases were stable without the fluctuations of from low valence to high valence to change. Thereby, the oxidized and reduction reaction became steadily.

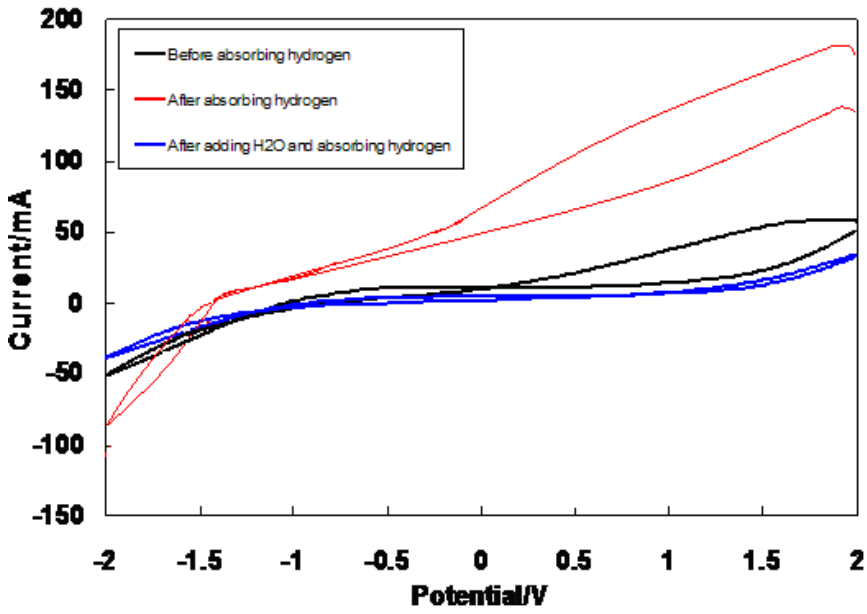

(a)

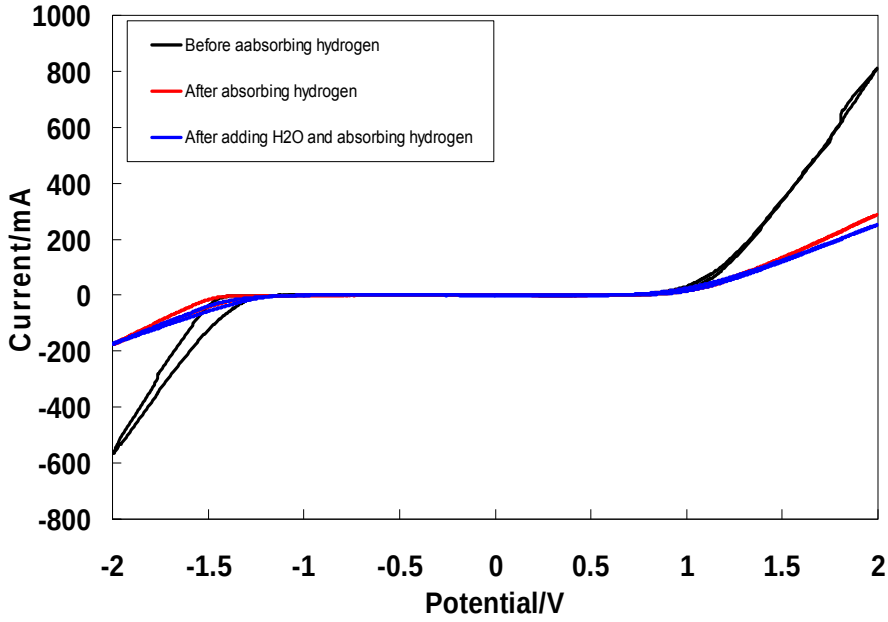

(b)

Fig. 5.4 Oxidation/Reduction of Mg/Ni/Ti (a) Neutral solution (PH7); (b) Alkaline solution (KOH).

5.3.3 Capacity evaluation of hydrogen absorption/desorption（from 340°C to 220°C）

In the early activation process, the amount of hydrogen absorption rapidly increase form room temperature up to 220°C within 30min. When maintaining 220 °C and 1MPa conditions, hydrogen absorption capacity did not change significantly, it is indicating that the temperature and hydrogen pressure was as switch for starting hydrogen storage in the initial stage. The increasing of absorbing hydrogen became slow with H_2 pressure to change under thermostatic state. The results showed that the adjusting for the system H_2 pressure made the amount of hydrogen absorption reach saturation and hydrogen desorption was starting with the decreasing of H_2 pressure so that completed the first cycle. In the process, the key of the first cycle of hydrogen absorption and desorption lie in the adjusting of H_2 pressure. In the second active process, while the temperature and H_2 pressure were adjusted at the same time, the second cycle of hydrogen absorption and desorption was

achieved within 1 hour. When hold constant temperature, the third cycle produced with adjusting H_2 pressure. It is indicated that the change of H_2 pressure play a decisive role, but the adjusting of H_2 pressure could make activated process longer. According to the sitting in the experimental conditions, although the activated time was long, but once the sample was fully activated, Life cycle, the amount and the rate of hydrogen absorption and desorption would be improved significantly. The differentiation with the previous determined condition was that conducted induced process under 3 kinds of different conditions. During the period, not only physical adsorption on the surface was achieved, but also rapidly achieved diffusion H atoms to the internal of the sintered body. It is shown that the main switch caused hydrogen absorption and desorption was the adjusting of the system H_2 pressure.

In order to activate the absorbing ability of hydrogen absorption and desorption on the surface as soon as possible, repeatedly adjusting H_2 pressure as the main condition according to H_2 pressure as switch. When H_2 pressure was adjusted repeatedly to 4MPa three times, the purpose is to confirm the loss of the capacity through the cycles of hydrogen absorption and desorption. As shown in Fig. 5.5, under thermostatic state 340°C, constantly adjusting the system hydrogen pressure, hydrogen absorption and desorption was significantly higher. The third time cycle about hydrogen absorption and desorption was completed under thermostatic process. It was shown that the material get very good activation during the period process, so that the whole of cycle of hydrogen absorption and desorption was completed within 30min. The results showed that H_2 pressure played a crucial role under a constant temperature, the level of H_2 pressure determines the beginning and end of hydrogen absorption and desorption of hydrogen.

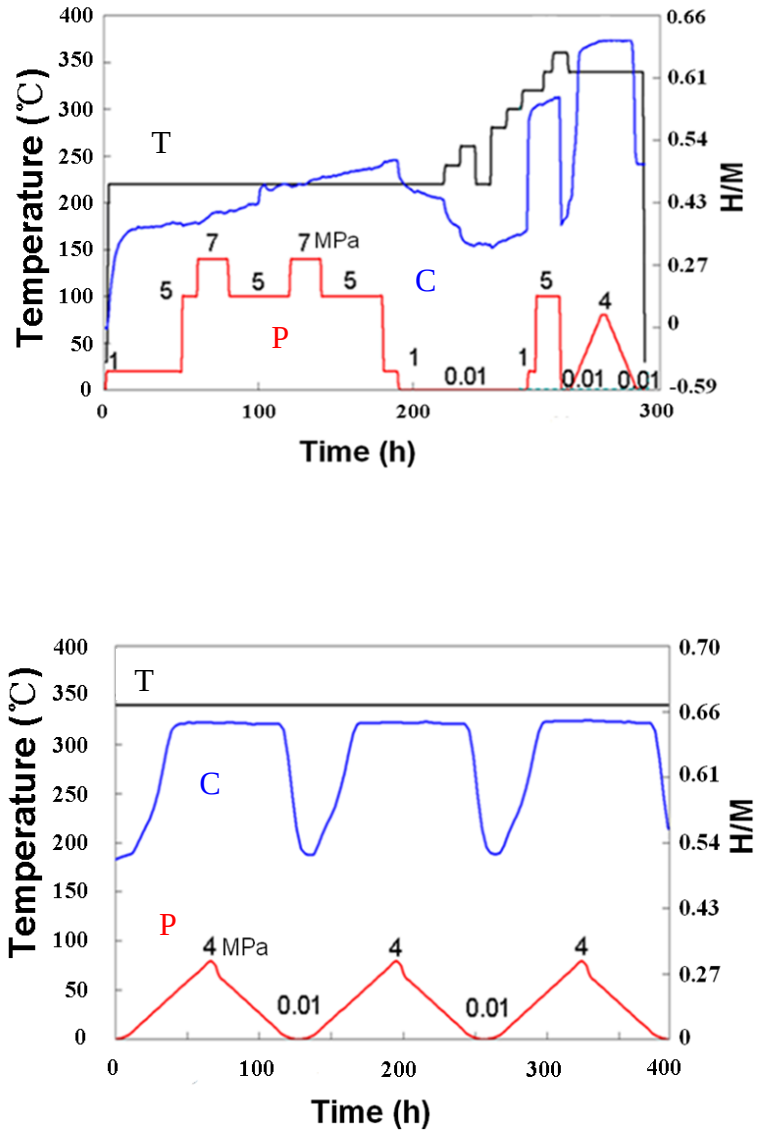

Fig. 5.5 (a) PCT curves of absorbing and desorbing hydrogen for activating process under different conditions of temperature and H_2 pressure; (b) PCT curves of absorbing and desorbing hydrogen for H atoms diffused process under constant temperature 340°C when adjusting repeatedly H_2 pressure from 0.01MPa to 4MPa.

(a) Quantitative analysis from 340°C to 220°C

Only depending on the extension of time can increase the capacity of hydrogen absorption and desorption from room temperature to 220°C, but the rate of hydrogen absorption and desorption was slowly by hours. The study conducted the subtle division and quantitative analysis for the above results. In the active process, absorb hydrogen process start while the temperature was surged. But under constant temperature and pressure, the increasing of hydrogen absorption became slow. The determination only depend on the prolong time made hydrogen absorption to saturation; the amount of hydrogen absorption reached up to 0.37 as shown in Fig. 5.6.

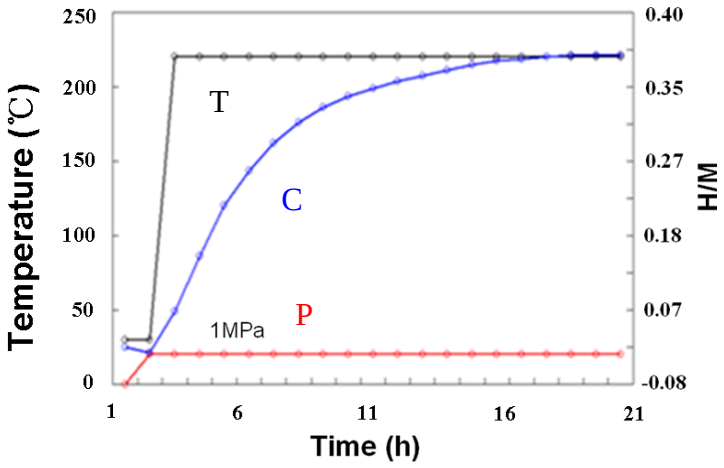

Fig. 5.6 Capacity of absorbing hydrogen when adjusting temperature (from room temperature to 220°C) and H_2 pressure (from 0.01MPa to 1MPa).

To maintain a constant temperature and to change hydrogen pressure, it is the result that small amounts of hydrogen absorption was obtained and needed a longer time, the hydrogen desorption process began when the hydrogen absorption is saturated; the rate of the hydrogen desorption was rapidly, there is a trend to continue to release hydrogen as shown in Fig. 5.7.

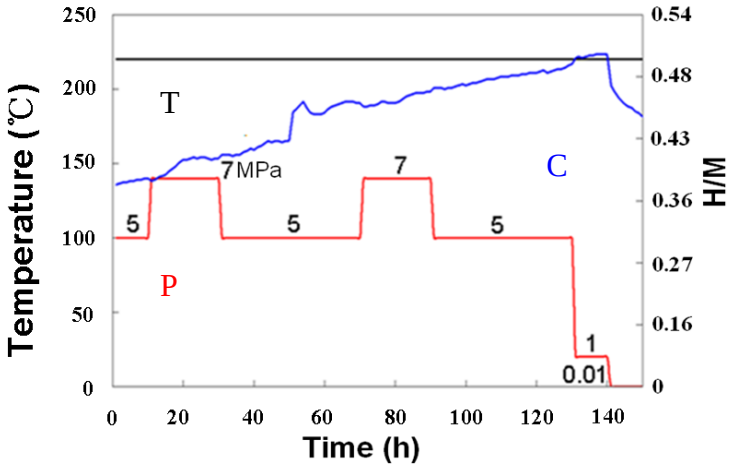

Fig. 5.7 Capacity of absorbing hydrogen under constant temperature 220°C when adjusting repeatedly H_2 pressure (from 5MPa to 7MPa).

In the preliminary absorbing process, the conditions that adjusting temperature and H_2 pressure were set at the same time because the cycle of hydrogen absorption and desorption was achieved in order to complete fully activation. When adjusting the temperature and H_2 pressure conditions, the first time of hydrogen desorption process is completed as shown in Fig. 5.8. Hydrogen desorption reached to 0.33. With the end of the first cycle to conduct the second cycle of absorption and desorption of hydrogen. The results showed that the hydrogen absorption capacity did not change significantly under constant H_2 pressure. When the temperature and hydrogen pressure were adjusted at the same time, the amount of absorption and desorption of hydrogen significant increased. Hydrogen storage capacity could reach about 0.42, the amount of hydrogen desorption also reached to 0.42. And the rate of hydrogen absorption was very fast just completed a secondary circulation within 1 hour. It is showed that the sample had been fully activated, so that achieved the rapid cycle of hydrogen absorption and desorption for the composite.

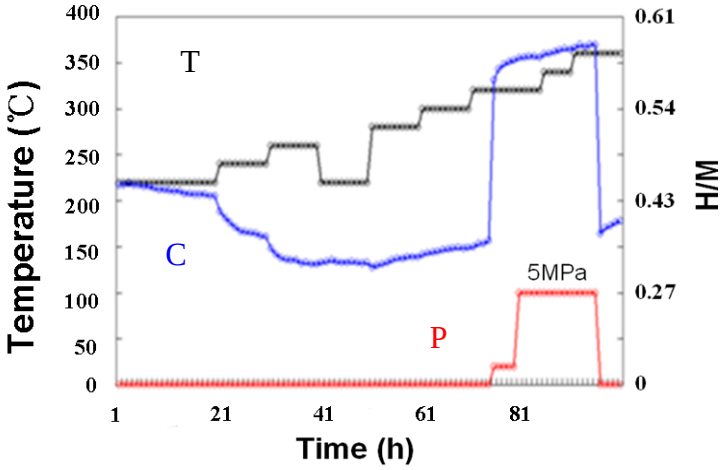

Fig. 5.8 Capacity of absorbing hydrogen when adjusting temperature (from 220°C to 340°C) and H_2 pressure (from 0.01MPa to 5MPa) at different times.

The determination was the good result mainly due to the improvement on the measurement conditions, 3 times cycles of hydrogen absorption and desorption were completed under the following constant temperature. The hydrogen was release to detect an amount and the rate of hydrogen absorption and desorption after activation. This method is easy to form a loose structure helps to sample more empty because the traces of H atoms diffused was reserved when hydrogen atoms were rapid released, resulting in an increasing of the grain boundary between the crystal grains, thereby increasing the effective area of the sample. The results showed that the hydrogen absorption capacity reached to 0.5, the amount of hydrogen desorption reached to 0.43 as shown in Fig. 5.9.

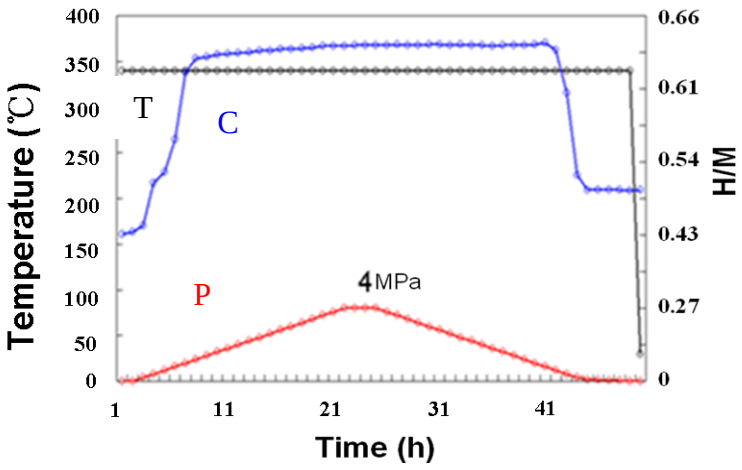

Fig. 5.9 1st cycle capacity of absorbing and desorbing hydrogen under constant temperature 340°C when adjusting H_2 pressure from 0.01MPa to 4MPa.

The same detected condition was set and the amounts of hydrogen absorption and desorption were 0.43 and 0.38 in the cycle process as shown in Fig. 5.10.

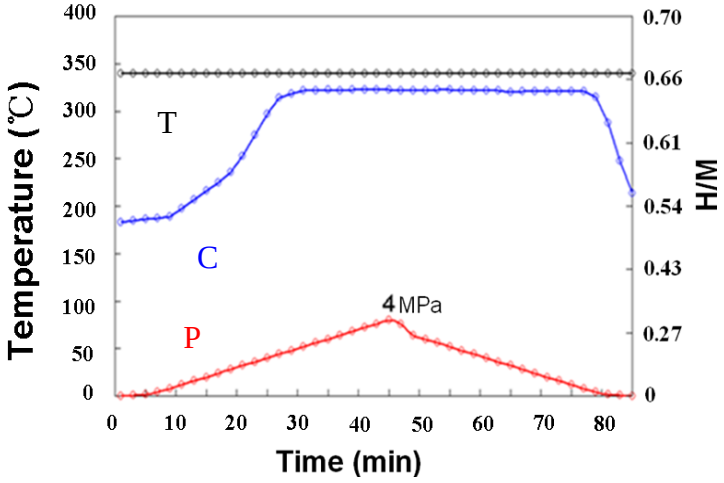

Fig. 5.10 2nd cycle capacity of absorbing and desorbing hydrogen under constant temperature 340°C when adjusting H_2 pressure from 0.01MPa to 4MPa.

In the third time cycle process as shown in Fig. 5.11, the amounts of hydrogen absorption and desorption were 0.43and 0.38.

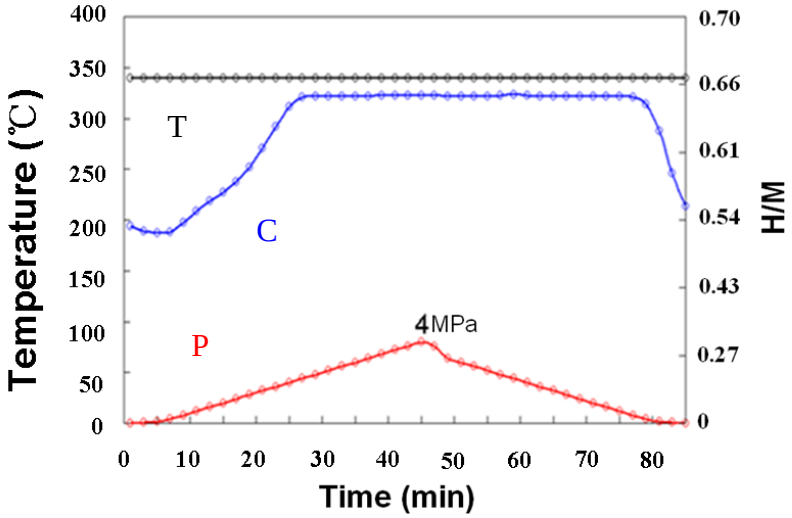

Fig. 5.11 3rd cycle capacity of absorbing and desorbing hydrogen under constant temperature 340°C when adjusting H_2 pressure from 0.01MPa to 4MPa.

(b) Quantitative analysis under H_2 pressure 4MPa and temperature 220°C

According to the most suitable H_2 pressure, the detected condition was adjusted directly to 4MPa under the temperature of hydrogen absorption and desorption 220°C. After several times cycles of hydrogen absorption and desorption, H pressure was confirmed at 4MPa was most suitable as shown in Fig. 5.12, hydrogen absorption capacity was significant increase and the rate was very fast with constantly adjusting H_2 pressure. The amount of absorption reached 0.54 within 3min under constant temperature; in 16min, the amount of hydrogen absorption had reach about 0.66. Under the constant temperature,

hydrogen absorption tended to saturated with repeatedly adjusting H_2 pressure. The time from starting absorb hydrogen to saturation took about 1 hour. For a sintered body, it is potential. It is indicated that the application of superposition method effectively increased the surface area of the sample. This result surpass than the result of powders prepared by the general milling method under the same conditions.

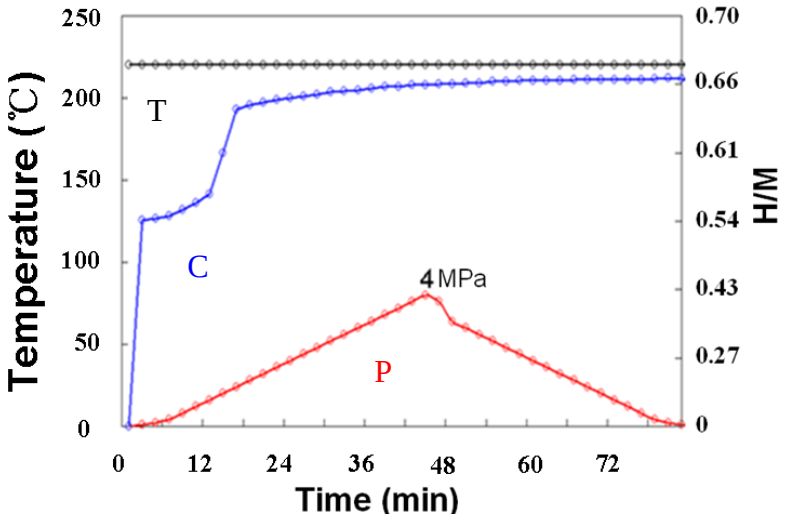

Fig. 5.12 Capacity of absorbing hydrogen under constant temperature 220°C when adjusting H_2 pressure from 0.01MPa to 4MPa.

When keeping temperature at 220°C, H_2 pressure was adjusted to 4MPa still promoted the diffusion of H atoms into the internal of the composite. But the capacity of hydrogen absorption was less and the rate was slowly in the short time. Among the continuous determination, hydrogen storage capacity increased more slowly, it is indicating that hydrogen absorption is about to reach saturation; the hydrogen absorption capacity had reached 0.67.

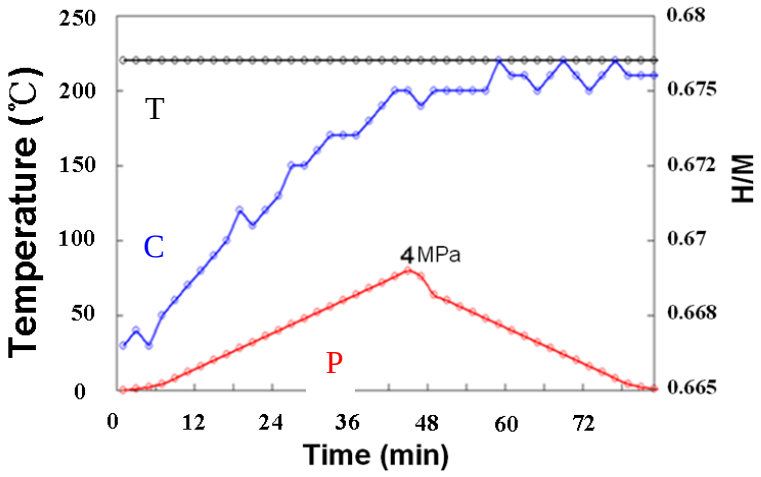

Fig. 5.13 Capacity of absorbing hydrogen closed to saturation under constant temperature 220°C when adjusting H_2 pressure from 0.01MPa to 4MPa.

The hydrogen desorption started when the capacity of hydrogen absorption reached saturation. The hydrogen desorption process was achieved, but the capacity of hydrogen desorption was less in the short time. As shown in Fig. 5.14, at a constant temperature, hydrogen desorption effect is not obvious under adjusting the same hydrogen pressure conditions. It is essential that the temperature conditions play an importance role in the hydrogen desorption.

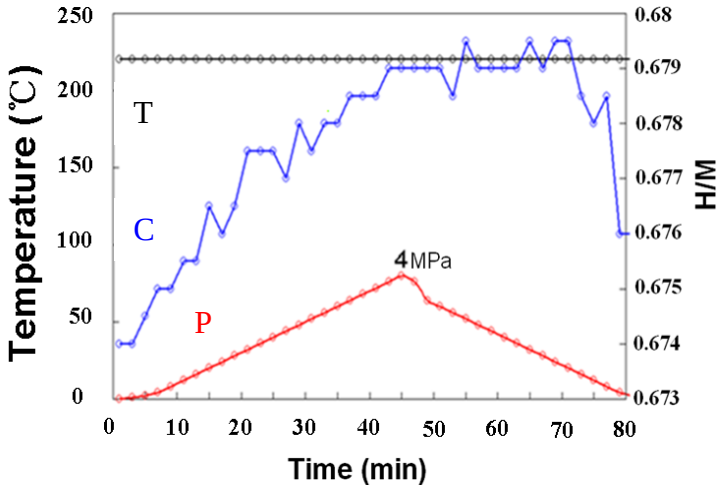

Fig. 5.14 Capacity of absorbing and desorbing hydrogen under constant temperature 220°C when adjusting H_2 pressure from 0.01MPa to 4MPa.

In order to compare the capacity of hydrogen absorption and desorption for composite with that of the powders, the study made detect under some condition and molar ratio. As shown in Fig. 5.15(a), the amount of hydrogen absorption reached 0.23. The rate of the powder was slowly because the powder easy to chalking, so that caused the capacity of hydrogen absorption was limited within long time. As shown in Fig. 5.15(b), when constant temperature was hold, the capacity of hydrogen absorption was slowly increased and reached quality fraction of 0.31.

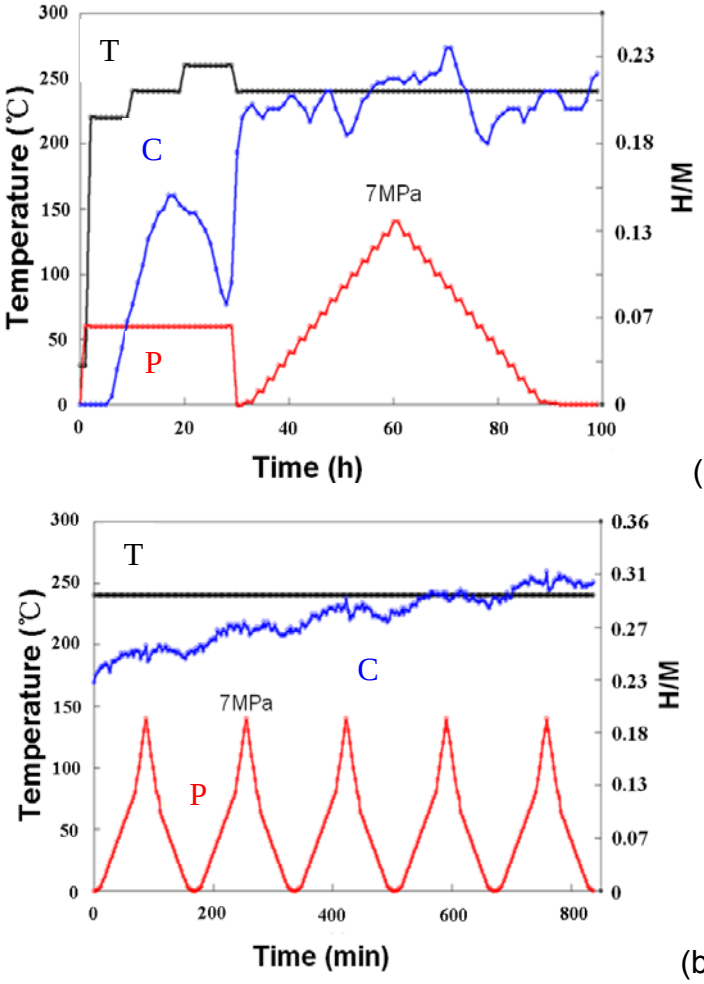

Fig. 5.15 (a) PCT curve of powder Mg/Ni(MgO)/Ti under adjusting temperature and H_2 pressure from 0.01MPa to 7MPa (b) PCT curve of powder Mg/Ni(MgO)/Ti under constant temperature 220°C when adjusting repeatedly H_2 pressure from 0.01MPa to 7MPa.

As shown in Fig. 5.16(a), the amount of hydrogen absorption reached 0.35 when MgO was added in sintering process. The rate of the powder became

relative rapid and the capacity of hydrogen absorption increased within the same time. As shown in Fig. 5.16(b), when constant temperature was hold, the capacity of hydrogen absorption increased and reached quality fraction of 0.37. in the short time, the absorbing hydrogen capacity reached to saturation state. The cycle of hydrogen absorption and desorption was achieved. The existing disadvantages were the main reason to prepare a new type composite material.

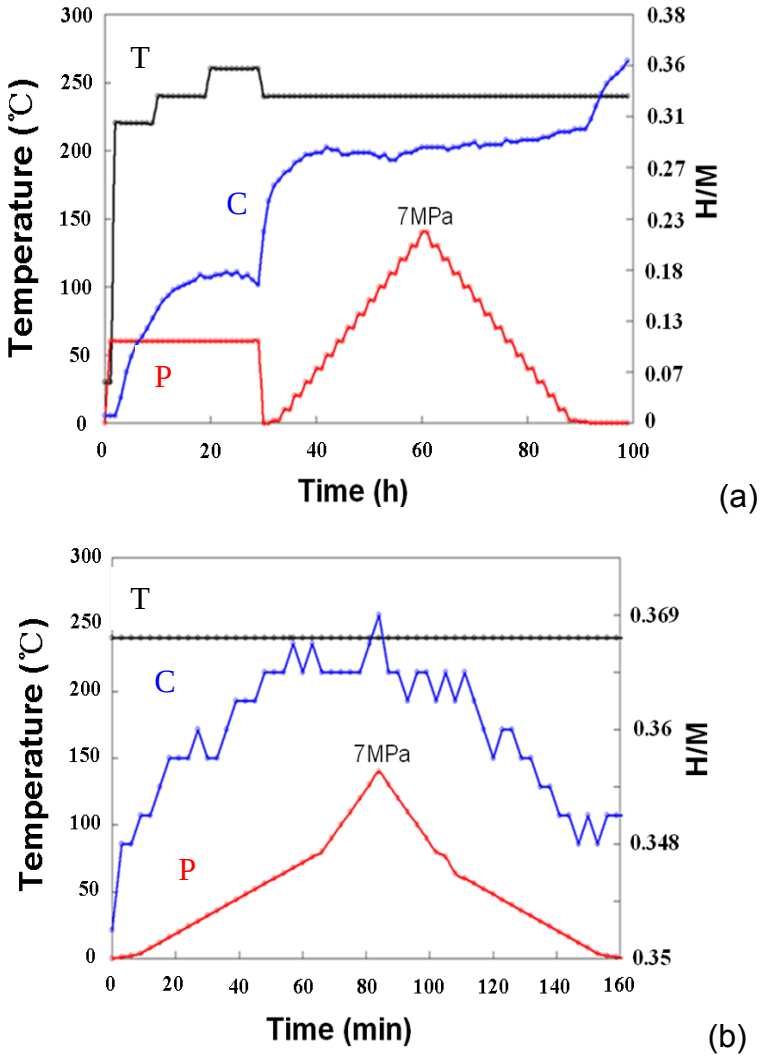

Fig. 5.16 (a) PCT curve of powder Mg/Ni/Ti under adjusting temperature and H_2 pressure from 0.01MPa to 7MPa (b) PCT curve of powder Mg/Ni/Ti under constant temperature 220°C when adjusting repeatedly H_2 pressure from 0.01MPa to 7MPa.

5.4 Concluding Remarks

High capacity and rapidly rate were achieved by the improvement on the determined conditions. The hydrogen absorption/desorption performance was improved due to the effective increase of surface area in the process of preparing the sintered body. A new method was used to avoid the disadvantages of other methods; the combination of powder and alloy was achieved. The sintered body had greatly improved the capacity and rate of hydrogen absorption/desorption. For the sintered body, absorbed and desorbed hydrogen rate became faster and even superior to effects from a powder. The capacity of hydrogen absorption reached 0.54 within 3min and the highest capacity reached 0.67 within 16min; the maximum amount of hydrogen desorption reached to 0.43 under certain detected conditions.

References

[1] W. Doenitz, R. Schmidberger, E. Steinheil and R. Streicher, Hydrogen production by high temperature electrolysis of water vapour, Int. J. Hydrogen Energy 1998, 5, 55-63.

[2] H. Gaffron, J.J. Rubin, Fermentative and photochemical production of hydrogen in algae, J.Gen. Physiol. 1942, 26, 219-240.

[3] D. H. Wang, Y. C. Luo, R. X. Yan, F. L. Zhang, L Kang, Phase structure and electrochemical properties of La0.67Mg0.33Ni3.0–x Cox (x=0.0, 0.25, 0.5, 0.75) hydrogen storage alloys. J. Alloys Compd., 2006, 413: 193.

[4] Y. X. Liu, L. Q. Xu, W. Q. Jiang, G. X. Li, W. L. Wei, J Guo, Effect of substituting Al for Co on the hydrogen-storage performance of $La_{0.7}Mg_{0.3}Ni_{2.6}AlxCo_{0.5-x}$ (x=0.0–0.3) alloys. Int. J. Hydrogen Energy, 2009, 34: 2986.

[5] L Jiang, G. X. Li, L. Q. Xu, W. Q. Jiang, Z. Q. Lan, J Guo, Effect of substituting Mn for Ni on the hydrogen storage and electrochemical properties of ReNi2.6–xMnxCo0.9 alloys. Int. J. Hydrogen Energy, 2010, 35: 204.

[6] O Arnaud, P Barbic, P Bernard, A Bouvier, B Knosp, B Riegel and M. Wohlfahrt-Mehrens, Study of the corrosion resistance of Cr, Zr, Y doped AB5 type alloys in KOH, J. Alloys Compd. 2002, 330-332, 262-267.

[7] A. Singh, B. K. Singh, D. J. Davidson and O. N. Srivastava, Studies on improvement of hydrogen storage capacity of AB5 type: =MmNi4.6Fe0.4 alloy, Int. J. Hydrogen Energy 2004, 29, 1151-1156.

[8] L. Schlapbach, A. Züttel, Hydogen-Storage Matcrials for Mobile Application, Journal of Nature, Vol. 414,353-358.

[9] M. V. Simičić, M. Zdujić, R. Dimitrijević, L. Niko-lić-Bujanović, N. H. Popović, Hydrogen Absorption and Electrochemical Properties of Mg2Ni-Type Alloys Synthesized by Mechanical Alloying, Journal of Power Sources, Vol. 158, 730-734.

[10] A. Ebrahimi-Purkani, S. F. Kashani-Bozorg, Nano-crystalline Mg2Ni-Based Powders Produced by High-Energy Ball Milling and Subsequent Annealing," Journal of Alloys and Compounds, Vol. 456, 211-215.

[11] D. Kyoi, T. Sakai, N. Kitamura, A. Ueda and S. Tanase, Synthesis of FCC Mg–Ta Hydrides Using GPa Hydro-gen Pressure Method and Their Hydrogen-Desorption Properties," Journal of Alloys and Compounds, Vol. 463, 306-310.

[12] J. L. Bobet, E Akiba, B Darriet, Study of Mg-M (M=Co, Ni and Fe) Mixture Elaborated by Reactive Mechanical Alloying: Hydrogen Sorption Properties, International Journal of Hydrogen Energy, 26, 493-501, 2001.

[13] A Zaluska, L Zaluski, Synergy of Hydrogen Sorption in Ball-milled Hy-drides of Mg and Mg_2Ni, Journal of Alloys and Compounds, 289, 197-206, 1999.

[14] C. W. Ostenfeld, I. B. Chorkendorff, Effect of oxygen on the hydrogenation properties of magnesium films. Surf Sci 2006; 600:1363–8.

[15] K. F. Aguey-Zinsou, J. R. Ares Fernandez, T Klassen, R Bormann, Using MgO to improve the (de)hydriding properties of magnesium. Mater Res Bull 2006; 41: 1118–26.

[16] A Zaluska, L Zaluski, Nanocrystalline magnesium for hydrogen storage. J Alloys Compd 1999; 288: 217–55.

[17] M Martin, C Gommel, C Borkhart, E Fromm, Absorption and desorption kinetics of hydrogen storage alloys. J Alloys Compd 1996;238:193–201.

[29] M Avrami, Kinetics of phase change. I general theory. J Chem Phys 1939; 7: 1103–12.

[18] W. A. Johnson, R. F. Mehl, Reaction kinetics in processes of nucleation and growth. Trans AIME 1939; 135: 416–68.

[19] P Hjort, A Krozer, B Kasemo, Hydrogen sorption kinetics in partly oxidized Mg films. J Alloys Compd 1996; 237: 74–80.

[20] K. B. Gerasimov, I. G. Konstanchuck, S. A. Chizhik, Hysteresis" in interaction of nanocrystalline magnesium with hydrogen. Int J Hydrogen

Energy 2009; 34: 1916–21.

[21] H. Y. Shao, Y. T. Wang, H. R. Xu, X. G. Li, Hydrogen storage properties of magnesium ultrafine particles prepared by hydrogen plasma-metal reaction. Mater Sci Eng B 2004; 110: 221–6.

Chapter 6 Conclusions

The study by using a new laminated cover method and changing element was conducted and was discussed to prepare the special structure sintered body. It had a large surface area can effectively conduct the cycle of hydrogen absorption and desorption; so that achieved the whole cycle was completed within very short time. In the process, the amount of hydrogen absorption and desorption was obviously improved. Some shortcoming of saving and inconvenient to carry from a powder was avoided and the shortcoming not easy to activate for an alloy was improved. The composite prepared in this experiment had uniform crystal structure and transitional layer promoted hydrogen absorption and desorption. The different diffused layers were composed based on the same size pure Mg ingot as substance; the different transitional layers were connected between each diffused layers and had good continuity, so that improved the performance of hydrogen absorption and desorption.

In this paper, effectively improved the amount and the rate of hydrogen absorption and desorption as the purpose to try to homemade refinement powder Ni by co-precipitation. By deliberately adding H_3BO_3 to refine the powder and form a simple substances or compounds phases can promote hydrogen absorption and desorption. It is showed that adding H_3BO_3 had not reach the experimental purpose, but only was to refine the powder. Therefore, based on above the study consider conduct restructuring for experimental method and adding element. Ti was selected add into powder Ni prepared and uniform mix powder was cover on pure Mg ingot, the purpose was to prepare a special structure sintered body. It was combining state between a powder and alloy; whose structure was loose and pores was more obvious. The structure provided a favorable condition for hydrogen absorption and desorption. In the prepared process, Mg_2Ni and NiTi as achieved absorbed hydrogen phase and

catalytic phase were formed. The ability and actual capacity of the sample were analyzed and discussed in detail. It is indicated that the materials had different degree activated performance and the cycle amount under different detected conditions. For the composite, it is a key that find out the most suitable activated condition to achieve rapidly absorb and desorb hydrogen. And contrasted to a powder and alloy, it has a great superiority on the amount of hydrogen absorption and desorption. Through several time activated conditions, the optimum results were obtained. According to H_2 pressure was main switch from room temperature surge to 220°C, all of H_2 was released after activating and conducted determination of hydrogen absorption and desorption again. The results were that the amount of hydrogen absorption was obviously and the rate was rapidly. The study analyzed highlights according to obtained results, at first, the experimental condition was special that powder and metal superimposed method each other was used in prepared process. Secondly, the activated process was more precise experimental condition and was explanted the whole absorbed and desorbed hydrogen process by many theoretical calculations. The third, the composite fully achieved high the absorbed and desorbed amount and rapidly rate. The study analyzed highlights according to obtained results, as shown in follows:

1. A new method was used to avoid disadvantages from other methods; fundamentally greatly improved the amount of hydrogen absorption and desorption；

2. The activated process was more precise and explanted the whole absorbed and desorbed hydrogen process by many theoretical calculations.

3. Sufficient diffusion between powder and metal;

4. Achieving multilayer composite structure

5. Effectively increasing surface area of composite;

6. Mg_2Ni absorbed hydrogen phase distributed the surface of composite, NiTi catalytic phase distributed the internal of sintered body;

7. Mg_2Ni phase effectively absorbed H atom on the surface, NiTi phase

penetrated the whole sintered body to achieve H atom diffused into inner;

8. MgO produced serious affect on hydrogen absorption/desorption due to the formation of $Mg(OH)_2$.

9. For composite, absorbed and desorbed hydrogen rate was obviously improved and even superior to effects from a powder;

10. Amount of hydrogen absorption and desorption reach to 3% within 3min and the high amount reach to 5.3% within 16min;

11. Hydrogen desorption process was completed within 30min and the released amount was about 2%. The preparation of the sintered body also achieved advantages.

In the future, the sample was prepared to be molded into a large-sized sintered body can be applied in various fields.

Table. 6.1 Comparison of the composite and recent Mg-based materials

Alloy phases	H mass%	Dissociation pressure (MPa)	Dissociation temperature (° C)	Rate of hydrogen absorption	△wt%
M-23.3%Ni	6.5	0.5-0.6	343	3h	
Mg_2Ni	3.6	0.1	250	6h	
Mg_2Cu	2.7	0.1	239	1h	△3%
$Mg_{12}Ce$	4.0	0.3	325	3h	
$Mg_{51}Zn_{20}$	3.6	0.4	200	20h	
$Mg_2Ni_{0.75}Cu_{0.25}$	3.5	0.1	227	80h	
$Mg_2Ni_{0.75}Ti_{0.25}$	3.6	0.1	263	5min	△ 1.5%
Mg_2Ca	5.5	0.5	350	10h	△ 3%
$Mg_{1.8}Ni_{0.5}Ca$	3.7	0.1	380	5h	
Mg_2Ni_2Ti	5.26	1	220	3min	

According to above results, the study achieved a high capacity of hydrogen absorption and desorption, and the rate of hydrogen absorption and desorption had been improved significantly. For other Mg-based material, the dissociation pressure was higher. The issue will be needed to resolve through improving experimental method and adding other elements in future.

Related publications of the author

[1] Ningning Zhou and Dongying Ju, A New Method of Electrode Material Preparation for Hydrogen Absorption-Desorption, Journal of The Electrochemical Society, 2013, Vol. 160(10), pp. A1863-A1869

[2] Ningning Zhou, Dongying Ju and Wanyu Ding, The effect of H_3BO_3 micro addition on microstructure of Ni/MgO sintered compact by Co-Precipitation method, Materials Science Forum, 2013, Vol.750(168), pp.168-171.

[3] Ningning Zhou and Dongying Ju, Study on preparation and properties evaluation of Mg/Ni/Ti hydrogen storage material, International Journal of Hydrogen Energy, accepted, in production.

[4] Ningning Zhou and Dongying Ju, Improvement on the performance of Mg_2Ni/NiTi/Mg hydrogen absorption/desorption, Materials Science Forum, accepted, in production.

Acknowledgements

I wish to express my sincere gratitude and appreciate to my directional Professor Dr. Dongying Ju, for taking me as his student and giving me the opportunity to pursue the Ph.D. degree in Saitama Institute of Technology. I owe him my sincere thanks for his support, encouragement and guidance throughout my study. Without his support I could not have achieved thus far.

I would like to thank Prof. S. Uchiyama, Prof. K. Tanaka, Prof. T. Yajima and Prof. M. Uchida for their productive suggestions and taking time away from their busy schedules to serve on the committee. Many thanks for their valuable advices enlightening me to understand the research deeply.

My thanks also go to all the peoples who engaged in or cooperated with our group in this research. I also would like to thank Prof. H. Matsuura in department of life science and green chemistry for his help on measuring electrochemical properties of hydrogen absorption/desorption. It is their cooperation that opened this research widely.

I wish to sincerely thank all the professors who supervised me or taught me at Saitama Institute of Technology. Thank them for giving me the high quality education. I also wish to thank all the professors and staff at SIT for their help and providing a pleasant study and work environment at SIT. Many thanks specially go to High Technology Research Center in Saitama Institute of Technology for the support through out my study. The support to my research work is gratefully acknowledged.

I would like to express my sincere gratitude to all the people who have been supportive of my endeavor towards my Ph. D. study. Finally, my deep appreciation is due to my parents for their love, support and encouragement throughout my graduate work.